AN ELECTRICAL RESISTIVITY STUDY OF THE AREA BETWEEN MT. SUSWA AND THE OLKARIA GEOTHERMAL FIELD, KENYA

STEPHEN ALUMASA ONACHA

A thesis submitted in accordance with the requirement for partial fulfillment of the Degree of Master of Science

DEPT. OF GEOLOGY

UNIVERSITY OF NAIROBI

1989

DECLARATION

This is my original work and has not been submitted for a degree in any other university

S.A. ONACHA

The thesis has been submitted for examination with our Knowledge as University Supervisors:

Prof. M.P. TOLE

Mr. E. DINDI

ACKNOWLEDGEMENTS

I wish to thank my supervisors Dr. M.P. Tole and Mr. E. Dindi for their invaluable help and advice during the course of my studies. I am grateful to the staff of the Ministry of Energy especially Mr. Kinyariro and Mr. Kilele for their tremendous help during the data acquisition. I also wish to express my appreciation of the University of Nairobi for their MSc Scholarship during my study. I am grateful to the British Council for their fellowship that enabled me to carry out data analysis at the University of Edinburgh.

Finally, I wish to thank the members of my family for their love and understanding during my studies.

ABSTRACT

The D. C. electrical resistivity study of Suswa-Olkaria region was carried out from July 1987 to November, 1988. The main objective was to evaluate the sub-surface geoelectric structure with a view to determining layers that might be associated with geothermal fluid migrations. The study also aimed at delineating the southern extent of the Olkaria geothermal field and of the structural discontinuities. The study was carried out using the Symmetrical Schlumberger array with a maximum current electrode spacing of 8000m.

The resistivity data analysis was carried out by curve matching and fitting, and I-D iterative computer modelling. Geoelectrical structural models on line profiles have identified horst-graben structures bound by normal to oblique N-S and oblique arcuate E-W trending discontinuities. Some of these discontinuities coincide with fault zones which are permeable zones of complex fluid migration. Geophysical and Geological data synthesis has identified four geoelectrical units with considerable variation in thickness. These are the overburden, a resistive cap rock, a conductive unit (3-15 Ωm) and an electrical basement (50-200Ωm). The resistivity of the conductive unit in the southern part of Olkaria is similar to that of Olkaria West. The conductive unit correlates with tertiary pyroclastics

intercalated with tuffs rhyolite and trachytes while the electrical "basement" correlates with Miocene Volcanics.

From this study, it is noted that the graben structures with a sub-surface conductive unit which is covered with a resistive "cap" rock offer good prospects for further geothermal exploration. The conductive unit has been attributed to a permeable layer that is part of a convective hydrothermal cell. The conductive unit continues southwards through the present area of study.

CONTENTS

Figures

TABLES

CHAPTER 1

INTRODUCTION

1.1 General Introduction

The present study evaluates the electrical resistivity structure of the area between the Olkaria geothermal field and Mt. Suswa. It is located in the rift floor in the central part of the Kenya Rift Valley. Suswa Market, which is about 85 km from Nairobi, lies on the eastern boundary of the study area. The study area extends for 225 square kilometres, and is bounded by latitudes $36^{\circ}\ 14'$ and $36^{\circ}20'$ east and longitudes $1^{\circ}05'$ south.

This section of the Rift Valley is one of the priority areas for the exploration of geothermal resources which if found would supplement Kenya's annual energy demand. The other priority areas are Eburru and Menengai. Presently the Olkaria geothermal field produces about 45 MW of electricity. Possible sites for further development at Olkaria are to the south and west of the exploited field. The nearby Eburru field is currently being explored.

The area of this study lies to the west of the Suswa-Longonot area in which the United Nations Development Programme (UNDP) undertook electrical resistivity soundings and gravity measurements in the period between April and July 1987. This UNDP project involved a total of 140 electrical resistivity soundings (E.S.) and 120 gravity stations with a spacing of 500m in an area covering approximately 900 square kilometres.

However, at the end of the UNDP project, there were very few electrical resistivity soundings to the south and west of the Olkaria geothermal field. After a reconnaissance survey of the area and familiarisation with the field equipment while on attachment to the project in early July 1987, the author started collecting data towards the end of July 1987. The Ministry of Energy provided logistical assistance with transport and labour.

The present study was carried out with the following objectives.

a) To establish the southern and western extent of the Olkaria geothermal field based on electrical resistivity structural analysis.

b) To establish the southern extent of the structural discontinuities observed in Olkaria.

c) To establish the western extent of the Suswa-Longonot low resistivity anomaly observed on the field resistivity curves from the UNDP project

i) To map the electrical "basement" which is estimated to be at a depth of 2-4 km and to evaluate possible fluid flow patterns.

Although the E.S. studies are expected to give an insight into the geothermal potential of this region, a thorough evaluation involves the integration of several methods including geochemistry, gravity, electromagnetics, seismics and magnetotellurics. Such integrated studies have not yet been used because of lack of equipment and funds. In view of these limitations, the resistivity method was chosen because of the availability of equipment; also it gives a good structural analysis based on the electrical properties of the rocks. The method can effectively delineate areas of geothermal potential associated with low sub-surface resistivities.

1.2 Physiography, Land Use and Communication

This region has topographic features ranging from plains, volcanic cones and domes. The most noticeable of these are the hilly Olkaria region to the north, the Njorowa gorge to the east, the Mau fault scarps to the west and Mt. Suswa to the south. The plains are relatively flat but they are occasionally interrupted by volcanic cones and domes. The hilly Olkaria region rises to more than 1680 m above sea level with the highest point above 2420m (Olkaria volcano). The hilly region (Plate 1) has been subjected to deep gully erosion. This makes the region highly inaccessible for electrical resistivity soundings

(Plate 1, 2 and 3). The drainage pattern is mostly parallel to the rift axis where seasonal streams have contributed to the gully erosion.

Most of the region receives poor rainfall for the greater part of the year. The heaviest rainfall is during the months of April and May and is usually concentrated in the highlands to the west. Due to the limited amount of rainfall, the people who live here are mainly pastoralists and keep large herds of cattle on group ranches. The ranches in the plains are covered by thorny bushes. The Olkaria region is covered by thick bushes (plate 4) which are sometimes inhabited by wild animals (plate 5).

The area can easily be reached through the Nairobi-Narok tarmac road which passes through the southern part. Within the study area, communication is rather poor especially to the south of the geothermal field where motorable tracks have turned into gullies. Most areas on the plains can be reached by driving on tracks or on the grassland during the dry season. This calls for strong four-wheel drive vehicles.

1.3 Geological Setting

The area is part of the presently tectonically active East African Rift System. It is a Miocene to Recent Rift which is regarded as representing an early stage of continental break up (Baker, et al. 1972). The Rift

Valley is characterised by an upwelling asthenosphere and it has a high thermal gradient. The Rift Valley has a general north-south trend and it is infilled by volcanic rocks associated with Quarternary Volcanism. The geology of parts of this region has been described by various authors (Thompson and Dodson 1963., Williams 1969, 1970., Saggerson 1970., Naylor 1972, Lagatchev et al. 1972., Woodhall 1987). The rocks are basically either of igneous origin or their reworked derivatives. The oldest rocks consist of a thick series of Miocene basaltic and phonolitic lavas which are covered by welded pyroclastics. These outcrop on the rift flanks to the west of Mt. Suswa and to the east of Mt. Longonot. Apart from the volcanic cones, domes and the Recent Ololbutot fault lava flow, bedrock exposures are rare. The rocks are covered by a series of pyroclastic material erupted form the Suswa and Longonot calderas.

Volcanic rocks are represented by phonolites, basalts, trachytes, commendites, rhyolites and pumiceous obsidians. Apart from the pumiceous obsidians, the other rocks are of Pleistocene age. The phonolite sequence which overlies the "basement" thins out southwards (Williams 1970). Cuttings and cores from the wells in the Olkaria area show that the area is made up of 2600 m of trachytes and rhyolites inter-calated with minor basalts. Since there are no wells in the southern part of the geothermal field, it is difficult to establish such a sequence. The commendites occur as small plugs and north-south trending dykes in the Njorowa gorge. Basaltic and pumiceous rocks are vesicular and these could trap fluids in them if the vesicles are interconnected. The various rock units observed in the Olkaria region are attributed to various magma chambers and different episodes of volcanicity while the rocks around Mt. Suswa show an evolutionary trend with decreasing silica content so that there is a gradual change from the original trachytic lava to phonolitic lava. This variation has been attributed to differentiation (Torfason 1987). Pyroclastics include the Mau ashes and reworked volcanic or sub-aqueously deposited pyroclastics (Fig 1) from Longonot and Suswa calderas.

The sediments found in this region are a manifestation of depositional and sedimentological patterns of the Rift Valley. Climatic and physiographic conditions have a strong control on the overall mode of deposition. Most parts of this region are starved of clastic sediments so that sedimentation is indicative of a dry continental rift. Deposition is controlled by structural geometry and physiography. In most cases, the down-dip side of the fault scarps play an important role in the

Fig 1. Geological Map of Suswa-Olkaria and part of The Mau Escarpment

transportation of sediment facies. Fine grained volcanic ash is transported by fault controlled seasonal streams while fluvial sands are deposited onto the plains from the Olkaria region through gullies and the Njorowa gorge. Recent sediments include reworked and redeposited sands, gravels, pebbles, soils and boulders.

1.4 Structural Morphology

The structural features observed in the Kenyan Rift are associated with volcanism and the tectonic development of the Great Rift Valley. Active faulting began in Mid-Miocene and still continues at the present time. Although the chronology of faulting has not been determined conclusively, the oldest rift structures have been estimated to be of Mid-Tertiary with a major episode of faulting at 7 Ma (Baker 1986).

The Rift Valley is a symmetrical, thermally initiated rift with a north-south tectonic pattern that is related to various stages of rifting. The north-south trend is exemplified by N-S trending normal to oblique faults affecting the Miocene-Pliocene volcanics on the rift shoulders. However, on the plains which are covered by volcanic soils and pyroclastics, the tectonic pattern can only be inferred from alignments of volcanic vents, cones and domes. The internal fault pattern has been portrayed as a series of anatomising and bifurcating faults with short segmented cross structures (Baker 1985, 1963, McCall 1967).

The observed surface geothermal manifestations (fumaroles and steaming grounds) in the Olkaria region are aligned along NS trending fractures. Some of these fractures are continuations of fractures from the area around Lake Elementaita. The steaming grounds show surface alterations to clay minerals. This is also evident on fractures exposed in the Njorowa gorge. This would imply that the steam vents and fumaroles occur in areas where fractures reach near the surface. In Mt. Suswa region, the fumaroles are concentrated in the crater and along radial fractures.

1.5 Previous Work

Much geological and geophysical work has been carried out in the Rift Valley as a whole. This review deals mainly with the geophysical work carried out in the study area. Some of the geological work has already been cited in the description of the geological setting.

The earliest written description of the thermal springs and steaming vents in the Olkaria region was by Thompson (1983). Scott (1953) suggested that the steam originated from a juvenile source trapped beneath the rocks. These surface manifestations encouraged people to carry out geophysical investigations to establish the structure of this region with a view of evaluating its geothermal potential. Most of the previous geophysical work has been carried out in the area surrounding the geothermal field.

In 1968 the Balfour and Beatty Survey team made some Wenner soundings in Olkaria with a maximum current electrode spacing of 500 m. The interpretation of this survey was seriously limited by the fact that the source of the current had a very high frequency (Hochstein 1971). The result however showed that most of the Olkaria region had high resistivities in the sub-surface except for areas around the geothermal field that show resistivities decreasing with depth. From the results of the Balfour and Beatty survey, it was clear that there was a need to establish the lateral markers of the geothermal reservoir around Olkaria. Group Seven Inc (1972) carried out a direct current dipole mapping augmented by Schlumberger and electromagnetic soundings. This survey provided little information about the variation of resistivity with depth. The dipole soundings were however useful in delineating the major lateral changes around Olkaria (Banwell 1972., Keller 1972). Meidav (1972) analysed the work by Group Seven Inc and found out that the roving dipole resistivity survey showed high resistivities along steaming grounds and that the vertical electrical soundings could be grouped into two types. The first type is in areas of steaming ground characterised by low to intermediate resistivity (10-30 Ωm) for surface layers, low to very low resistivity for layers between 50-300m depths and high resistivity for layers between depths of 300 - 1000 m. The second type of curves is encountered in areas away from the steaming regions where the surface layer has very high resistivities attributed to superheating of water or conversion into steam. It was concluded that H type curves ($\rho_1 > \rho_2 < \rho_3$) were characteristic of areas with a rapid increase in temperature while the surrounding areas would be characterised by Q-type curves. To test these hypotheses a set of closely spaced soundings were recommended to be carried out in areas of known thermal manifestations. The above resistivity studies were augmented by the magnetic survey since hydrothermal alterations cause magnetic minerals to change into non-magnetic ones. These magnetic studies helped in mapping out possible electrically conducting zones which might be due to permeable formations containing hot waters and those due to alterations of volcanic rocks (McEuen 1970., Duprat 1970).

Furgerson (1972) carried out an electrical resistivity survey in the northern section of this area. The soundings had a maximum current electrode spacing (AB) of 5400 metres. The survey showed that the Olkaria field could be divided into two areas by a NNE-SSW discontinuity and that the depth to the basement is much greater to the west of this discontinuity than to the east. The southern extent of this discontinuity was not established but it was noted however that the Olkaria region has high resistivities at the surface with the southern and eastern parts showing favourable geothermal targets.

Further understanding of the structural set up of Olkaria was contributed by Naylor (1972) who postulated that the region is a remnant of a large ring structure which was later infilled by thick flows of commendite followed by large quantities of rhyolitic pyroclastics. This ring structure was later cut by fractures along which pumice cones and bedded lavas erupted. Seismic refraction studies (Hamilton et al, 1973) were carried out to establish the stratigraphy (Table 1). The study underestimated the thickness of the rhyolitic-trachytic sequence which has been estimated at about 2600m from cores and cuttings. It has been postulated from gravity and resistivity surveys (Skinner 1977) that a deep heat source at about 2.5 km depth exists along the axis of the rift where the mantle derived intrusion coincides with the depth of the crystalline basement. Bhogal (1978) carried out further investigations using the polar-dipole method and recommended that further work should be carried out to establish the southern extent of the Olkaria geothermal field. He estimated the width of the Olkaria field to be about 8km with a source depth 3-4 km.

DEPTH/km	p velocity/km s^{-1}	inferred rock units
0.00 - 0.40	3.22	rhyolitic volcanics
0.40 - 1.68	3.80	trachytic volcanic
1.68 - 3.50	5.00	phonolitic volcanics
>3.50 -	6.38	basement system

Table 1. Depths and velocity of P waves in the inferred rock units (After Hamilton et al, 1973)

field to be about 8km with a source depth of 3 - 4 km.

The gravity survey of the shallow crust beneath Olkaria (Ndombi 1981) suggested a three-layered horizontal volcanic sequence overlying the "basement" system. This sequence was found to be downfaulted on the western part of Olkaria and is intruded by denser dyke-like material of rhyolitic composition. The survey also noted a prominent N-S gravity high to the north-west of the Oloserian dome. However the southern extent of this gravity high was not delineated.
In an attempt to establish the structural pattern of the floor of the rift valley, the Kenya Rift International Seismic (KRISP 85) carried out both E-W and N-S refraction profiling. Part of these profiles covered the southern end of the area of the present study. The E-W profile did not yield good results. This was attributed to a thick pyroclastic cover. Nevertheless a 2-dimensional velocity structure for the rift axis was proposed with a thickening of the crust between Mt. Suswa and Lake Elementaita (Khan et al, 1987).

Further work in Olkaria using electrical resistivity soundings has not established the boundaries of the field (Mwangi 1986). Geovolcanological, geochemical and hydrogeological projects have been carried out in the Suswa-Longonot-Olkaria region to augment the geophysical data (Torfason 1987; Woodhall 1987; Clarke 1987). The geochemical studies proposed the existence of two geothermal reservoirs while soil gas surveys have identified an anomalous zone between Njorowa gorge ad Mt Suswa which coincides with a large positive gravity anomaly. It is probable that this anomalous zone extends into the present area of study. The difficulty of correlating the previous work with the present work is compounded by the fact that there are no wells drilled in the southern part of this region.

The geological and geophysical review reveals that the comprehensive synthesis of the available data is seriously limited by the structural evolution and geological complexity of the region due to the variation in faulting and volcanic episodes. Stratigraphic correlation is not well documented for the whole region. Furthermore, the geophysical surveys have not established the source of the geothermal manifestations and the boundaries of the geothermal field.

CHAPTER 2

THEORY OF THE METHOD

2.1 Introduction

The theory of the electrical resistivity method has been outlined in various texts (Grant and West 1965; Zohdy 1965; Keller and Frischknecht 1966; Bhatachyra and Patra 1968; Telford et al 1983). These authors have outlined the theories behind the practical use of the electrical resistivity method for geophysical prospecting.

The method identifies resistivities and thicknesses of rock formations. The resistivities of the rock formations depend on state, fluid content, porosity, permeability, temperature and degree of hydrothermal alteration.

The electrical resistivity method of sub-surface exploration involves the introduction of an artificial current through two current electrodes and measuring the potential difference (p.d) between two potential electrodes. The artificial current may be propagated in the sub-surface in three different ways. These are;

a) Ohmic propagation which is based Ohm's law.

b) electrolytic conduction where resistivity varies with the mobility, concentration and degree of dissociation of the ions, and c) dielectric conduction where the variation of the electric field produces a relative displacement of atomic electrons propagating the flow of current. The electric properties of earth materials and their modes of current conduction have been outlined extensively by Keller and Frischknecht (1966). In this study, ohmic propagation is assumed since the instruments used were designed to measure current and potential difference based on Ohm's law. To minimise the effects of the other modes of propagation low (up to 1 amp) dc current was used.

The Schlumberger array was used to determine the variations of resistivities with depth. The most important target of this survey is the location of zones of low resistivity that can be associated with geothermally altered and permeable formations, while the electrical "basement" and cap rock will generally be associated with high resistivities. In measuring the values of potential differences, the basic assumptions are that; the electric field between the potential electrodes remains constant during measurements and the earth layers are horizontal, homogeneous and isotropic so that resistivity is constant for any electrode arrangement. However, if the Sub-surface is not homogeneous and the electrode spacing is varied, the measured resistivity is not constant. It varies with the electrodes arrangement and is known as the apparent resistivity (ρa). This value is diagnostic of the resistivity of a zone near the electrode arrangement and depends on the potential and current distribution.

2.2 Potential and Current Distribution in the Earth

The potential difference (p.d) measured in electrical prospecting between any two specified points is created by a continuous current flow (I). If the earth was homogeneous and isotropic, the potential (v) due to a current electrode on the surface would be a function of resistivity (ρ) and the current. The depth of penetration of the current is increased by increasing the current electrode spacing.

The potential $V_{(r)}$ at a point on the surface a distance r from a single electrode is expressed as

$$V_{(r)} = I\rho/2\pi r \qquad 2.1$$

where r is the radius of the hemispherical shells due to equipotential surfaces (fig. 2.1a). The direction of current flow is perpendicular to the equipotential surfaces. For the case of two current electrodes (A and B) as used in this survey (Fig 2.2a), the potential at any nearby point on the surface of the earth is affected by both current electrodes. There is a distortion of equipotential lines between the two current electrodes (Fig. 2.1b). The net potential difference between the potential electrodes (M and N) can be obtained for a

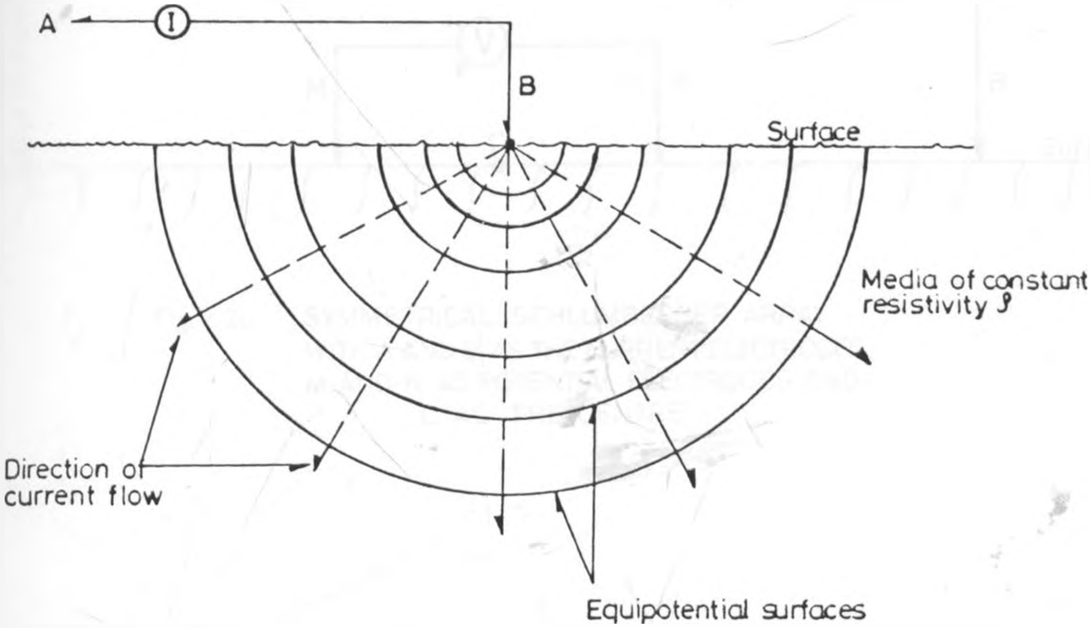

Fig 2.1a EQUIPOTENTIAL SURFACES AND THE DIRECTION OF CURRENT FLOW DUE TO A SINGLE CURRENT ELECTRODE ON THE SURFACE OF THE EARTH

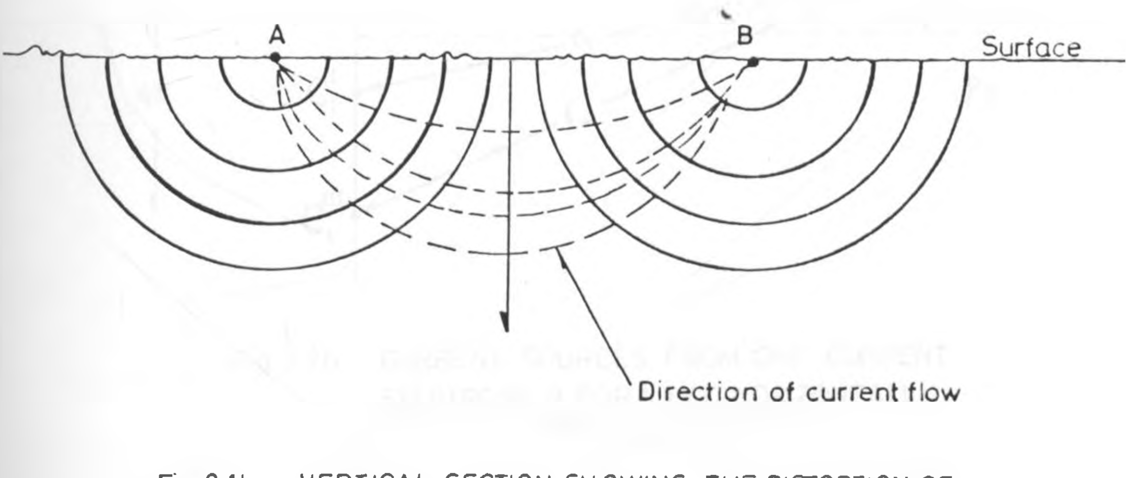

Fig. 2.1b VERTICAL SECTION SHOWING THE DISTORTION OF EQUIPOTENTIAL SURFACES AND DIRECTION OF CURRENT FLOW BETWEEN TWO CURRENT ELECTRODES

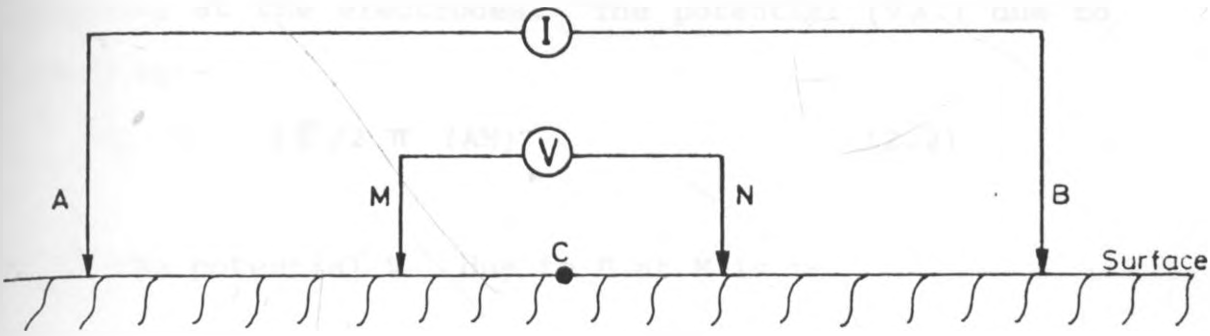

Fig.2 2a SYMMETRICAL SCHLUMBERGER ARRAY WITH A AND B AS THE CURRENT ELECTRODES, M AND N AS POTENTIAL ELECTRODES AND C AS THE CENTRE

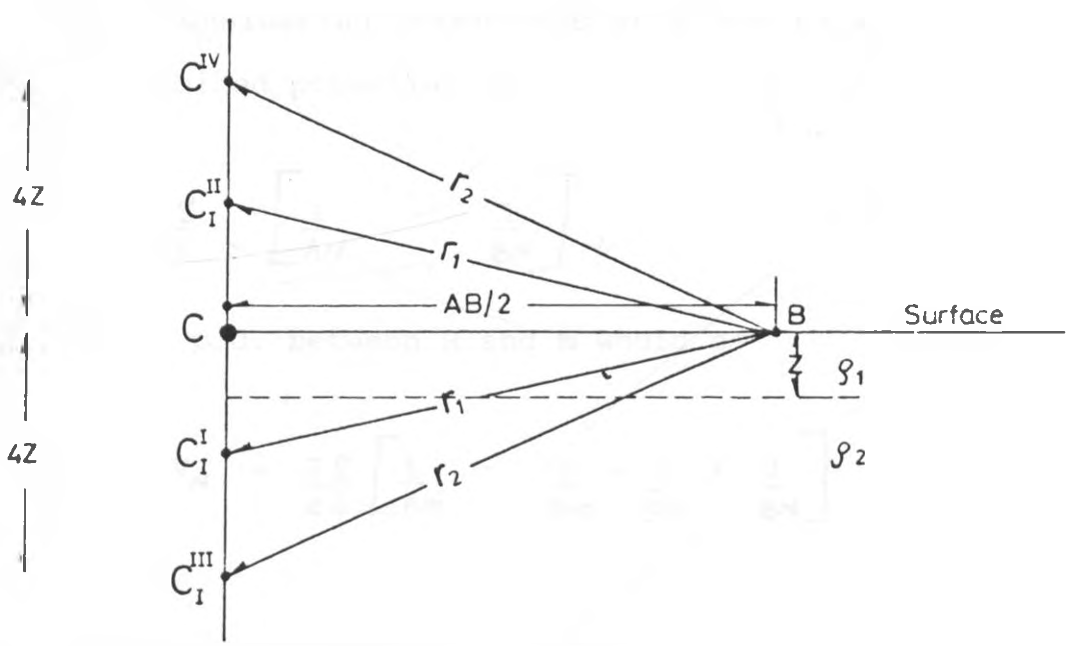

Fig. 2.2b CURRENT SOURCES FROM ONE CURRENT ELECTRODE B FOR A TWO HORIZONTALLY LAYERED MODEL

homogeneous earth by considering the distribution of the potential at the electrodes. The potential (V_A) due to A at M is:-

$$V_A = I\rho/2\pi(AM) \qquad (2.2)$$

while the potential V due to B at M is :-

$$V_B = -I\rho/2\pi(BM) \qquad (2.3)$$

Combining eqns 2.2 and 2.3, we obtain the total potential at M (V_m) as:-

$$V_m = V_A + V_B = \frac{I\rho}{2\pi}\left[\frac{1}{AM} - \frac{1}{Bm}\right] \qquad 2.4$$

Similarly, by considering potentials at N due to A and B we obtain a combined potential of

$$V_N = \frac{1\rho}{2\pi}\left[\frac{1}{AN} - \frac{1}{BN}\right] \qquad 2.5$$

The measurable p.d. between M and N would be

$$\text{p.d} = V_m - V_N = \frac{I\rho}{2\pi}\left[\frac{1}{Am} - \frac{1}{Bm} - \frac{1}{AN} + \frac{1}{BN}\right] \qquad 2.6$$

Eqn. 2.6 can be expressed as

$$\rho a = \frac{\Delta V}{I} \quad K$$

where $\Delta V = V_M - V_N$ and $K = \pi\left[\frac{AM.AN}{MN}\right]$ for the symmetrical array used.

Since the earth is made up of layers, the method of electric images is a better approximation of the potential distribution because it takes into account the effect of the layer parameters (Hummel 1932). The potential is obtained by the summation of the potential of a semi-Infinite medium of resistivity ρ_1 and the potential due to current sources C^{I}, C^{II}, C^{III}, C^{IV}, for two horizontal beds (Fig 2.2b). This can be extended to any number of layers. Stefanesco et al., (1930) established the fundamental equation for the distribution of potential around a point source of current on the surface of a layered earth as:

$$V_{(r)} = \frac{\rho_1 I}{2\pi}\left[\frac{1}{r} + 2r\int_{-\infty}^{\infty} B_1(\lambda, k, z)\, J_0(\lambda, r)\, d\lambda\right]$$

$$= \frac{I}{2\pi}\int_0^{\infty} T(\lambda)\, J_0(\lambda r)\, d\lambda \qquad 2.8$$

Where

λ = integration variable between 0 and .

Z = thickness of layer

J_0 = Bessel function of zero order

k = reflection coefficient of the resistivities

ρ_1 = resistivity of the first layer.

r = distance at which potential is considered

B_1 = Kernel function which contains all information on layering

$T(\lambda)$= resistivity transform function

For the Schlumberger array used, the apparent resistivity can be obtained from:

$$\rho_a = (AB/2)^2 \int_0^{\infty} T(\lambda) \; J_1(\lambda s) \, \lambda \, d\lambda \qquad 2.9$$

and

$$T(\lambda) = \rho_1 \left[(1 + 2B(\lambda)) \right] \qquad 2.10$$

Eqn. 2.8 is the basis of filter designs used in the computer analysis of electrical resistivity data (Appendix A). Koefoed (1968, 1970) developed methods of determining the kernel function and the resistivity transform function from the apparent resistivity curves. The quantitative results obtained for layer parameters depend on the types of resistivity curve.

The case of dipping beds is not considered in this study but it is worthwhile mentioning that dipping beds have the overall effect of reducing resistivity contrasts that would be inferred from single layer master curves. The dip of the beds is usually difficult to establish and could therefore give ambiguous results.

2.3 Types of Resistivity Curves

The various types of theoretical resistivity curve depend on the distribution of the resistivities in the subsurface. To illustrate this, three layer model curves are considered. The types of curve express the differences in the resistivity contrasts in the layers. There are four main types of curve but in practice a combination of these curves can be encountered. If the resistivities of the three layers are defined as ρ_1, ρ_2

and ρ_3 then the following types (Fig. 2.3) are defined.

i) <u>Minimum Types (H-type)</u> - $\rho_1 > \rho_2 < \rho_3$

Under these conditions for a linear symmetrical array, the flow of current is concentrated in the second layer.

ii) <u>Maximum type (K-type)</u> - $\rho_1 < \rho_2 > \rho_3$

The curve shows a clearly defined maximum due to the second layer being more resistive than the other two layers. In this case, depending on the electrode spacing, when ρ_3 is much less than ρ_1 then the current flow is concentrated in layer 3 and the lines of current flow are vertical in the second layer.

iii) <u>Ascending type (A-type)</u> - $\rho_1 < \rho_2 < \rho_3$

For this type of curve, the current flow is not primarily parallel to the stratification. If ρ_1 is highly conductive, the current flow is concentrated in the first layer resulting in an increase of pseudoresistivity and pseudothickness.

iv) <u>Descending Type (O-type)</u> - $\rho_1 > \rho_2 > \rho_3$

In this case, the presence of the conductive substratum results in the reduction of pseudoresistivity and thickness.

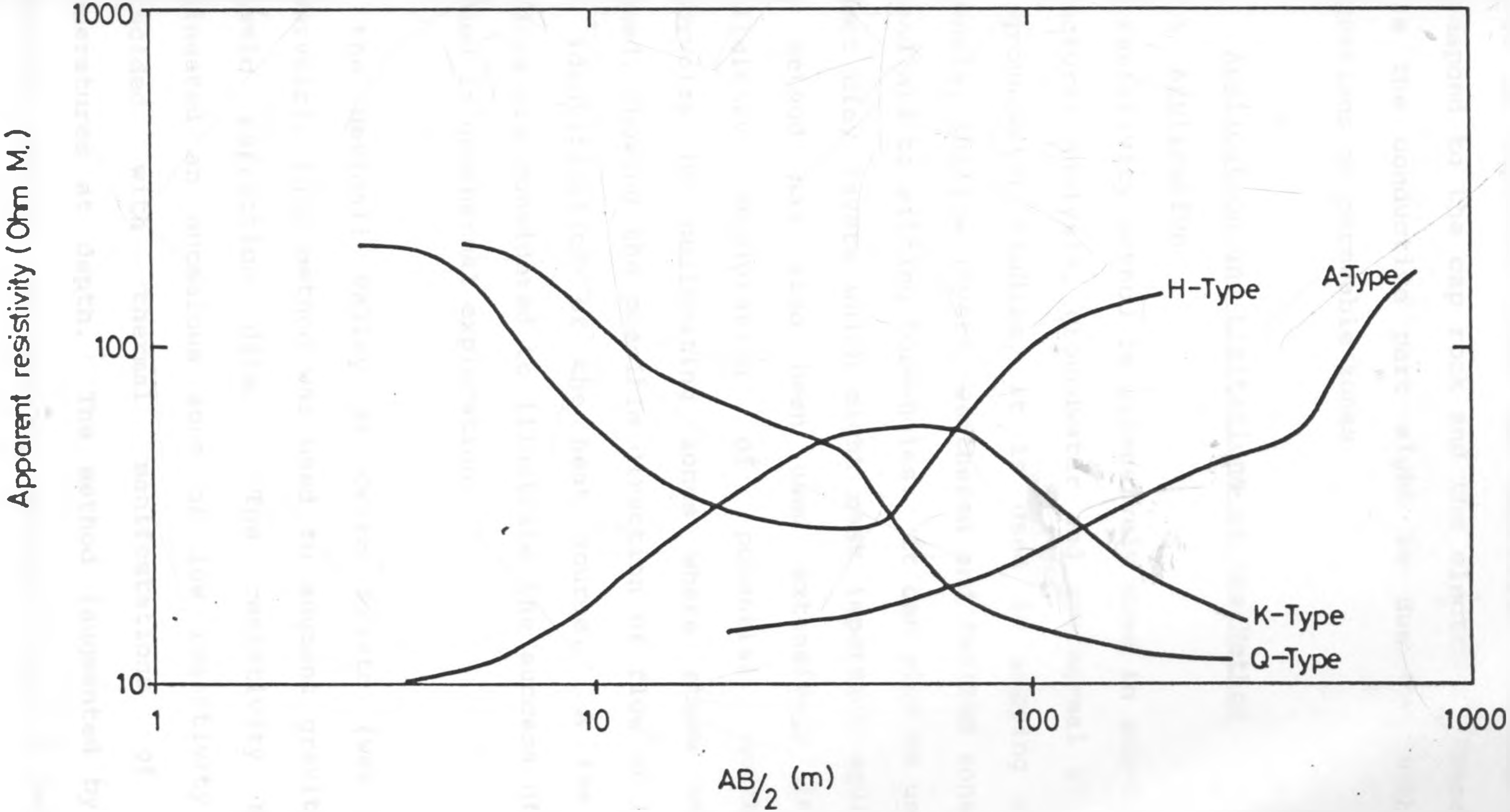

Fig 2.3 TYPES OF RESISTIVITY CURVES FOR A THREE LAYER EARTH MODEL

In the present survey, a combination of H and K type curves is expected since the resistive sections might correspond to the cap rock and the electrical "basement" while the conductive part might be due to geothermal alterations or permeable zones.

2.4 Application and Limitations of the Method

2.4.1 Application

The resistivity method is extensively used in sub-surface structural analysis, groundwater and geothermal studies. In groundwater studies, it is used in mapping stream channels, shallow layers, weathered and faulted zones and as and aid to sitting bore-holes. It can also be used to detect clay layers which might mask important aquifers. The method has also been used extensively in the preliminary exploration of potential geothermal reservoirs by delineating zones where steam can be tapped, showing the possible direction of flow of fluids and identification of the heat source. A few case studies are considered to illustrate the success of this method in geothermal exploration.

In the Mexicali Valley at Cerro Prieto (wet steam reservoir), this method was used to augment gravity and seismic refraction data. The resistivity method delineated an anomalous zone of low resistivity that coincided with thermal manifestations of high temperatures at depth. The method (augmented by very detailed magnetic and gravity studies) gave a detailed sub-structural picture concealed by pyroclastics and sediments (Goldstein et al., 1980). Detailed resistivity surveys were later carried out to give electrostratigraphic sections and the probable extent of the field. It was established that the low resistivity areas are zones of high porosity due to fracturing. However, Razo et al, (1980) considers this method as being ineffective for mapping the "basement" surface or other deeply buried resistive horizons.

In the Roosevelt hot springs, the resistivity surveys established a low resistivity zone parallel to a dome fault. The resistivity low was attributed to intense fracturing and water saturated rock formations with a resistive "basement" that is non-porous and unaltered. It was further established that the hot springs situated along faults delineated as vertical inhomogeneities. The method did not however resolve the complexity of the homogeneities (Tripp et al., 1978) and did not differentiate between clay conduction and fracture conduction effects. Other fields where resistivity surveys have been used successfully to delineate the depth and the possible extent of geothermal fields include the Wairakei-Taupo field and Broadlands in New Zealand (Risk et al., 1970; Banwell and MacDonald 1965; Hatherton et al: 1966), Larderello in Italy (Breusse and Mathiez 1956), Yellowstone National Park in U.S.A. (Zohdy et al; 1973), Java and Chile (Hochstein 1975a 1975b) and the Long Valley geothermal area, California (Stanley at al, 1976).

From the results of resistivity augmented by Magnetotelluric and other geophysical studies, a basic model of a geothermal steam field reservoir comprises a source of natural heat usually a Magmatic intrusion with temperature of 600-900^{o}C at a depth of 5 - 15 km, an aquifer or permeable reservoir rock and a cap rock which is a layer of rock with low permeability overlying the aquifer.

2.4.2 Limitations of the Method

Although the method has proved successful in establishing the general characteristics of the surface layers, there are serious limitations to the interpretation as a result of surface and structural inhomogeneities, topography, and the principles of equivalence and suppression. The principles of equivalence and suppression express the fact that different resistivity distributions may show the same apparent resistivity curve. Equivalence arises from the fact that all layers for which the product of thickness and resistivity is the same are electrically the same.

This means that thickness and resistivity cannot be determined uniquely. Suppression can arise in two different ways. Firstly, if the thickness of a given layer is very small compared to its depth, its effect on the apparent resistivity curve is not noticeable on the curve (i.e. it is suppressed). Secondly if a thin resistive layer is sandwiched between very conductive layers, its effect is not distinguishable on the apparent resistivity curve. This is also the case when a thin conductive layer is sandwiched between two resistive layers. The two principles might lead to the masking of important horizons and therefore give ambiguous interpretations.

Structural inhomogeneities that might limit the interpretation include surface and buried structures (dykes, shear zones, faults and veins). The effect of concealed sub-surface structures on the apparent resistivity curves might not be easily noticeable. For instance, the effect of a conducting sphere whose depth from the surface is much more than 1.5 times its radius cannot be detected on apparent resistivity curves (Van nastrand 1953). Structural inhomogeneities may arise from the anisotropic nature of the rock formation (anisotropy means that the properties of the rock formation are not uniform laterally and vertically). There are basically two types of anisotropy:- Micro and Macro anisotropies. Microanisotropy results from the anisotropy of the structures of individual grains in the rock so that the resistivity at any point can only be described by a tensor rather than a scalar function (Maillet 1947).

Macroanisotropy results from a formation containing several different facies (either isotropic or anisotropic) alternating regularly. The resistivity (or conductivity) varies both longitudinally and transversely. Both type of anisotropy are difficult to determine independently and in most cases they are superimposed to give the total anisotropy of the formation.

Potential difference measurements may include spurious electrochemical potentials between the current electrodes and electrolytes in the earth. This limitation is easily minimised by using non-polarizing electrodes, low frequency alternating current or reversing the directions of current flow to cancel out the effect of spurious potentials. There is no direct method of evaluating the effect of topography on the measured potential differences. Variations in the physical and geometrical patterns of surface formations cause variations in electric resistivities because of the variable moisture conditions, and the extent of weathering and erosion. The distortions obtained due to these effects can be corrected by smoothing the graphs. Sometimes the distortions portray false anomalies. Although limitations generally introduce ambiguities in the determination of layered parameters of the formations the electrical resistivity method offers a practical tool for sub-surface prospecting. This method is relatively fast and cheaper than most of the other geophysical methods.

CHAPTER 3

FIELD WORK

3.1 Introduction

The field work started in July and ended in early September 1987. The field camp for the project was at the Longonot Satellite Station which is about 70km from Nairobi along the Nairobi - Narok tarmac road. The working crew was composed of an average of 20 field assistants, four drivers and a game ranger. Four assistants were used at the centre for connecting the AB and MN lines and coordinating radio communication using Motorola radio sets. A minimum of four vehicles were used for transporting the field crew and equipment (Plate 6).

Most of the soundings had N-S azimuths. The density of the sounding stations is higher in the southern region where there is one "deep" sounding every 2 - 2.5 km. A total of 45 deep soundings cover the study area giving a coverage of one "deep" sounding every five square kilometres. Data acquisition was limited by poor radio communication, breakdown of vehicles and the inaccessibility of some areas especially in the hilly Olkaria region.

3.2 Field Equipment

3.2.1 Geo-Resistivity Meter GRM 3000

The GRM 3000 is a product of Geostudi of Italy. It is specially designed for deep electrical resistivity soundings and allows fast and accurate measurements even if field conditions are unfavourable, e.g. resistive soils, deep conductive layers and variable disturbing potentials. Unstable conditions in potential difference measurements are easily recognized on the meter by unstable deflections of the needle. Calibration errors are minimised by using the same meter for both current and potential difference measurements. Other advantages of the equipment include (a) the provision for minimising electrolytic polarisation effects due to unidirectional current by reversing the current in the AB electrodes (b) the elimination of spurious potentials using compensation circuits, and (c) possibility of measuring the electrode resistances to give an indication of the conditions at the electrodes. This last feature helps the control of data quality by the elimination of spurious measurements associated with the positioning of the electrodes.

The main disadvantages of the equipment are (a) the increased effect of disturbing potentials when the current electrode spacing is more than 6000 m (b) the risk of taking the reading in the wrong scale, and (c) the increased reading error in the higher scale. The various measurements and operations are carried out by the switches on the panel (Fig 3.1).

3.2.2. Transmitter

The transmitter was manufactured locally by Kenya Electronics. It is specially designed to give measurable potential differences at large AB spacings. It operates in the time domain in the range 50 - 500V. The maximum voltage used for this survey was 400V. Low voltages were used for small current electrodes spacing, while high voltages were used for AB spacing of more than 5000 m. The transmitter was powered by a 12 volt battery.

3.3 Resistivity Measurements

Resistivity measurements were carried out at predetermined sites to give maximum structural information for this region. The azimuths of most of the stations were N-S except in a few cases when this was limited by the terrain. The locations were plotted on a field map on a scale of 1:50,000 (Fig. 3.2 a and b). The electrodes were spaced along a straight line with potential electrodes placed at equal distances from the centre (C) - which was taken as the position for the stations (Plate 7). The AB spacing ranged from 6m to a maximum of 8000 m while MN spacing ranged from 1 to 250m. Before measuring the potential difference and the current, it was necessary to determine the resistances of the electrodes.

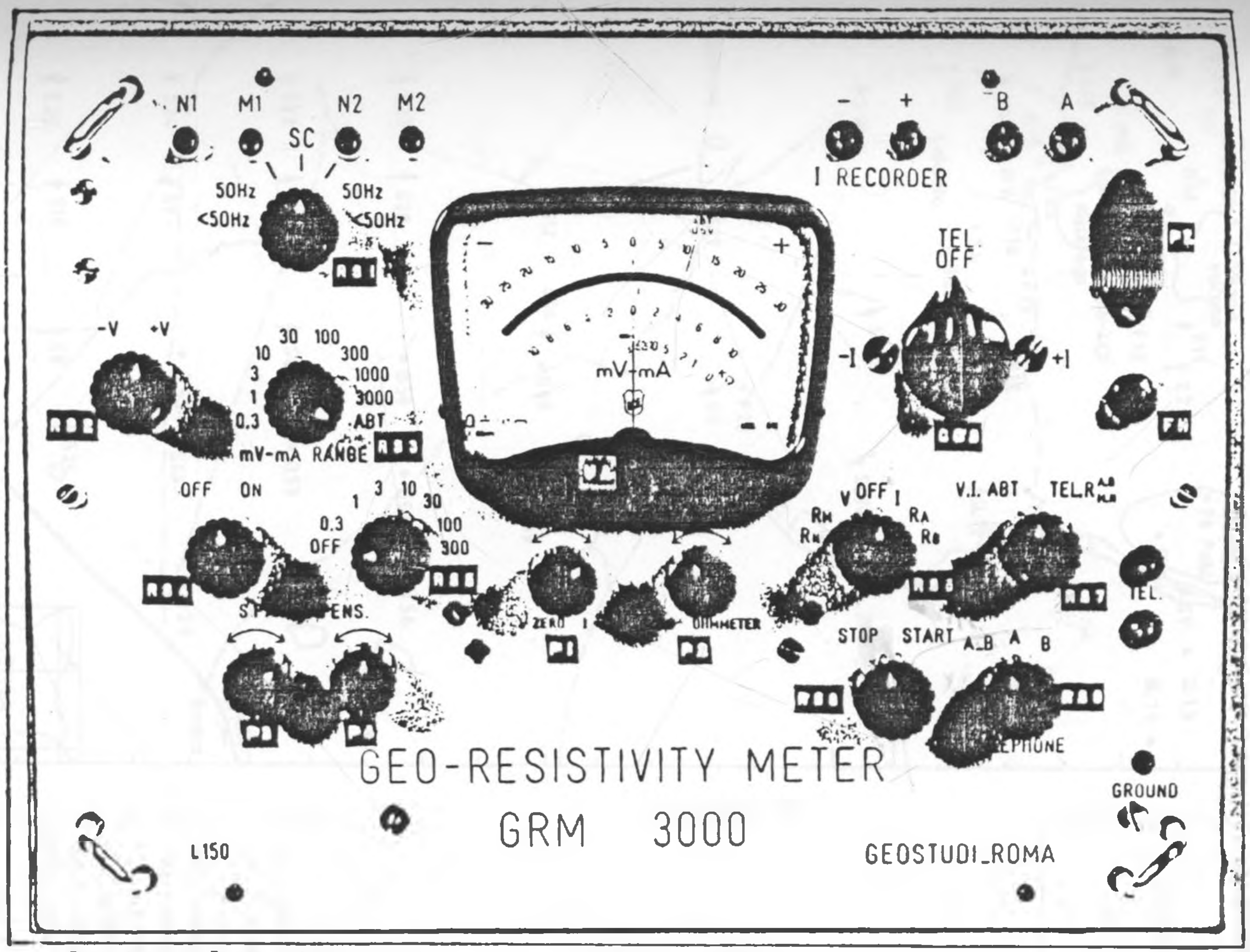

Fig. 3·1 Panel for operating the GRM 3000

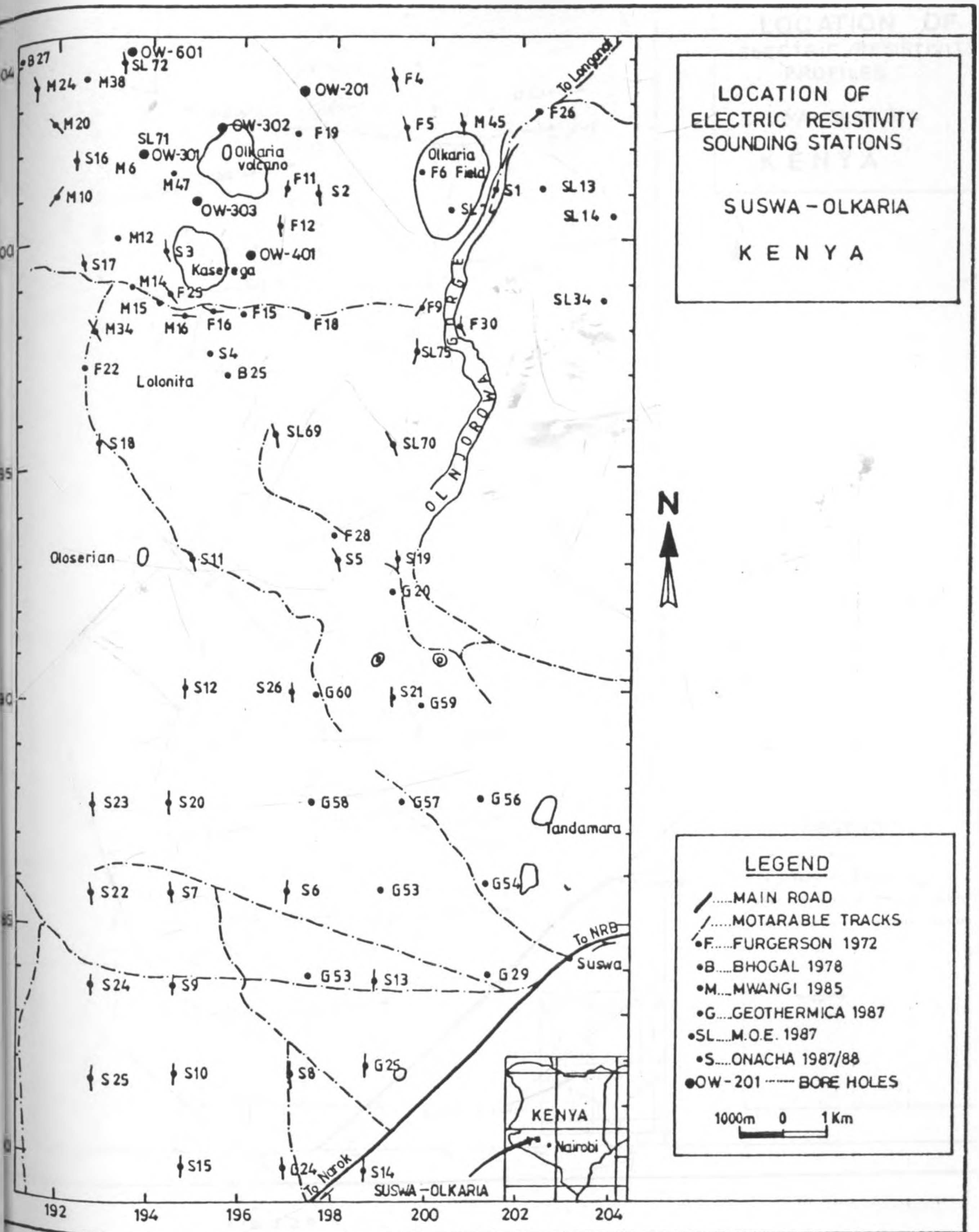
LOCATION OF
ELECTRIC RESISTIVITY
SOUNDING STATIONS
SUSWA – OLKARIA
K E N Y A
LEGEND
MAIN ROAD
MOTARABLE TRACKS
F.....FURGERSON 1972
B.....BHOGAL 1978
M.....MWANGI 1985
G.....GEOTHERMICA 1987
SL.....M.O.E. 1987
S.....ONACHA 1987/88
OW-201 BORE HOLES
1000m 0 1 Km
N
KENYA
Nairobi
SUSWA – OLKARIA
Olkaria volcano
Olkaria F6 Field
Kaserega
Lolonita
Oloserian
Tandamara
Suswa
To Longonot
To NRB
To Narok
OLNJOROWA GORGE
OW-601
OW-201
OW-302
OW-301
OW-303
OW-401
192
194
196
198
200
202
204

Fig. 3.2a

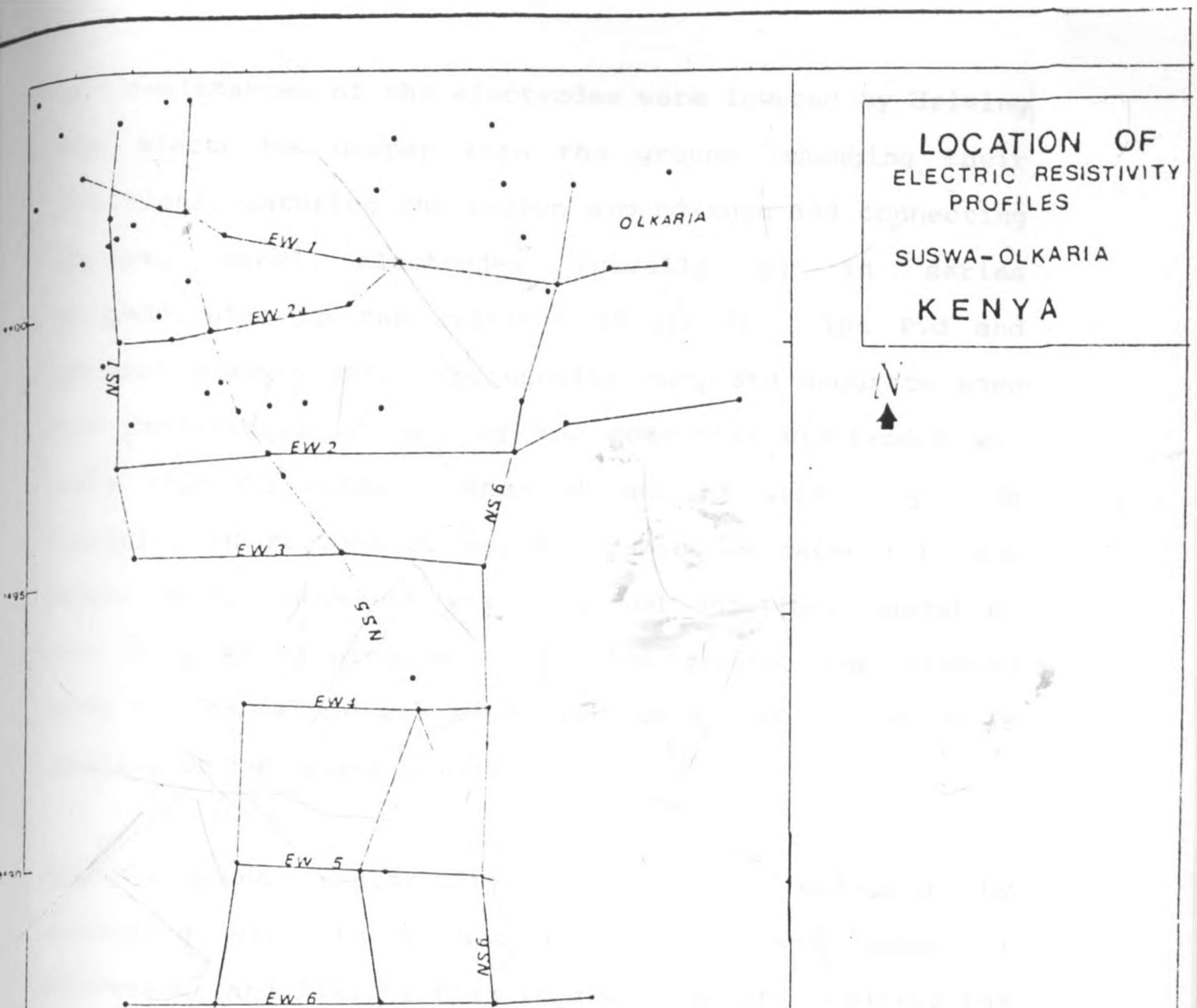
LOCATION OF
ELECTRIC RESISTIVITY
PROFILES
SUSWA-OLKARIA
KENYA
N
OLKARIA
EW 1
NS 1
EW 2
NS 6
EW 3
NS 5
EW 4
EW 5
NS 6
EW 6
NS 4
EW 7
NS 2
NS 3
EW8
EW 9
EW10
SUSWA
KENYA
SUSWA-OLKARIA
LEGEND
MAIN ROAD
SOUNDING STATION
NORTH-SOUTH PROFILE NUMBER
EAST-WEST PROFILE NUMBER

Fig. 3.2 b

The resistances of the electrodes were lowered by driving the electrodes deeper into the ground, changing their positions, watering the region around them and connecting several steel electrodes (usually 8) in series perpendicular to the azimuths (Plate 8). The P.d and current measurements were usually easy and accurate when the resistances of each of the potential electrodes was less than 15 KOhms. When RM and RN were very high (usually in regions of surface pumiceous material), the meter needle movement was slow and sometimes unstable. For long AB spacing on conductive ground, the slowing down of the needle was more noticeable than for short AB spacing on resistive ground.

The apparent resistivity values were obtained by measuring separate values of current and potential difference and filling them in a data sheet. Usually the current was measured first and then the P.d so that the current reading could be checked later to establish any change during P.d measurements. The current value was obtained by taking the average value for both readings on either side of the central zero.

Spontaneous potentials were compensated by using either RS4-P3 or RS5-P4. The coarse compensation circuit RS4-P3 was used when the P.d to be measured was over 30mv. (ie at small AB spacings.) RS5-P4 was used for longer AB spacings. For actual P.d measurements, two readings were enough for short AB spacing while at longer AB spacing and in the presence of variable spontaneous currents, various sets of six or more readings were used to calculate an average value. To check the validity of the average, an equal number of measurements with both polarities of the current was used.

3.4 Data Quality

Data quality depends among other factors on the instrumentation, field procedures and the properties of the rocks in the sub-surface. Some of the data used by the author is from the UNDP (1987), Furgerson (1972) and Mwangi (1986). The same equipment was used in the acquisition of data in the UNDP and the author's surveys. Data quality was mainly affected by errors due to reading of the meter, lateral inhomogeneities and in a few cases the presence of water pipes in the ground. At AB of more than 6000 m, the potential differences measured were usually small. In most cases they were less than 1 mV. The percentage scale reading error for the upper scale was 0.83%.

For perfectly symmetrical arrays, the apparent resistivity calculation has a combined error due to the readings of the P.d and current. The error due to reading the scale is only significant for long AB spacings when the potential differences to be measured are small. The calculated apparent resistivities can also be affected considerably if there is a significant offset from the proposed azimuths. In this case the most significant error would occur in determining the geometrical factor. To minimise this error, the offset was kept to within 30 metres from the azimuths. The maximum combined error in apparent resistivity measurement can be obtained from.

$$\delta\rho_a/\rho_a = (\delta V/V + \delta I/I + \delta MN/MN + \delta AB/AB) \qquad 3.1$$

where $\delta\rho_a$ = error in apparent resistivity

δV = error in potential difference measurement

δI = error in current measurement

δMN = error in MN

δAB = error in AB

The percentage error in apparent resistivity is obtained by the summation of the percentage errors in Eqn. 3.1. A conservative error of 100m for the longest AB/2 spacing and 5m for the longest MN/2 spacing have been used in this survey to give.

$$\delta\rho_a\ \% = (1 + 1 + 2.5 + 2) = 6.5\%.$$

The error due to lateral inhomogeneities caused by changes in lithology, presence of boulders and loose rock fragments are hard to determine. However, loose fragments tended to give high contact resistances of the electrodes. The effect of lateral inhomogeneities was controlled by taking readings at two different MN spacing for the same AB spacing. Spurious apparent resistivities significant error would occur in determining the geometrical factor. To minimise this error, the offset was kept to within 30 metres from the azimuths. The maximum combined error in apparent resistivity measurement can be obtained from.

$$\delta\rho_a/\rho_a = (\delta V/V + \delta I/I + \delta MN/MN + \delta AB/AB) \qquad 3.1$$

where $\delta\rho_a$ = error in apparent resistivity

δV = error in potential difference measurement

δI = error in current measurement

δMN = error in MN

δAB = error in AB

The percentage error in apparent resistivity is obtained by the summation of the percentage errors in Eqn. 3.1. A conservative error of 100m for the longest AB/2 spacing and 5m for the longest MN/2 spacing have been used in this survey to give.

$$\delta\rho_a\,\% = (1 + 1 + 2.5 + 2) = 6.5\%.$$

The error due to lateral inhomogeneities caused by changes in lithology, presence of boulders and loose rock fragments are hard to determine. However, loose fragments tended to give high contact resistances of the electrodes. The effect of lateral inhomogeneities was controlled by taking readings at two different MN spacing for the same AB spacing. Spurious apparent resistivities were represented as kinks on the field curves. In this case it was necessary to take one or two more readings and obtain an average value. Sometimes the kinks on the graphs were so sharp that it was difficult to establish their causes. For instance S11 (Fig 3.3a) shows a kink between AB/2 2000 and 4000m. It is difficult to determine whether its source is to the south or north of the station. In other places, apparent resistivity values were affected by the presence of pipes. A good example of this is at S19 (Fig 3.3b). Both 19A and B have a NS azimuth but are separated by a distance of 10m. The effect at S19A is attributed to MN/2=10m being located on a pipe and MN/2=40 between two pipes. The net effect is to give high apparent resistivities when the orientation of the pipes is away from the sounding station. This effect can be attributed to the current being concentrated in the conductive pipes so that a low current is recorded at the sounding station. If the pipes are concealed, the apparent resistivity obtained could erroneously be attributed to a resistive layer in the sub-stratum.

The quality of the data from previous surveys (mainly Furgerson 1972 and Mwangi 1986) is mainly considered in terms of the length of the soundings and the instrumentation deployed. Furgerson used a transmitter system which consisted of a 1.2 Kw, 240V a.c. and 60 Hz portable generator. The frequencies used in the survey varied between 0.1 and 0.0125 Hz. The apparent

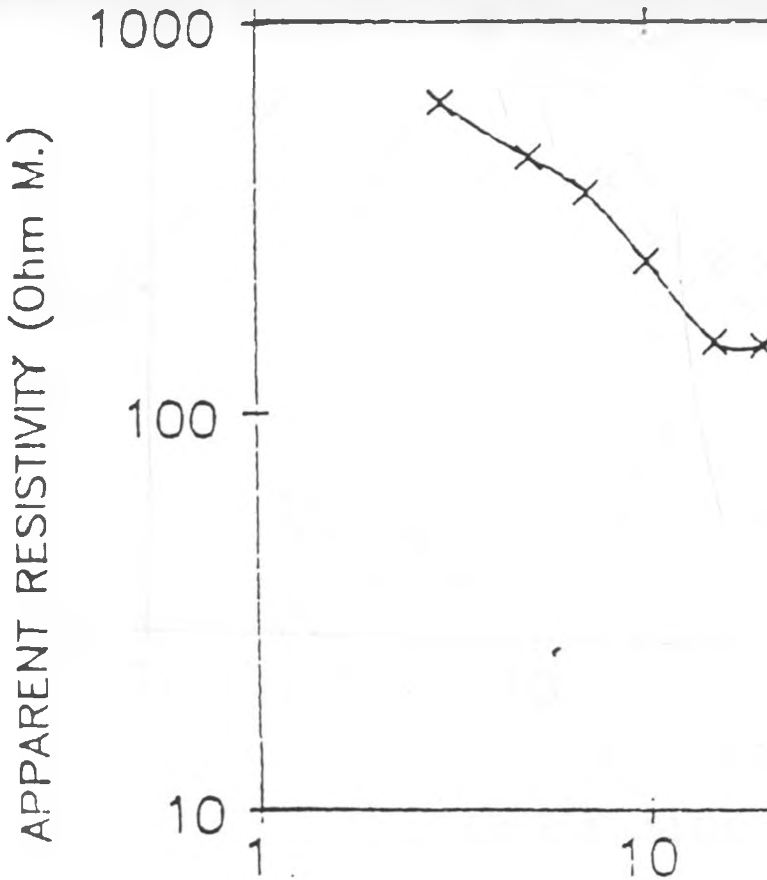

Fig. 3.3a

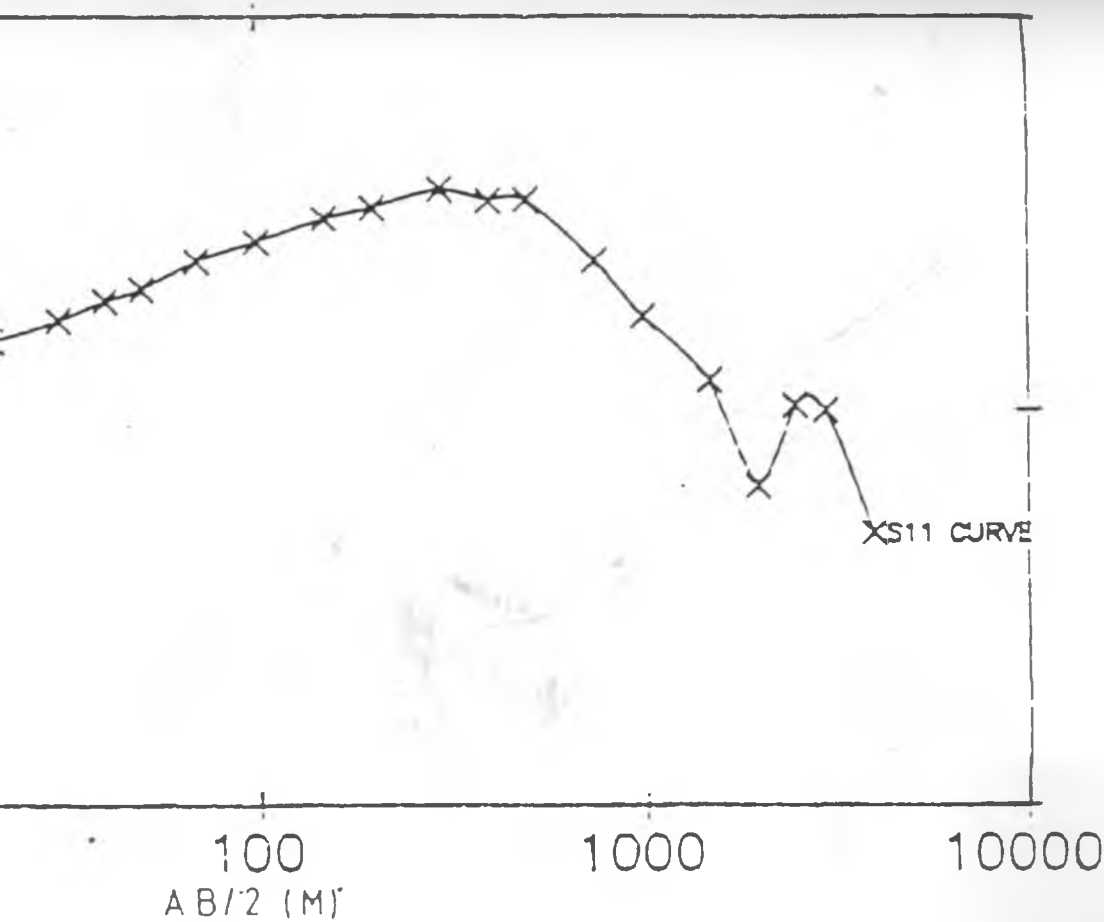

SITE S11 Apparent Resistivity Curve

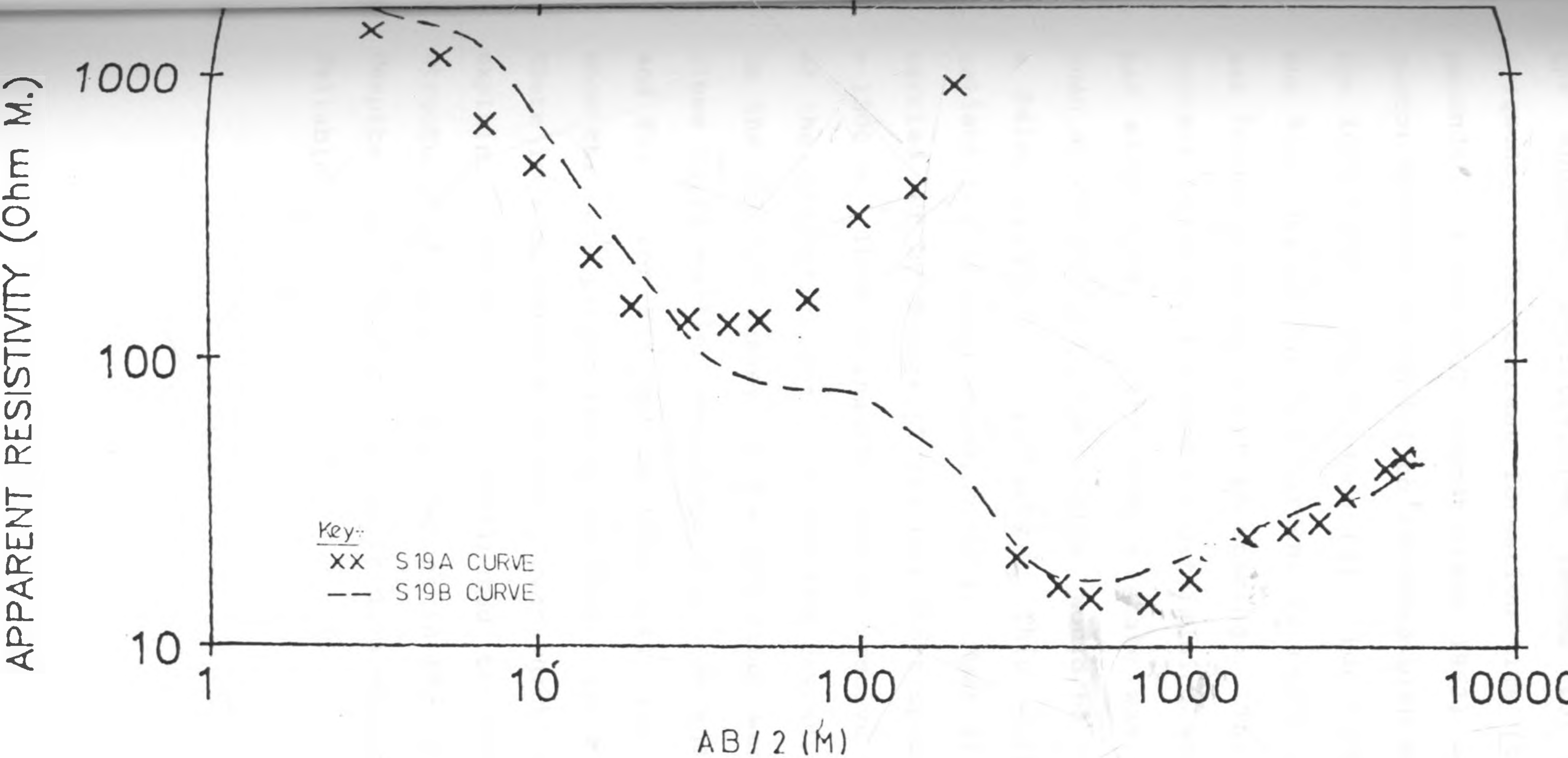

Fig. 3.3 b SITES S19A and B Apparent Resistivity Curves

resistivities measured were frequency dependent such that the apparent resistivities tended to increase with frequency. The current formation time (tc) defined in seconds = 1.99S.AB/2 (Verdrintsev 1963) was a limiting factor because it tended to increase with AB spacings and the longitudinal conductance (S). For long AB spacings, the time needed for the current to reach a stable state was longer than for short AB spacings. The values of the current recorded depended on determining when the current had stabilized. If the stable state was not attained, then an erroneous current value would be recorded giving a false apparent resistivity. This would reduce the reliability of long sounding data. Most of the soundings carried out by Mwangi (1986) had short spacings with AB/2 = 1300 m. This is insufficient to resolve the properties of the conductive horizons and the resistive substratum. In the present survey, a few soundings were carried out close these earlier soundings e.g. F28 and S5, and SL74 and F7. For F28 and S5 (Fig 3.4), the two soundings show the same properties up to AB/2 = 500 m. After 500 m there is a difference in the curves which is difficult to explain. It would be attributed to lateral changes, structural changes or differences in the instrumentation. Despite these limitations, their data quality is high and reliable.

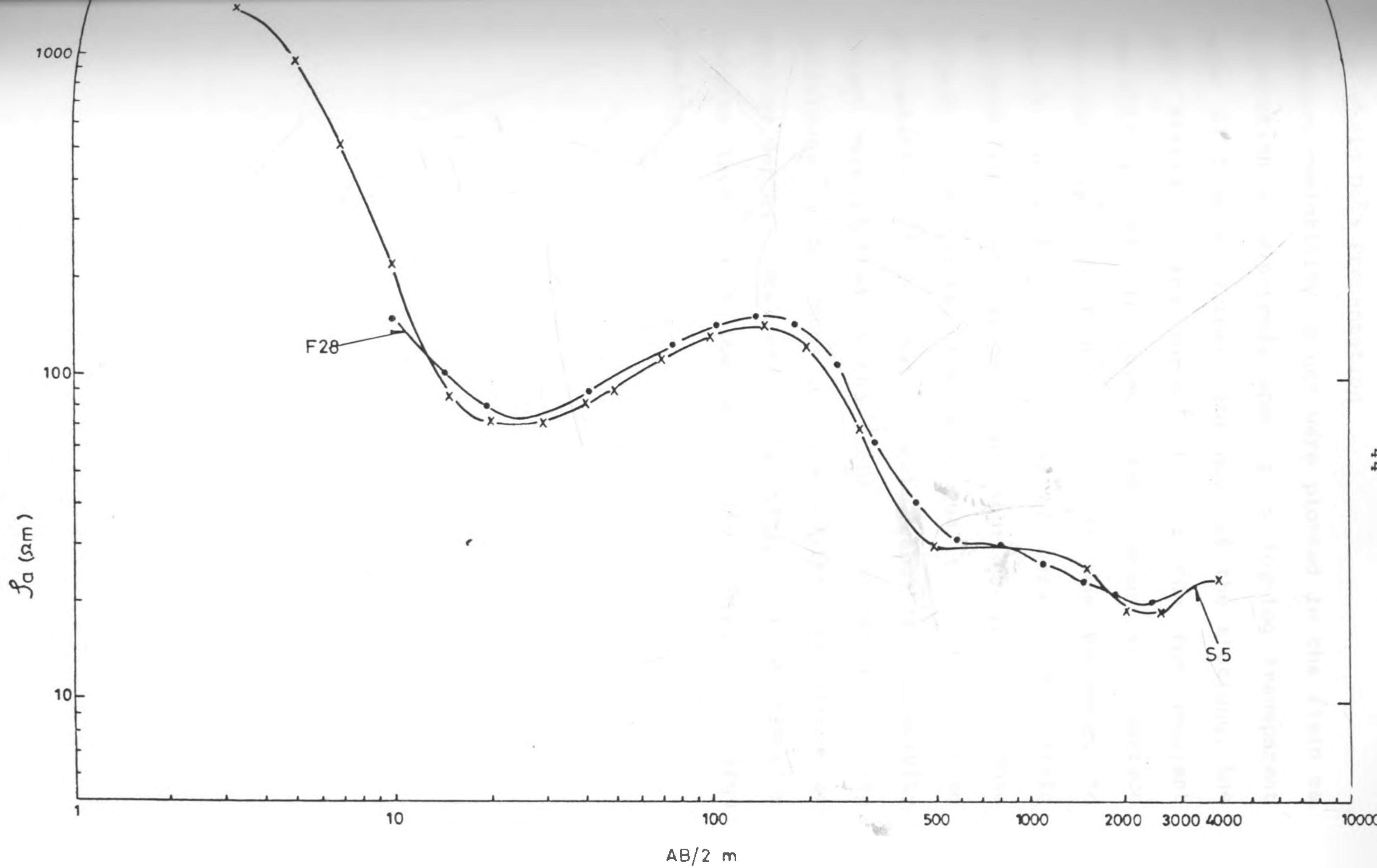

Fig. 3.4 APPARENT RESISTIVITY CURVES FOR F 28 AND S 5

3.5 Field Data Presentation

Apparent resistivity values were plotted in the field as a function of electrode spacing on log-log transparent paper of 3 by 4 cycles. For most of the stations, the data fitted in the range 1 - 1000Ωm for apparent resistivity but in some cases when the surface resistivities were high e.g S2, it was necessary to modify the scale. The plotting of data in the field allowed the determination of any spurious results. This helped in monitoring the data quality. The log-log presentation ensure that a wide rang of resistivity values were plotted in the field and enhanced both the variations in thickness and low resistivity values at shallow depths. However, it is difficult to distinguish between layers with low resistivity contrast at large depths.

CHAPTER 4

DATA ANALYSIS

4.1 Introduction

The aim of the data analysis is to determine true resistivities and thickness of the sub-surface layers so as to establish generalized structural and geological models. This chapter evaluates the electrical resistivity data. There are various methods of quantitative electrical resistivity data analysis. The approximate method uses theoretical curves (Campagnie Generale de Geophysique 1963; Mooney et al 1956; Orellana et al 1966; Rikwaterstaat 1979) in conjunction with the auxiliary point method (Zohdy 1965). The direct method (Slichter 1937; Pekeris 1940; Kunetz et al 1970; Marsden 1973; Bichara et al 1976 and Niwas et al 1987) determines layer parameters by fitting a theoretical kernel function to the observed field data. The iterative methods involve numerical computation of infinite integrals containing Bessel functions. In the later case, iteration can either be carried out in the apparent resistivity domain (Inman et al 1973, Johansen 1977) or in the kernel domain. In determining layer parameters, linear filter coefficients (Ghosh 1971a, 1971b, Nyman et al 1977; Anderson 1979, O'Neill 1975, O'Neill et al 194) are used in successive iterations because of their high accuracy, flexibility and the high speed at which they may be computed. An outline of the derivation of the filter coefficients used is given in appendix A.

A brief outline of the analysis procedures used in this study is given below but their detailed mathematical derivation is not discussed. In this chapter, qualitative and quantitative comparison of the results of the procedures used is also given.

4.2 Qualitative Analysis

The qualitative analysis was carried out to gain an insight into the general characteristics of the study area. It mainly involved the study of the types of sounding curve drawn on the same axes for each profile and noting their areal distribution. Visual inspection of the types of curve gave the minimum number of layers and possible discontinuities to be found along the profiles. The ρ_a curves show a combination of all the types of theoretical curves described in Chapter 2. Most of them are smooth and indicate the presence of discernible resistivity and thickness contrasts. From visual inspection of the ρ_a curves, it was possible to group them into six types as described below.

(i) Type 1 curves are mainly encountered in the Olkaria region. These show one clearly defined conductive layer (C1) at apparent depths of less than 1000 m e.g. SL 74 (Fig 4.1a). There are distortions on the

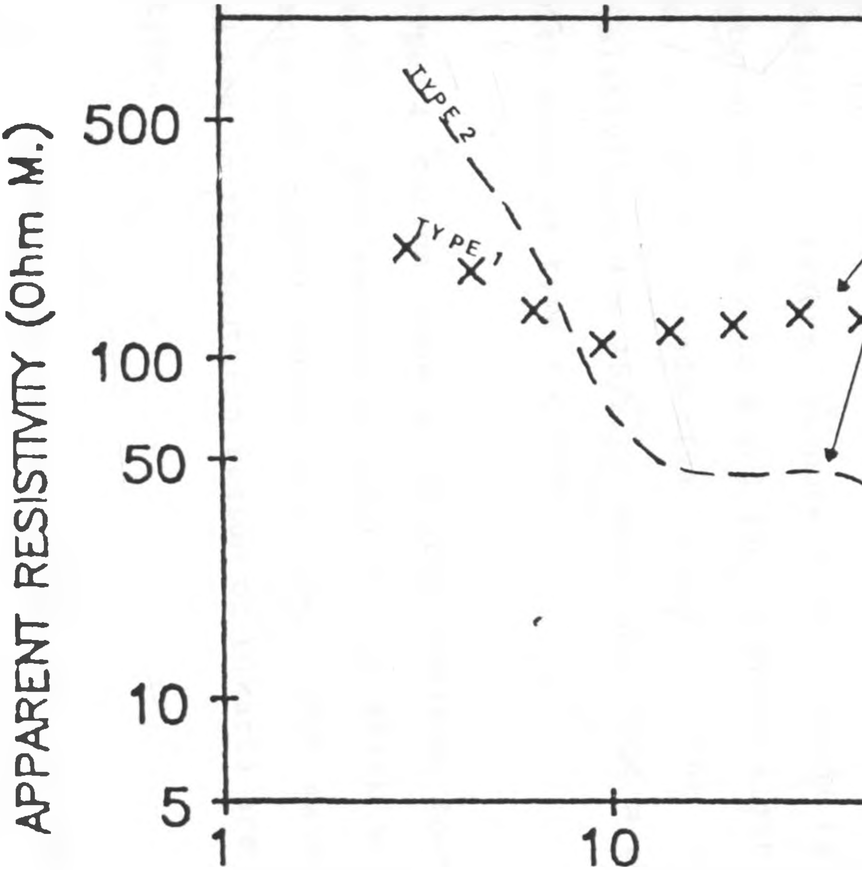

Fig 4.1a Type

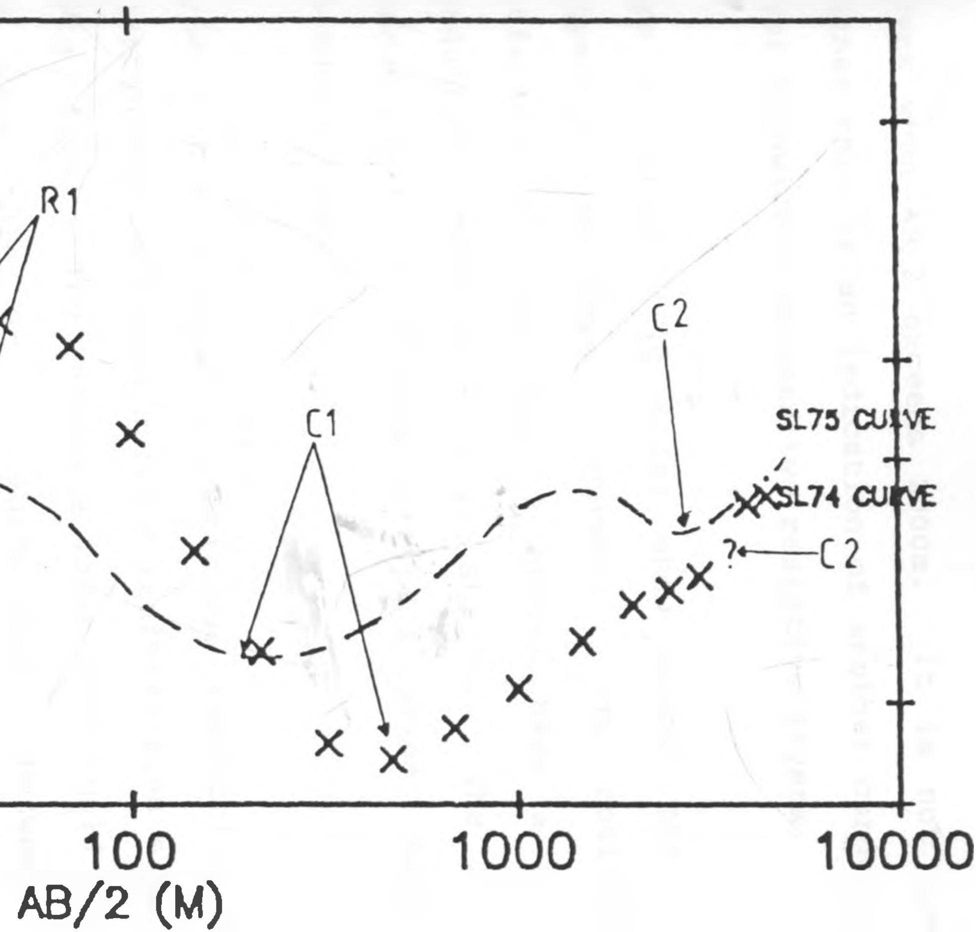

1 and 2 Apparent Resistivity Curves.

curves when AB/2 exceeds 2000m. It is not clear whether this is an indication of another conductive layer sandwiched between two resistive layers.

ii) Type 2 curves (Fig 4.1a) show almost the same properties as type 1 curves. the noticeable difference is that type 2 curves have a second conductive layer (C2) e.g. SL 75. The second conductive layer in areas of type 1 curves might be much deeper.

iii) Type 3 curves show a continuous conductive sub-stratum and very high surface resistivities e.g. S19 (Fig 4.1b). The resistive layer (R1) could either be very thin or sandwiched between two conductive layers (suppression). There is a cusp between AB/2 at 2500 m and 4000 m which might be due to a second conductive layer. The apparent resistivities for AB/2 of more than 2000 m coincide with those of type 4 curves.

iv) Type 4 curves show a clearly defined four layer model. The resistive layer R1 is thick with high apparent resistivities e.g. S8. The majority of curves in the southern region of Olkaria are of this type.

v) Type 5 curves are basically the same as type 4 but show a conductive layer (CR) within the

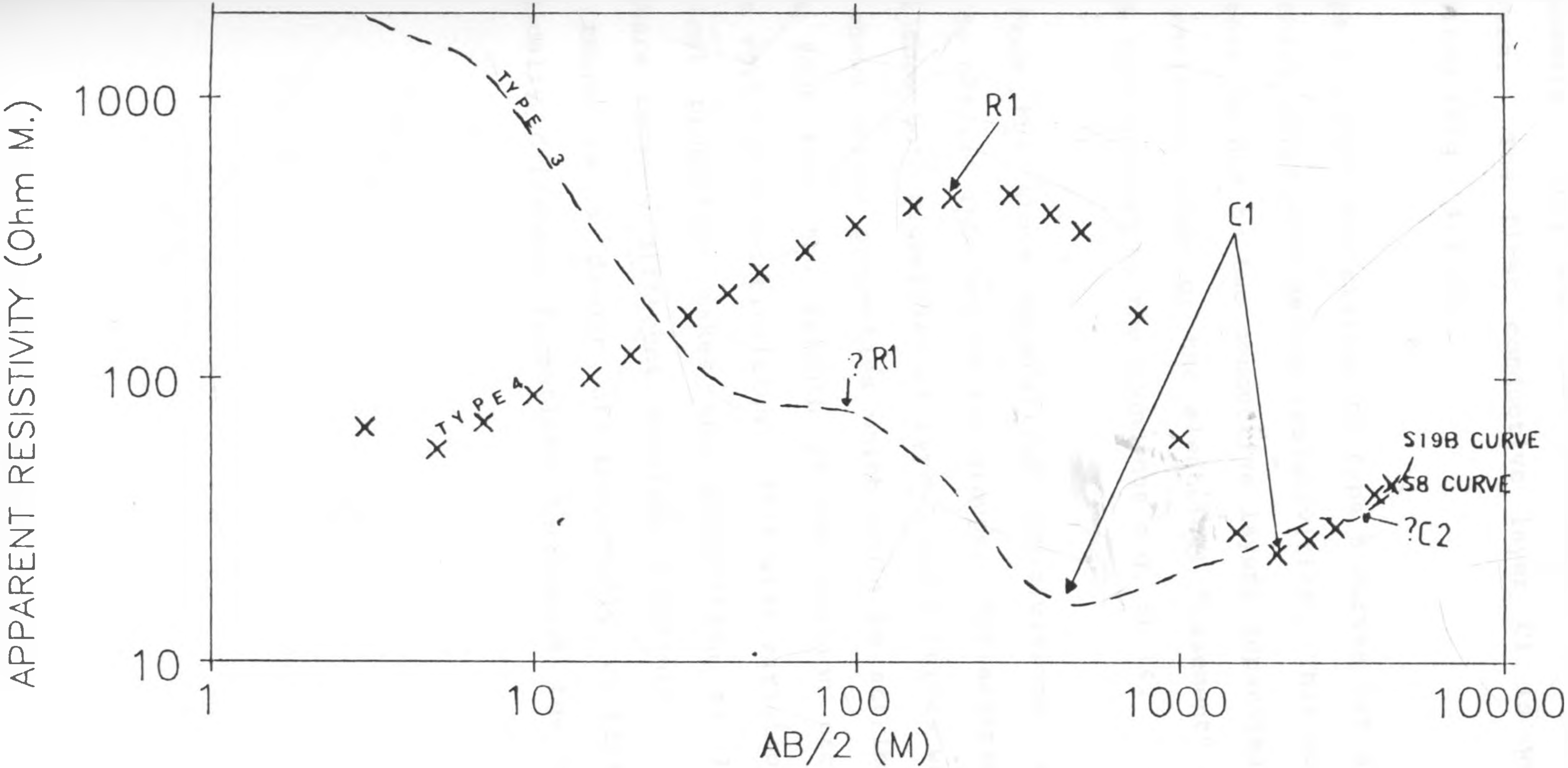

Fig. 4.1b Type 3 and 4 Apparent Resistivity Curves .

resistive layer R1. They are found to the west of Tandamara. They show some resemblance to type 2 curves. The first conductive layer C1 is well defined (Fig 4.1 c).

vi) Type 6 curves are similar to type 5 curves but show a thick layer with medium resistivities. This could either be due to two conductive layers separated by a resistive layer or the electrical "basement" has not been defined by the soundings e.g. SL 14.

Apart from the above generalized sub-divisions, some curves do not fit into any of the groups. For example S5 and S21 show both properties of type 3 and 4 curves while SL 69 shows unique properties which could be attributed to the fact that the azimuth of the station crosses various vertical discontinuities. This wide variation in electrical properties makes the correlation of layer parameters between different stations difficult. This means there is a danger of incorrectly correlating geologically different formations throughout the study area.

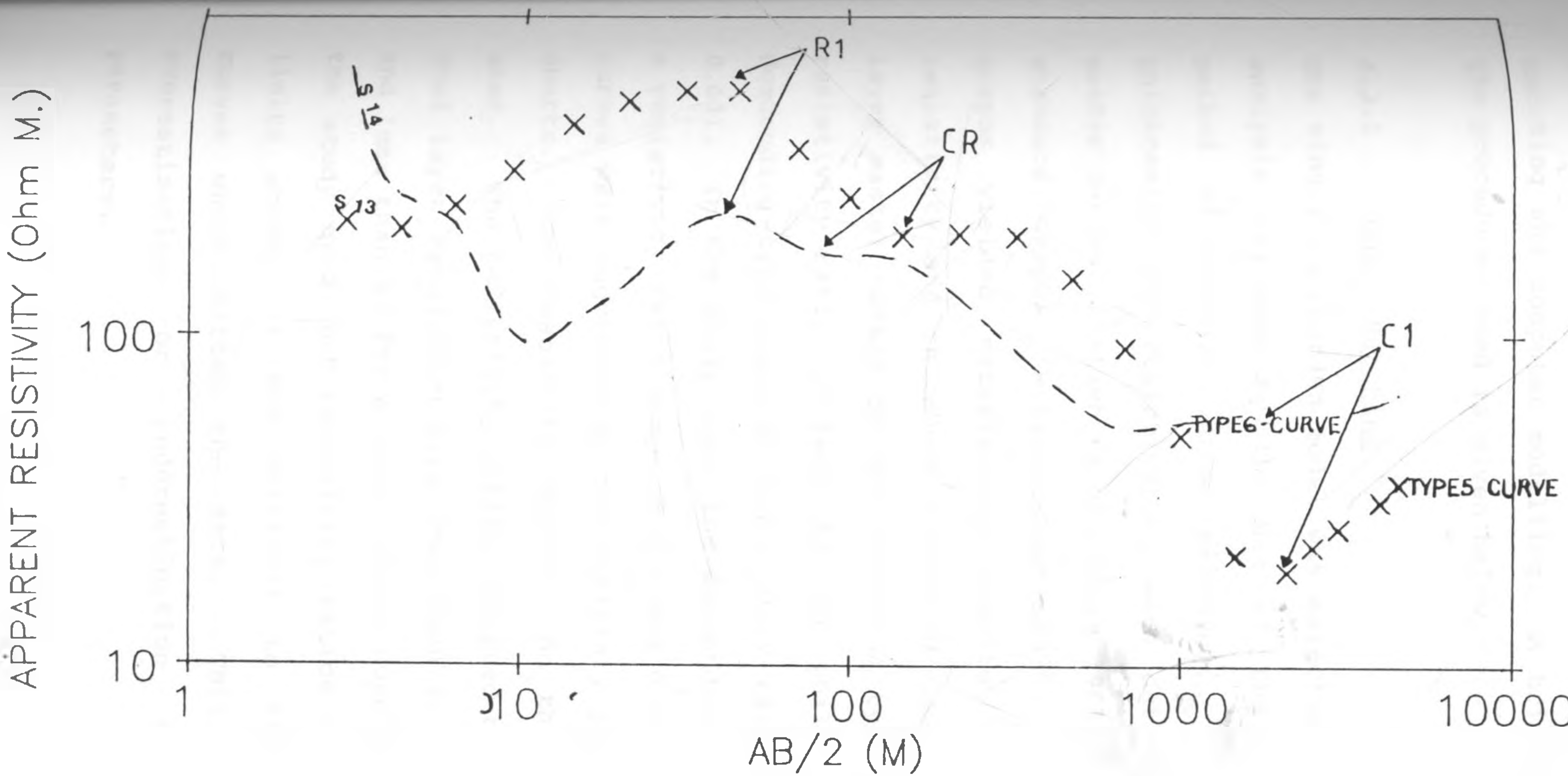

Fig. 4.1c Type 5 and 6 Apparent Resistivity Curves

4.3 Quantitative Analysis

The quantitative data analysis was carried out by curve matching and computer modelling. A brief description of the procedures used is given below.

4.3.1 Curve Matching

The single overburden model was selected as the basis of analysis followed by the use of the auxiliary point method of partial curve matching. The overburden thicknesses and resistivities were determined by using master curves (Bhatachyra and Patra 1968) supplemented by standard graphs (Rikwaterstaat 1979). The standard graphs yielded satisfactory results for layers with resistivity and thickness ratios of less than 25. Two layer master curves of the ascending type were used for resistivity ratios of less than 100 while the use of the descending type required resistivity ratios of more than 0.001. In the study area, the descending type curves had a resistivity ratio range of 0.1 and 0.026. These master curves were augmented by two auxiliary point (HA and KQ) charts. The resolution depended on the type of chart used. The resistivity ratios required by the charts for good layer resolution were less than 20 for the K type, and less than 40 for A type. Since some of the curves in the study area had resistivity ratios greater than the limits above, it was difficult to find satisfactory curves which fitted the data. This led to either overestimation or underestimation of the layer parameters.

A detailed description of the auxiliary point method is not given but briefly, it involves lumping together two or more homogeneous and isotropic layers to form a single anisotropic layer that is electrically equivalent to a homogeneous and isotropic layer. Details of this method are outlined by Zohdy (1965) who showed that the thickness determined by this method is greater than the true thickness by a factor of $(\rho_{\perp}/\rho_{p})$ where $\rho_{\perp}$ is the vertical resistivity and ρ_{p} the horizontal resistivity of the layer. The results of curve matching were used as the initial models for computer modelling.

4.3.2 Computer Modelling

The first step in computer modelling was the computation of O'Neill curves (Appendix C) using an M24 Ollivetti PC from the Ministry of Water Development (M.O.W.D.). The computation was based on Ghosh's convolution method using O'Neill filter coefficients (O'Neill 1975). The layer parameters were obtained by adjusting the parameters of the initial input model until calculated apparent resistivities fitted the field data. The surface layers were well resolved but there was a noticeable disagreement between the results obtained by curve matching and computer modelling for deeper layers. As expected the results of curve matching showed overestimation of thicknesses while resistivities were well resolved. This could be attributed to the fact that in curve matching a probing depth equal to AB/2 spacing is assumed. In practice, there is a decrease in current penetration to the deeper layers so that the apparent resistivities measured at large current electrode spacings are only representative of resistivity structures at shallower depths. On the other hand, at shallow depths probed by small electrode spacings, the effects of deeper layers are minimal so that the ratio of 1:1 for probing depths versus AB/2 current spacing is almost valid. The programme used for computing O'Neill curves has good resolution when there are appreciable contrasts in layer parameters e.g at S12 (Fig. 4.2). There is poor resolution when there are abrupt changes and small contrasts in the layer parameters with increasing depths e.g. SL 75 (Fig 4.3). This means that a "good fit" to the field data does not necessarily indicate an accurate determination of the layer parameters. The actual modelling for one curve took 20-60 minutes minutes while the computation of the curve took about 40 seconds. The thicknesses of the deeper layers obtained using the computer programme were appreciably less than those obtained by curve matching. Hence it is apparent that an effective probing depth of about half the AB/2 spacing was common for most of the data. Details of the programme are not available because of the copyright protection.

After computation of the O'Neill curves, it was necessary to assess the validity of the results by using a different programme. The first step was carried out by the programme "RESINV 88" (Resistivity Inversion 88) -

Resistivity model

Nr.	Depth(m)	Res.(ohmm)
1.	1.5	1000.0
2.	6.0	20.0
3.	230.0	315.0
4.	1450.0	13.0
5.	9999.0	110.0

S12

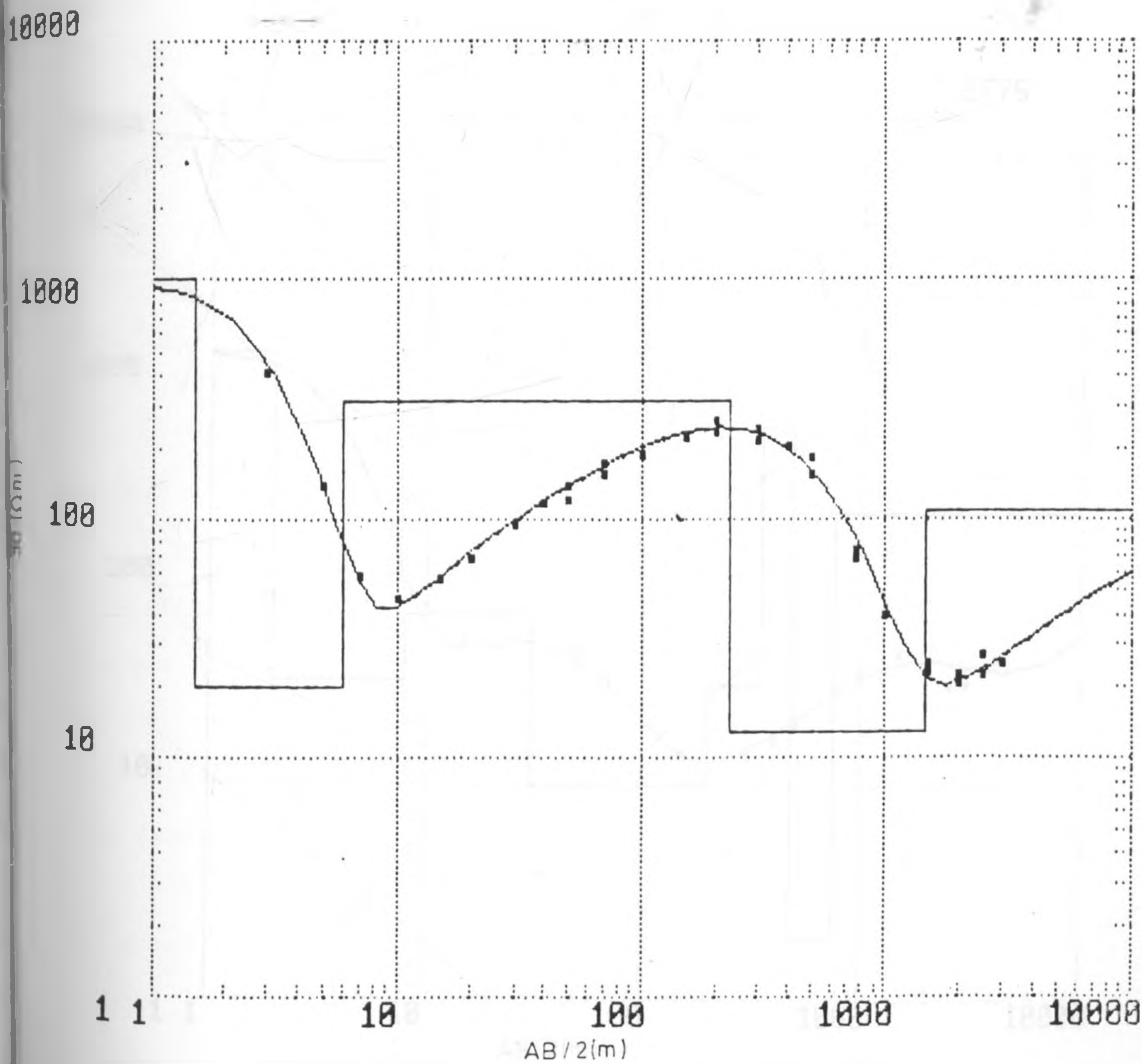

Fig. 4.2 O'neill curve fitting model for S12

Resistivity model

Nr.	Depth(m)	Res.(ohmm)
1.	2.0	1100.0
2.	8.0	32.0
3.	30.0	65.0
4.	200.0	10.0
5.	350.0	30.0
6.	480.0	500.0
7.	750.0	2.00
8.	9999.0	200.0

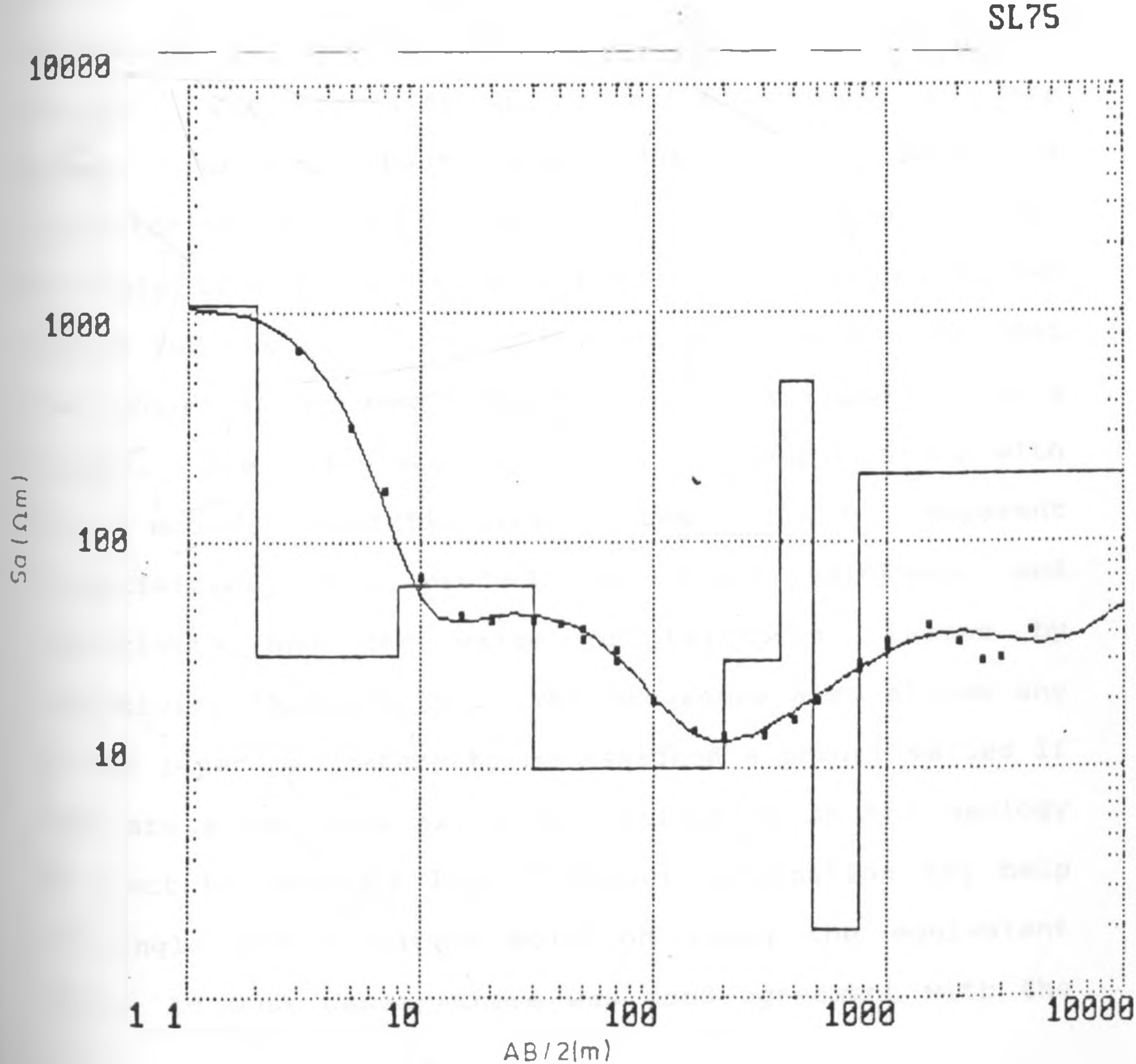

Fig. 4.3 O'neill curve fitting model for SL 75

Appendix B. This was a modification of the programme "Inverse" based on the concept presented by Merrick (1977) and written by David et al (1980). "Resinv 88" computes a layered earth model (up to fifteen layers) whose theoretical apparent resistivity closely agrees with the field curve using the least squares method. The initial model parameters from O'Neill curve matching were then successively modified automatically using a maximum of 15 iterations. In most cases, there was good agreement with the models obtained from the O'Neill curves. After a few iterations, the misfit between the predicted response of the model and the data rapidly decreased to less than 10% (root mean square percentage error). The programme which can accommodate 29 data points performs best with data where AB/2 is logarithmically distributed with 6 points per decade. The data from the study area contains 8 data points per decade for the second and third decades. This means that the programme interpolates to fit 6 data points in a decade. The calculated spacings are output along with the model resistivities, the field apparent resistivities, the product of layer thickness and resistivity and the value of thickness divided by resistivity (Appendix D). The programme also allows any of the layer parameters to be assigned a priori values if they are known from existing information on the geology or electric borehole logs. Priori information may help to single out a unique solution among the equivalent ones. In most cases, there was good agreement with the layer parameters for the intermediate layers obtained form the O'Neill curves. RESNIV 88 indicated poor resolution for the surface and last layer parameters because there are few data points in the first and fourth decades.The interpolation procedure of the programme also leads to the loss of data because fewer points of the field data are used.This might introduce errors in the computation of output model parameters.

The next step in the data analysis was to gain insight into the nature of the non-uniqueness of the models and the equivalence between the models determined by the methods described above. This was carried out by an automatic iteration programme "MAINO" consisting of two parts.The first part involved the computation of most squares models (Patrick et al 1969), Inman et al 1973) based on iteration by approximate inversion (Bostick 1977) and the comparison of the solution with the data using the exact forward computation. This part of the programme carries out an exhaustive computation of all possible layer parameters using ridge regression (Levenberg 1944, Foster 1961 Marquardt 1970, Hoel et al 1970, Hoversten et al 1982).The output shows the range of models or the non-uniqueness of the average model (appendix E). This range increases with the percentage error in data. The models obtained from O'Neill curves and RESNIV 88 were input as the initial models. Throughout the analysis, an 8% error was assumed. To evaluate the effect of increasing the percentage error, errors of 8 % and 10% were used for S12 (Fig.4.4a and b). In both cases the layer parameters are well resolved but with a slight decrease in resolution with the higher percentage. The first and last layers are the least resolved. Some sounding stations showed considerable non-uniqueness e.g. G29 (Fig. 4.5). In this case, it was difficult to determine the model parameters.It was then necessary to remodel the layer parameters and the procedure described above was repeated starting from the Resniv 88 programme.

The second part of the programme used the Occam technique (Meju 1988). In this programme, the initial apparent resistivities of a large number of layers are fixed at logarithmic intervals as the starting model which is then modified automatically by reducing the misfit between the field data and the output model. The output gives the general characteristics of the layer parameters (Fig 4.6). The programme was modified to give models with fifteen layers (Appendix F) spaced at constant logarithmic intervals which were reduced by half to give an approximation of the effective probing depths (from the analysis of the field data using the methods above, it is seen that the effective probing depths for deeper layers is about AB/4). Ideally, the programme should produce a very smooth layered structure if all the field data points are sampled to evaluate the layer parameters. This would result in a large number of unresolved layers. A reasonable geoelectric structure was obtained when the

MOST-SQUARES SM DC MODELS FOR SITE SUS-OLK S12

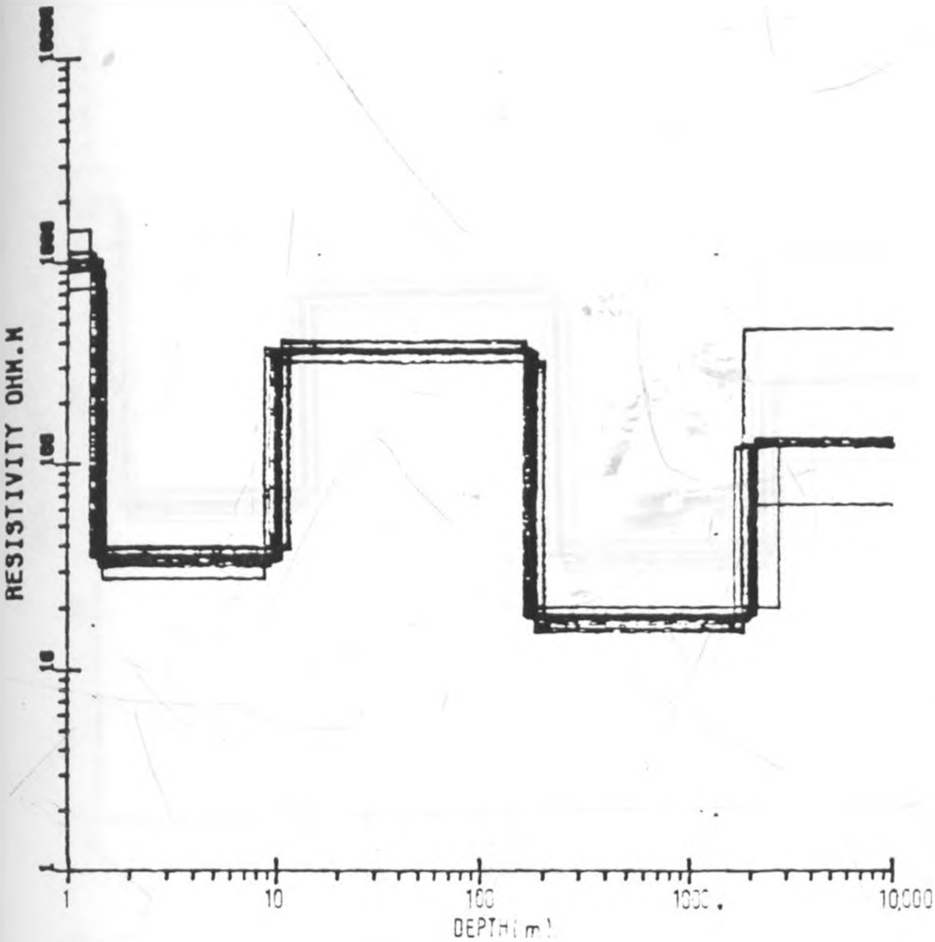

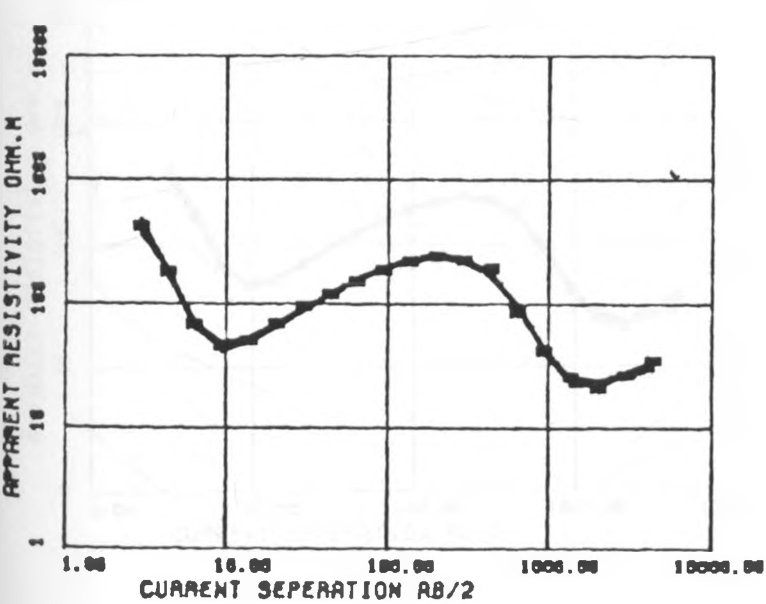

Fig. 4.4 a Equivalent models for 8% error .

MOST-SQUARES SM DC MODELS FOR SITE SUS-OLK S12

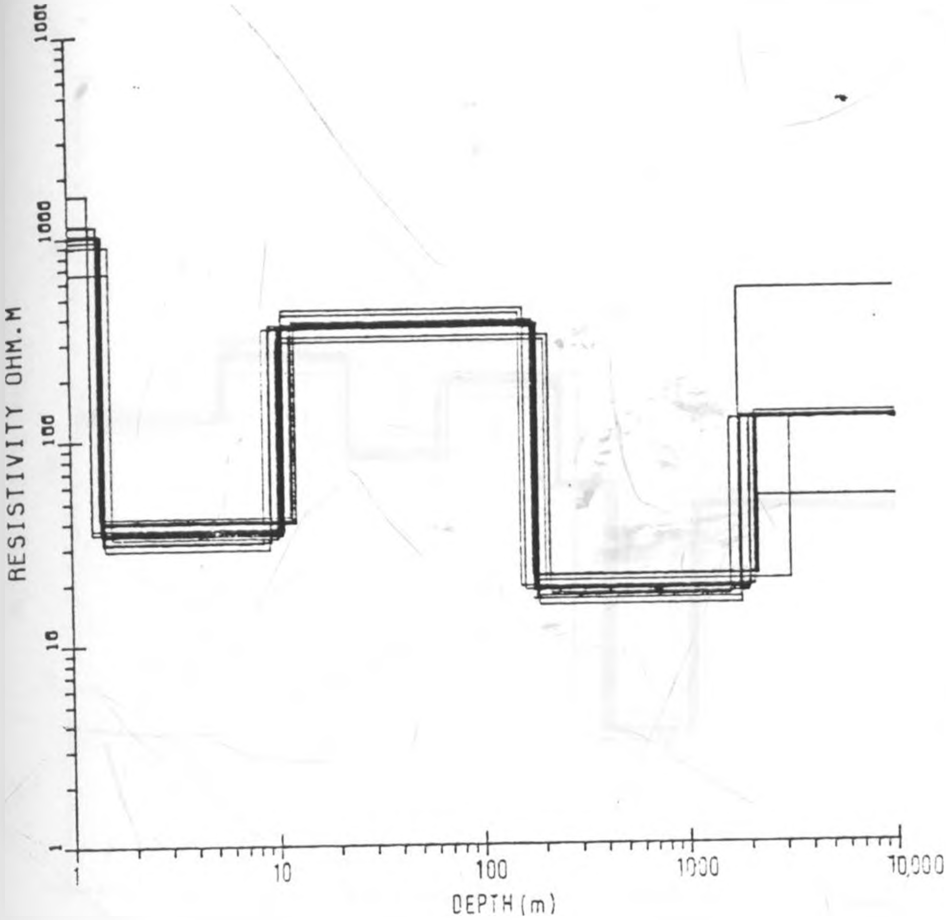

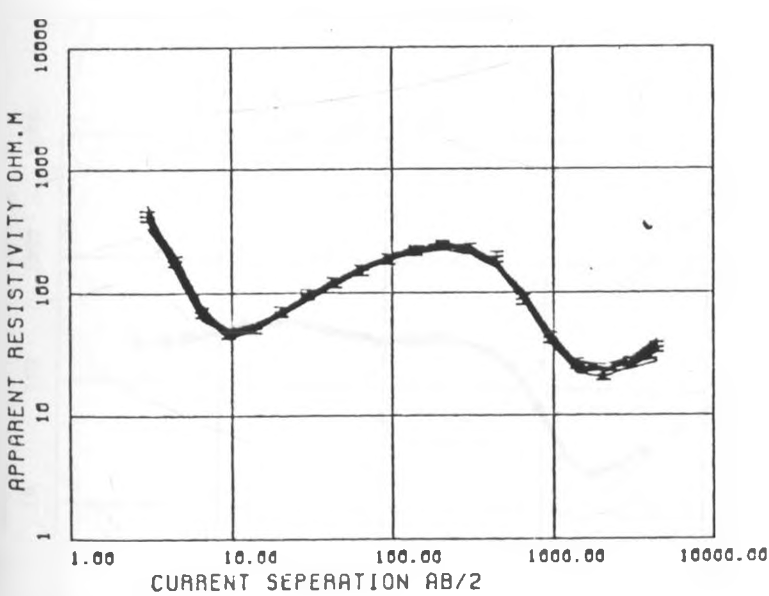

Fig. 4.4b Equivalent models for 10 % error.

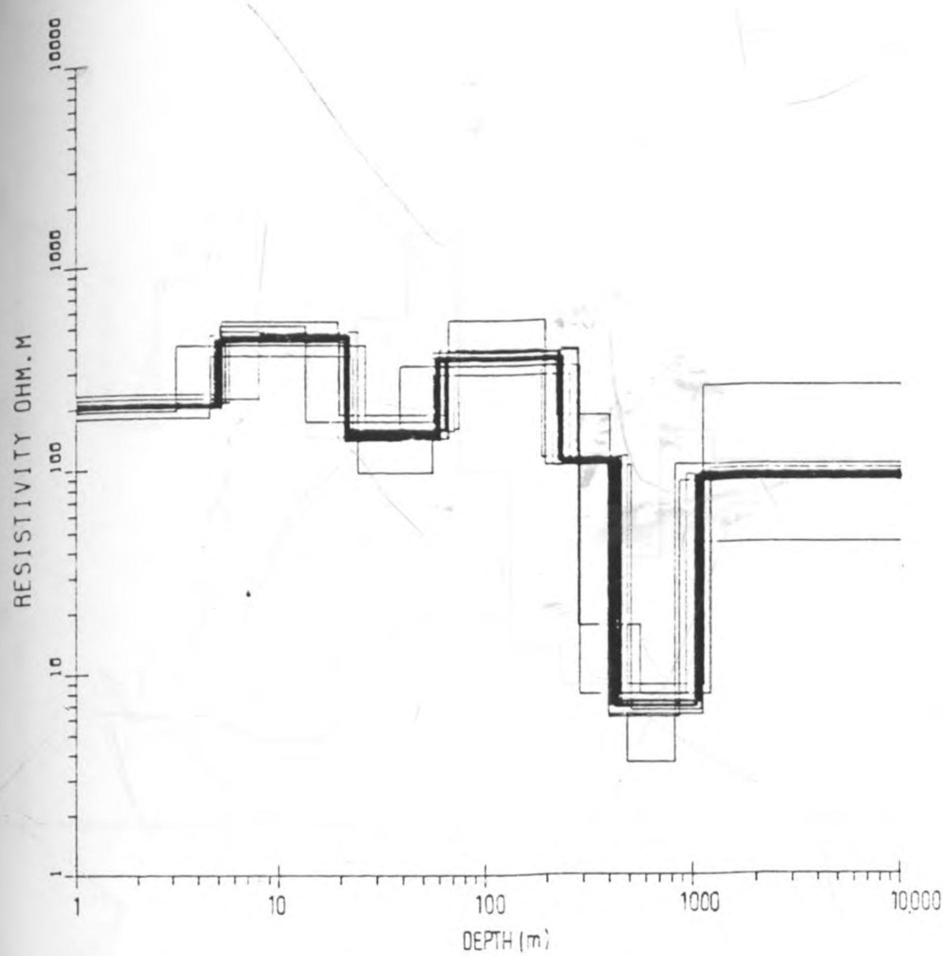

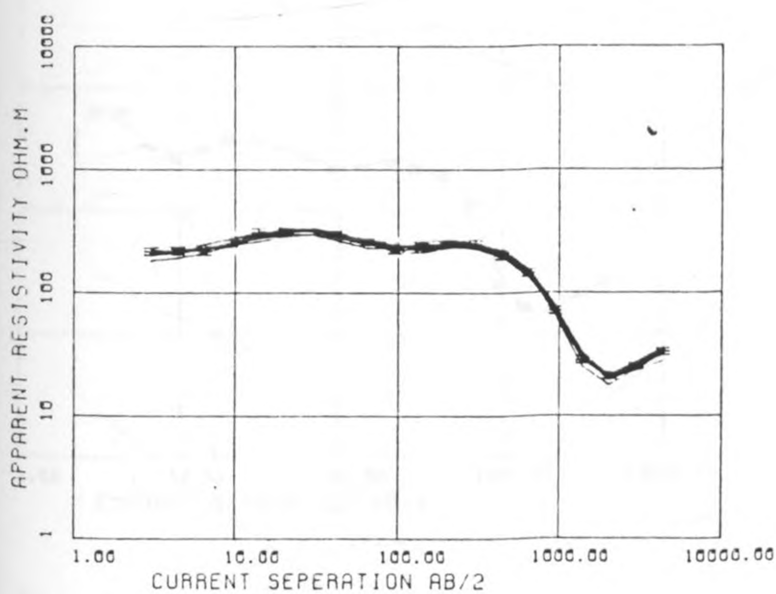

Fig. 4.5 Most squares modes for G29 snowing poor resolution

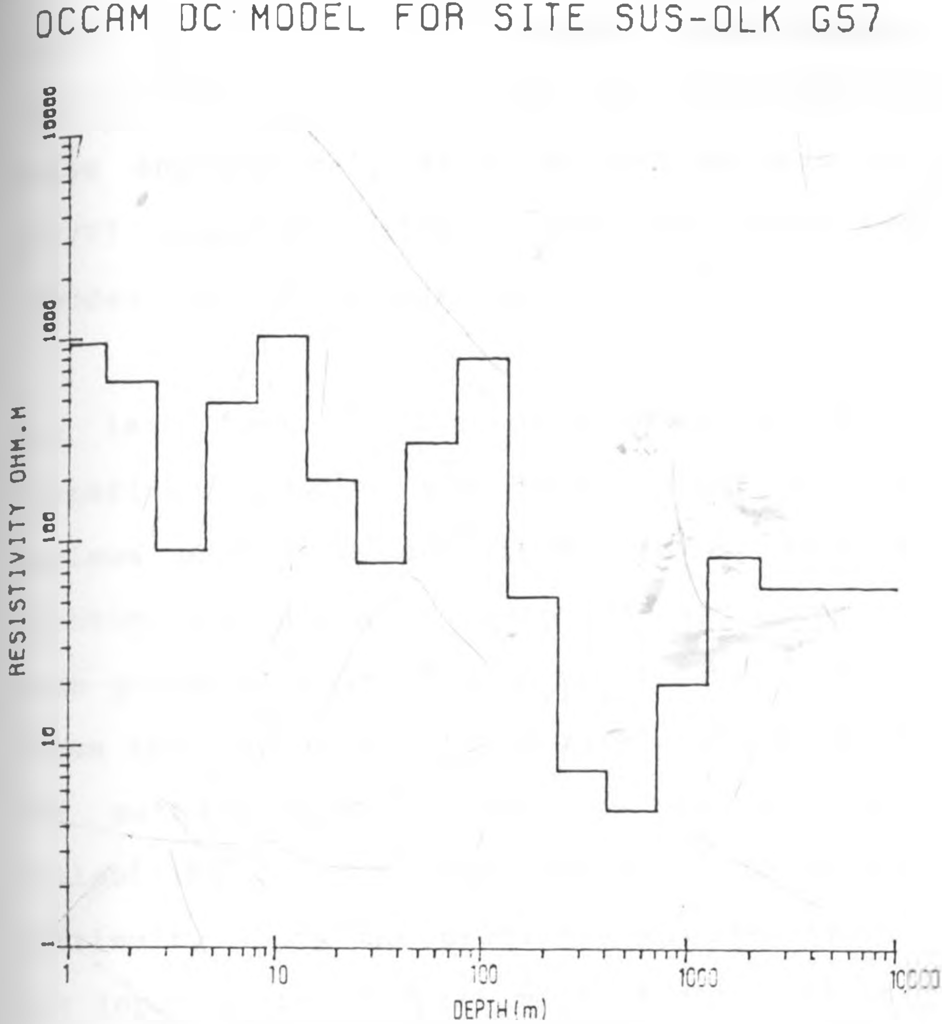

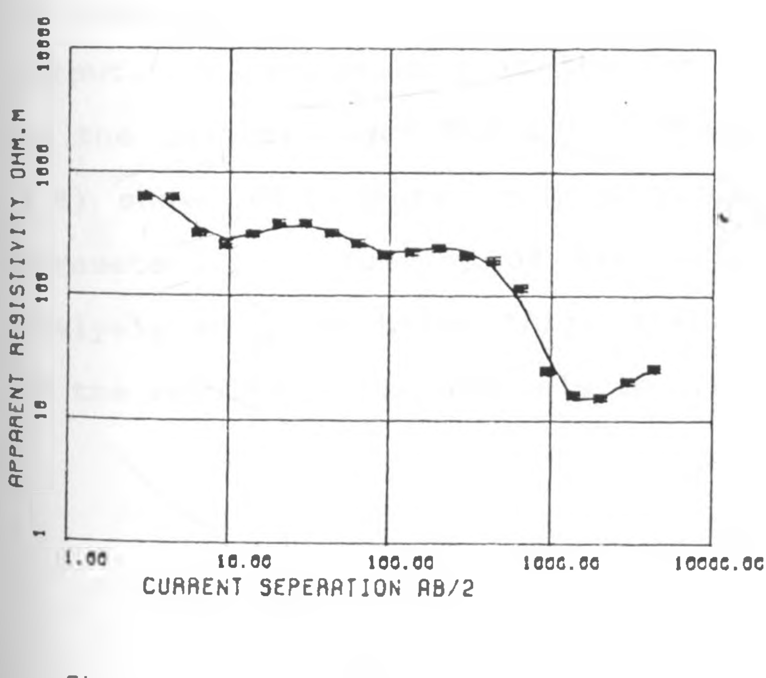

Fig. 4.6 General characteristic for 1-D model

layers were reduced to fifteen. The execution time of the programme depend on the type of graph but generally takes approximately 45 - 60 CPU seconds on an Amdahl 470/V7 computer. The results of Occam were used to remodel some of the curves.

The last part in the data analysis was to draw a comparison between the best output models from the various procedures described above. This was done by plotting the output of Resinv 88, and Occam models on the same graph as that of the field data. (Fig 4.7. This shows that there is a "good fit to the field data for all the methods used. This is an indication of the reliability of the final models. To evaluate lateral continuity along the profiles, a model from one station was input as the initial model for the adjacent station. In some cases there was no significant difference in the output. A good example is the use of the model for S13 as the initial model for G55. The output for G55 (Fig 4.8) shows that there is good resolution of the layer parameters. A summary of the procedures used in the analysis is given below (Fig 4.9). The interpretation of the results of the analysis is given in Chapter five.

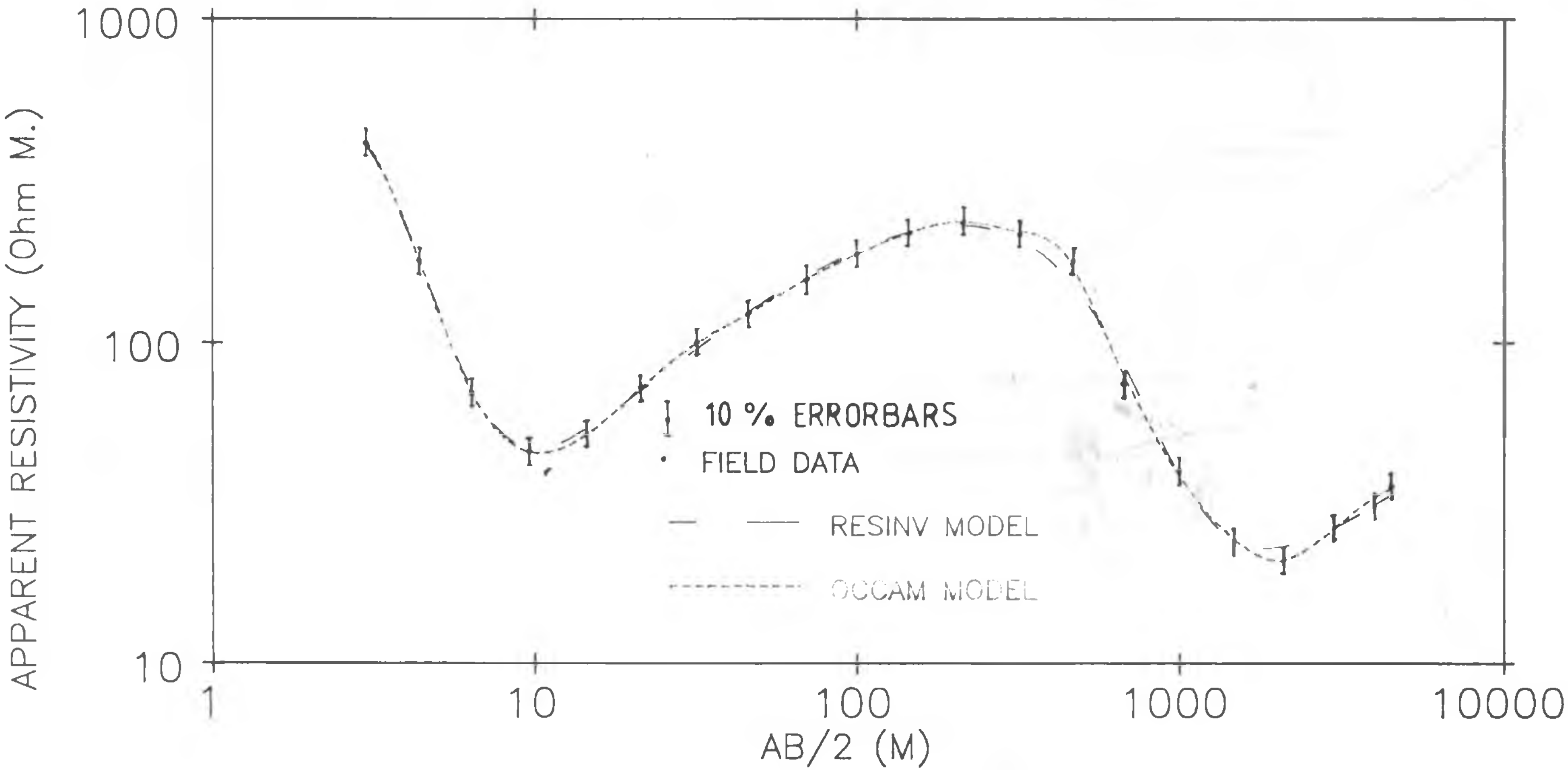

Fig. 4.7 Comparison of "best" output models for S12

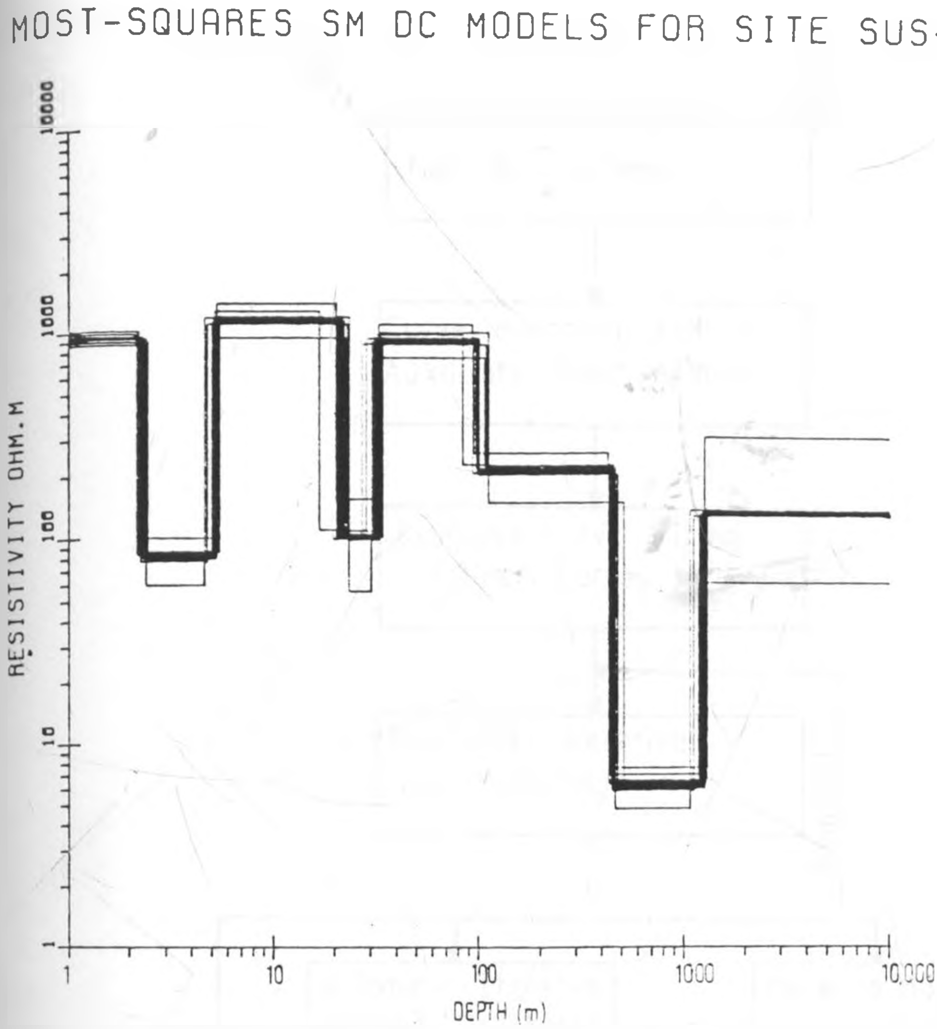

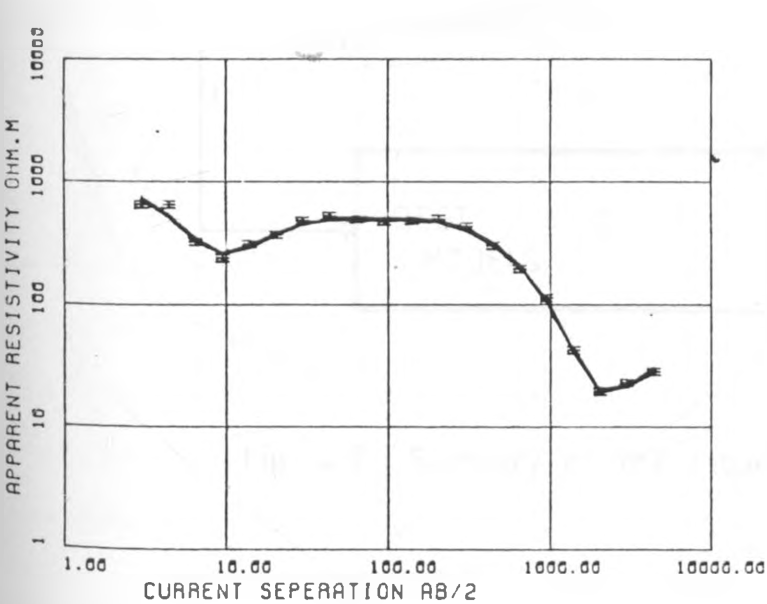

Fig. 4.8 Resolution of equivalent models

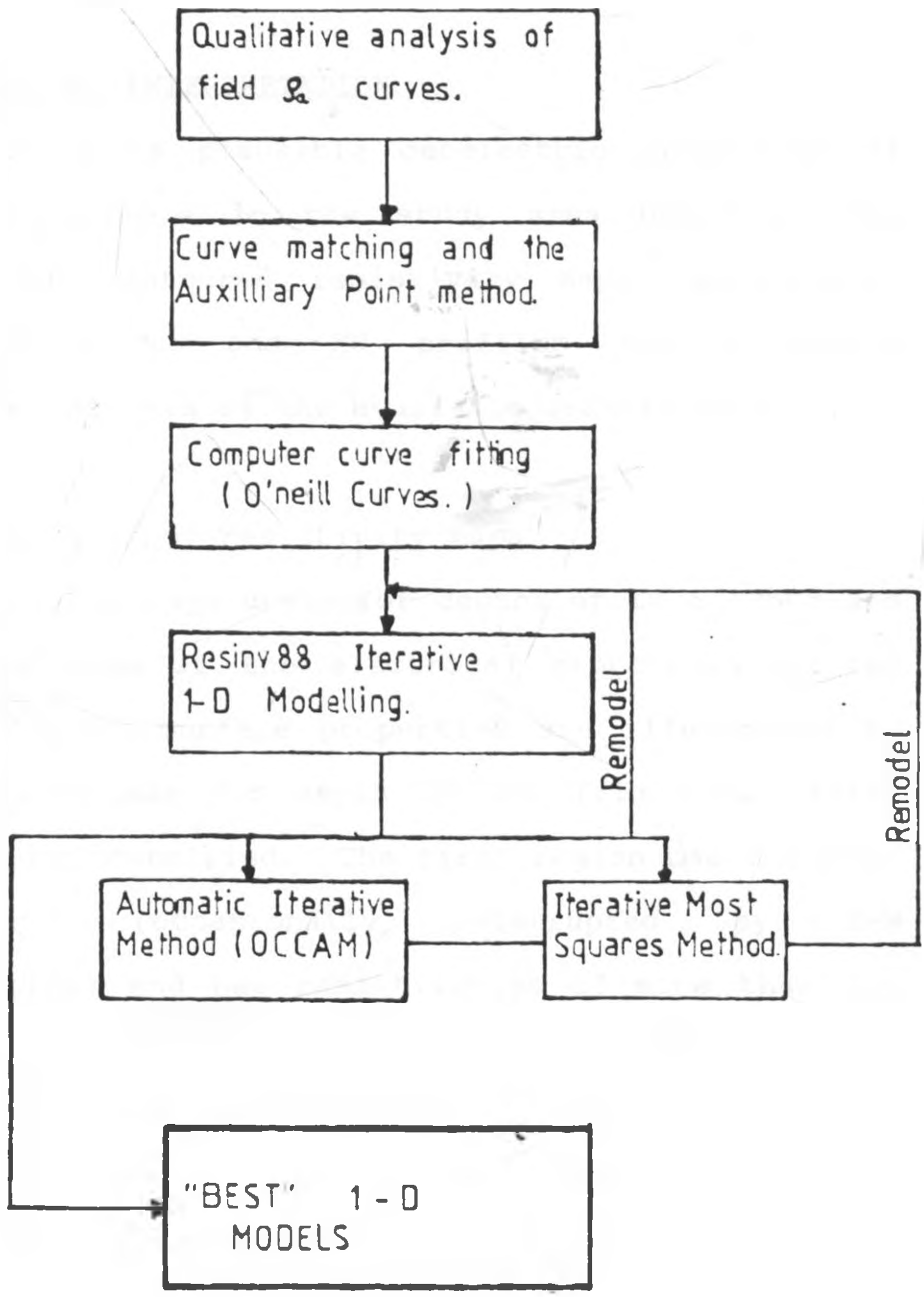

Fig. 4.9 Summary of the sequence of data analysis.

CHAPTER 5

INTERPRETATION OF THE RESULTS

5.1 GEOPHYSICAL INTERPRETATION

This section gives plausible geoelectric properties of the rock formations in the study area based on the evaluation of contoured resistivity maps, geoelectric sections along NS and EW profiles and a simple quantitative analysis of the available gravity data.

5.1.1 Analysis of resistivity maps

Three resistivity maps drawn for depths of 10 m, 750m and 2000 m show some of the electrical properties of the study area. The surface properties are illustrated by the resistivity map for depth of 10m (fig 5.1). Three regions can be identified. The first region has a north-south trend (occasionally interrupted by E-W discontinuities) and has resistivities of more than 300 Ωm. Within this region, higher resistivities (more than 500 Ωm) are found around Ololbutot lava flow, to the West of Tandamara and towards the foot of Mt Suswa. These are areas which are covered with recent lava flows and pumiceous material. The second region surrounds the first one and has resistivities of 100 - 300Ωm . The third region surrounds these two and has a resistivity of less than 100Ωm.

The maps for 750m (Fig 5.2) represents the average subsurface resistivity of the conductive unit. Two

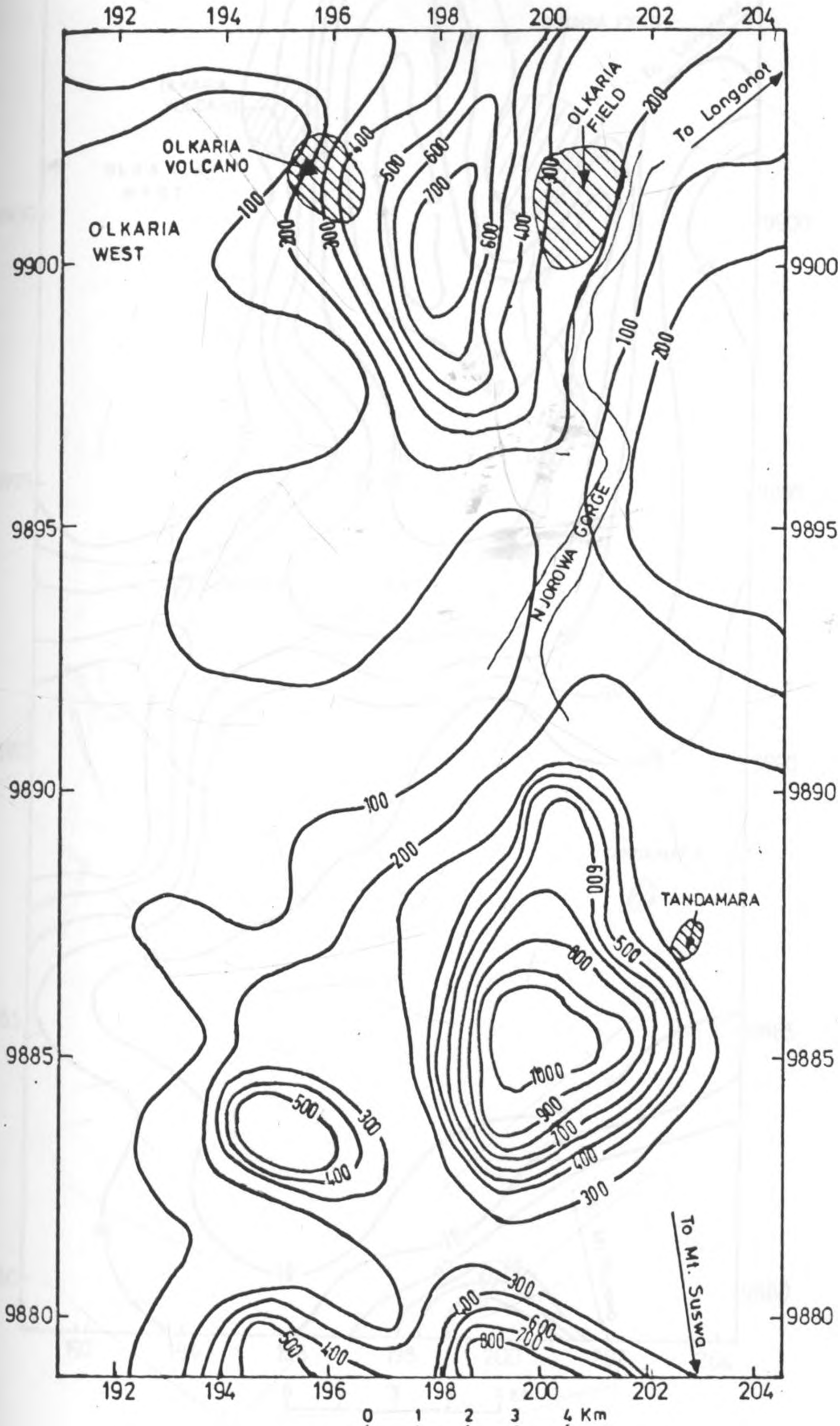

Fig.5.1 Resistivity(Ωm) map at a depth of 10m

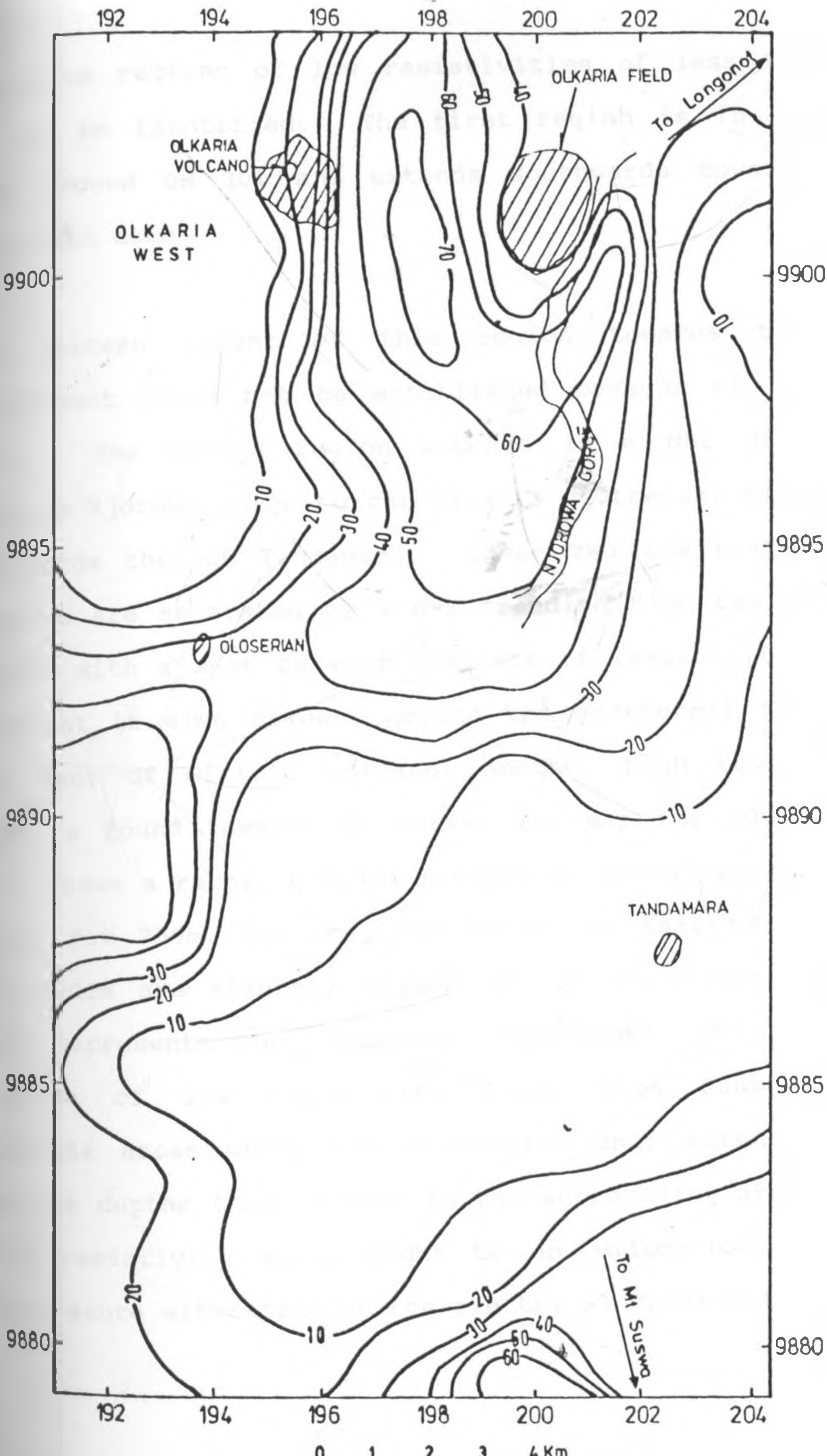

Fig. 5.2 Resistivity (Ωm) map at a depth of 750m in the Suswa Olkaria region

anomalous regions of low resistivities of less than 20 Ωm can be identified. The first region is in Olkaria West around OW 301 and extends southwards towards the Oloserian dome.

The western extent of this region towards the Mau escarpment could not be established because of lack of data. The second region extends in a NNE direction through Njorowa gorge to the Olkaria geothermal field and eastwards through Tandamara. These two low resistivity regions are separated by a NNE trending high resistivity region with a west to east gradient of resistivity. The gradient is also evident around the geothermal field to the east of Olkaria volcano. Another high resistivity area is found towards Mt Suswa. The map for 2000m (Fig 5.3) shows a rather similar pattern of anomalies as those drawn for 750m. The only difference is that the values for 2000m are slightly higher. It is not clear whether this represents the electrical "basement". The isolated regions of low resistivity (less than 50Ωm) could indicate areas where the conductive unit extends to a greater depths than it does in the surrounding areas. The high resistivity areas might be an indication of high temperature alteration of the electrical "basement".

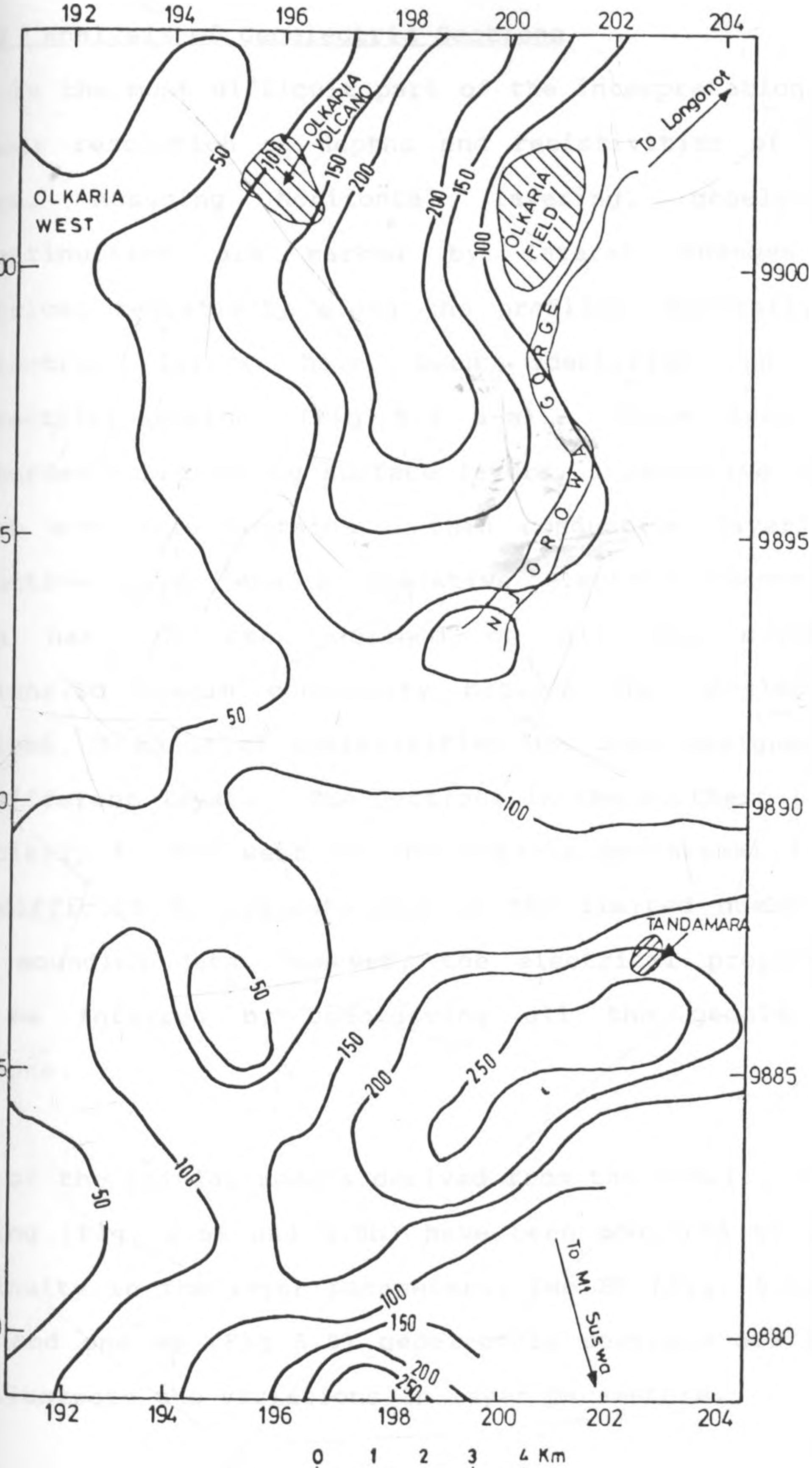

Fig. 5.3 Resistivity (Ωm) map at a depth of 2000m.

5.1.2 Analysis of Geoelectric Sections

This is the most difficult part of the interpretation due to poor resolution of depths and resistivities of some layers. Assuming horizontal layering, geoelectric discontinuities are marked by lateral changes in electrical resistivity along the profiles. Generally, 4 geoelectric layers have been identified on the geoelectric sections (Fig 5.4 a-m). These are, the overburden representing surface layers, a resistive layer (Which sometimes contains a thin conductive layer), a conductive layer and a resistive electric "basement" which has not been defined on all the sounding stations.To obtain continuity between the geoelectric sections, a range of resistivities has been assigned to the different layers. The sections in the northern part, especially to the west of the Olkaria geothermal field are difficult to evaluate due to the limited number of deep sounding data. However, the electrical properties can be inferred by considering all the geoelectric sections.

Some of the initial models derived from the O'Neill curve fitting (Fig. 5.5a and 5.5b) have been modified to give continuity in the layer parameters. Two EW (Fig. 5.6 and 5.7) and one NS (Fig 5.8) geoelectric sections are used to illustrate the variations in layer parameters.

In the southern part of the study area (see profile EW 8, Fig 5.7) a surface resistive layer (300-1000Ωm) thins out

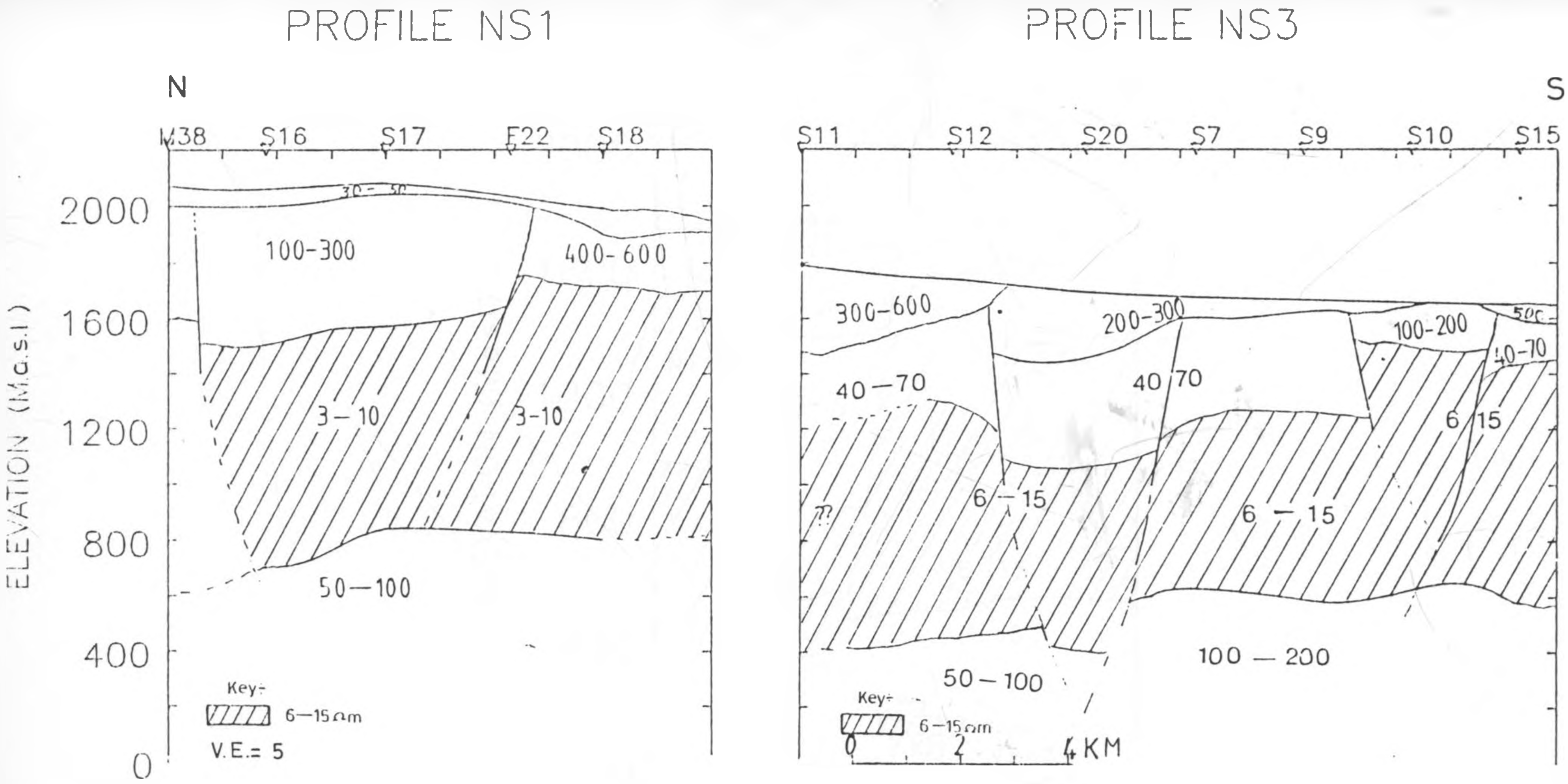

PROFILE NS1
PROFILE NS3
N
S
M38
S16
S17
E22
S18
S11
S12
S20
S7
S9
S10
S15
ELEVATION (M.a.s.l.)
2000
1600
1200
800
400
0
30 - 50
100-300
400-600
3-10
3-10
50—100
300-600
200-300
100-200
50c
40-70
40—70
40 70
6 15
6 — 15
6 — 15
100 — 200
50 — 100
Key:
6—15 Ωm
V.E.= 5
0
2
4 KM

Fig. 5.4a

PROFILE NS2

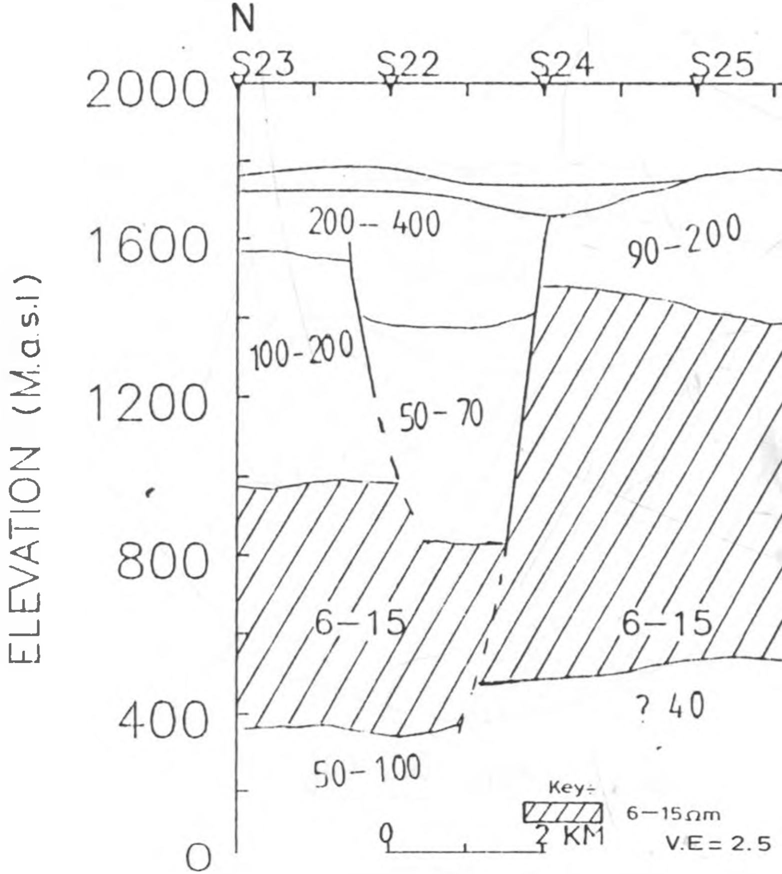

Fig. 54b

S

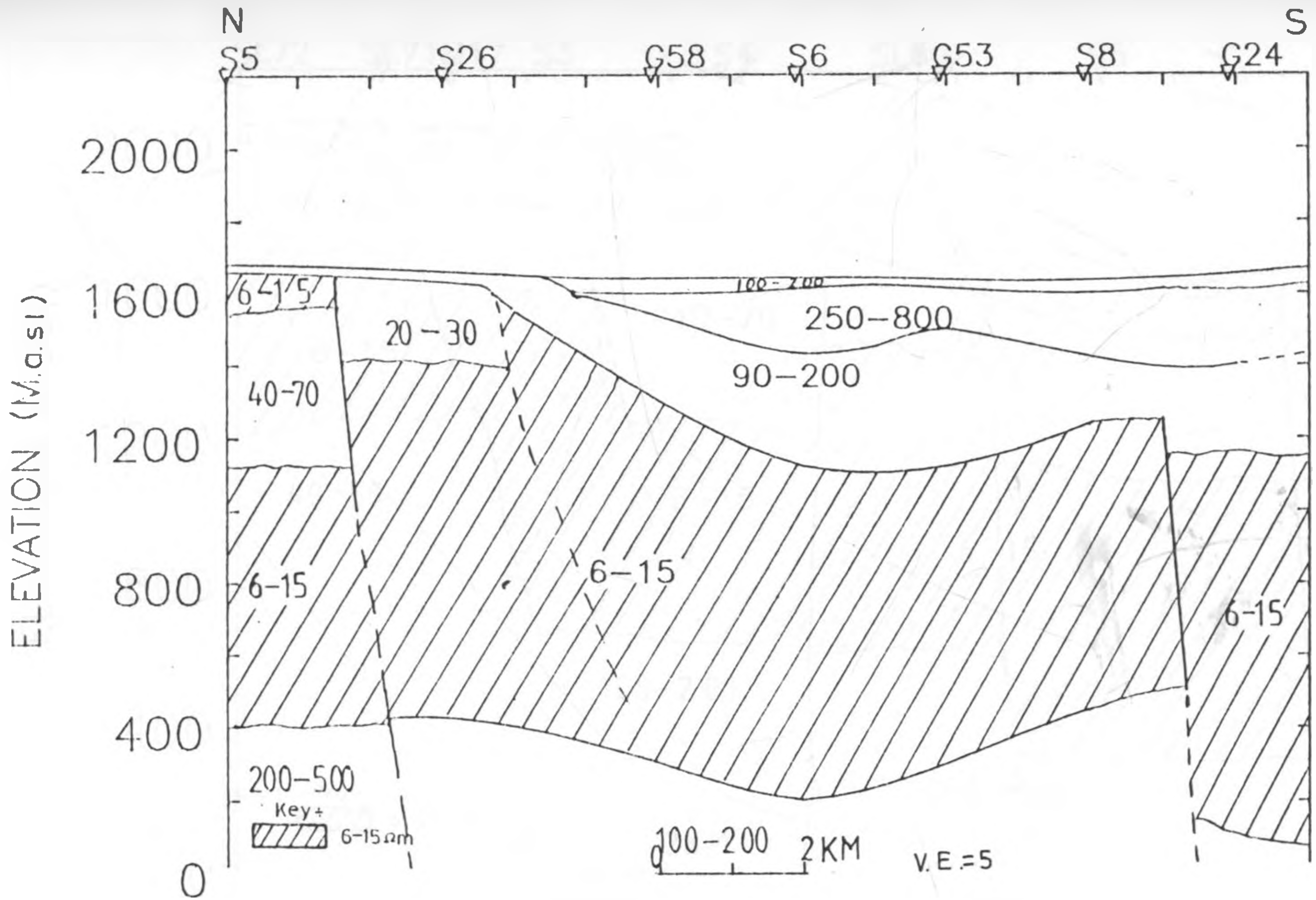

N
S
S5
S26
G58
S6
G53
S8
G24
2000
1600
1200
800
400
0
ELEVATION (M.a.sl)
100-200
250-800
20-30
90-200
40-70
6-15
6-15
6-15
200-500
Key:
6-15 Ωm
100-200
0
2 KM
V.E.=5

Fig. 5.4c

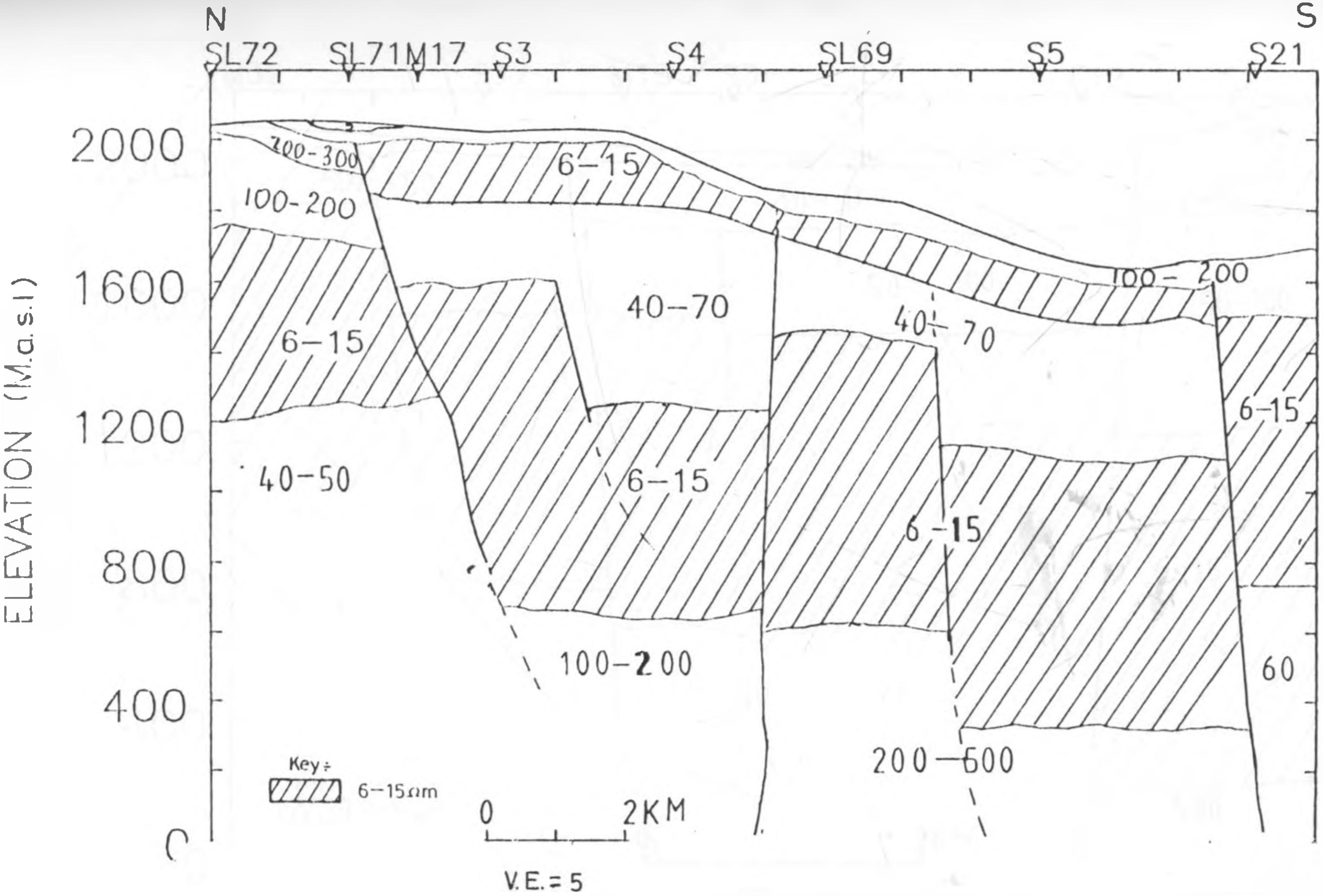
N
S
SL72
SL71
M17
S3
S4
SL69
S5
S21
2000
1600
1200
800
400
0
ELEVATION (M.a.s.l)
200-300
100-200
6-15
40-70
40-50
100-200
200-600
100-200
60
Key:
6-15 Ωm
0
2KM
V.E.= 5

Fig. 5.4d

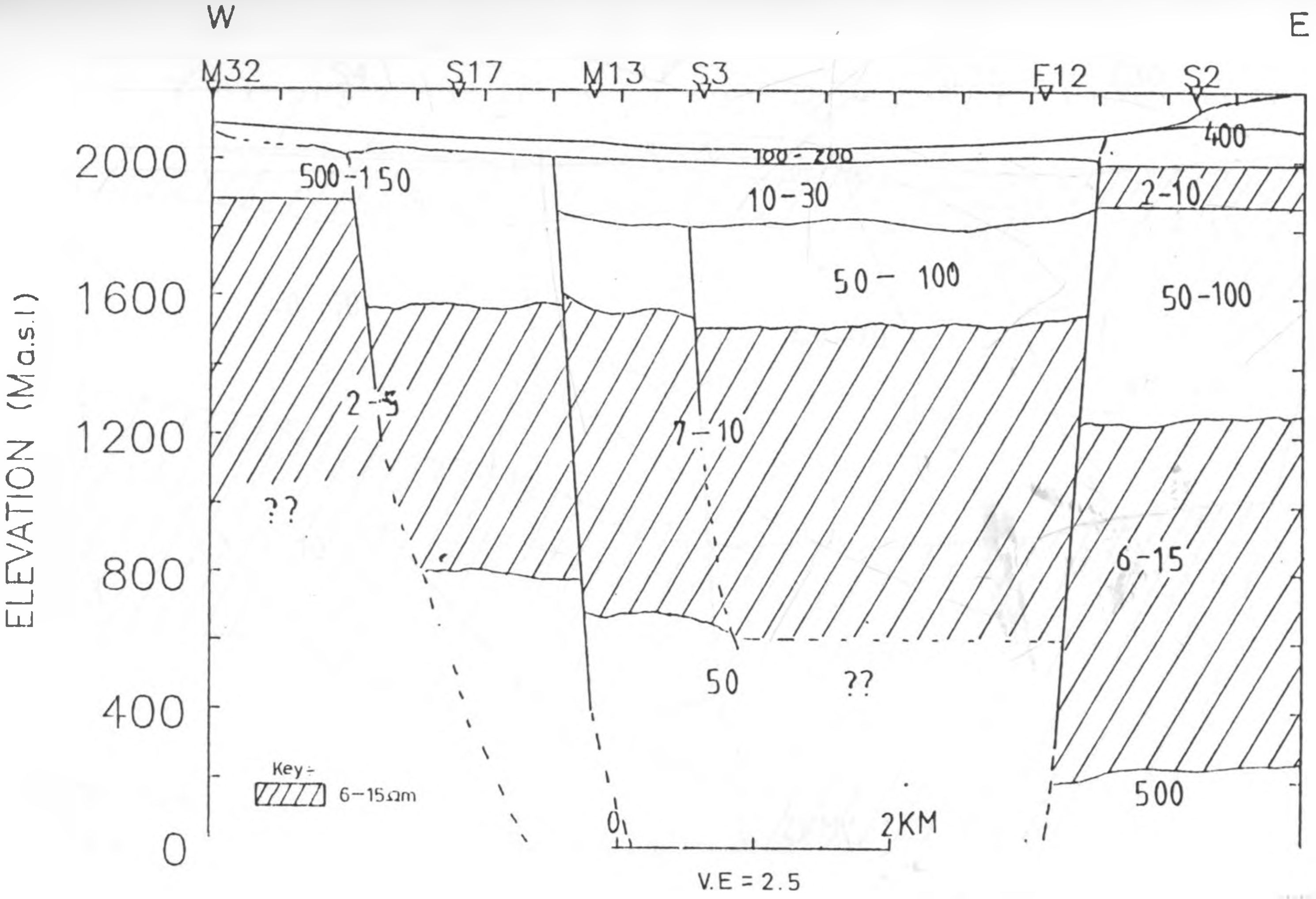

W
E
M32
S17
M13
S3
F12
S2
ELEVATION (M.a.s.l)
2000
1600
1200
800
400
0
500-150
100-200
10-30
400
2-10
50- 100
50-100
2-5
7-10
??
6-15
50
??
500
Key:
6-15Ωm
0
2KM
V.E = 2.5

Fig. 5.4e

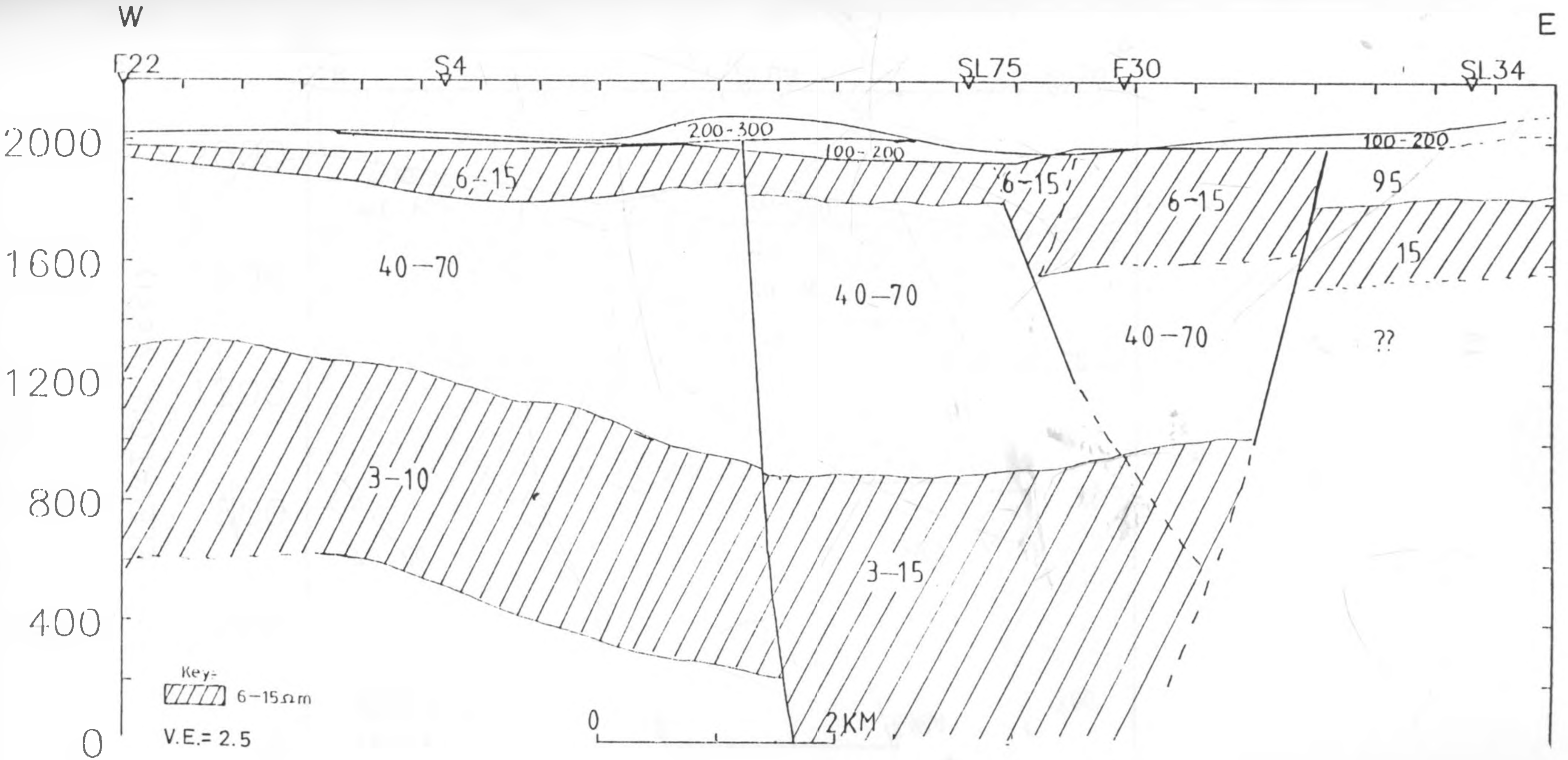

W
E
F22
S4
SL75
F30
SL34
2000
1600
1200
800
400
0
200-300
100-200
100-200
6-15
6-15
6-15
95
15
40-70
40-70
40-70
??
3-10
3-15
Key:-
6-15Ωm
V.E.= 2.5
0
2KM

Fig. 5.4f

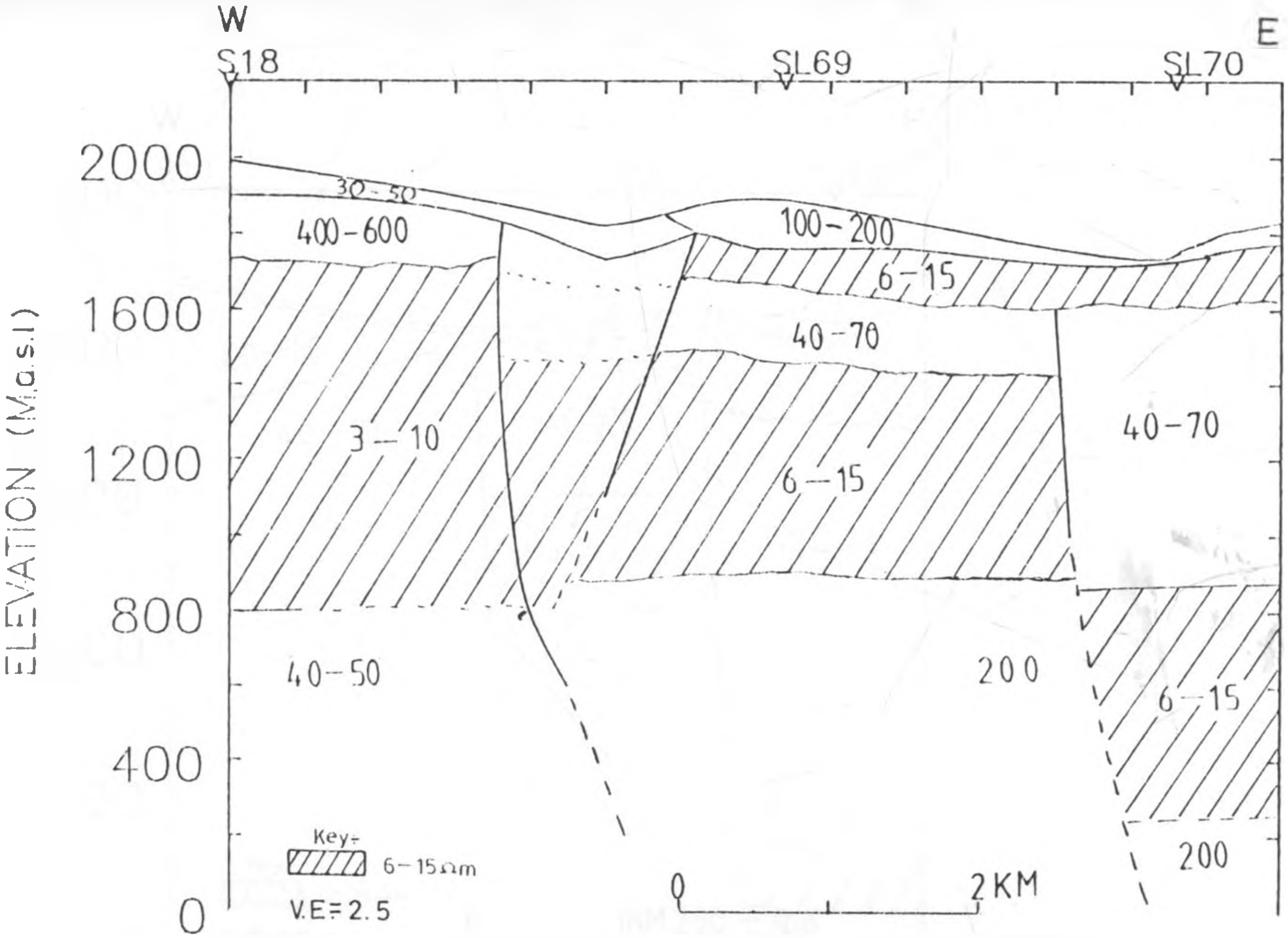

W
E
S18
SL69
SL70
2000
1600
1200
800
400
0
ELEVATION (M.a.s.l)
30-50
400-600
100-200
6-15
40-70
3-10
6-15
40-70
40-50
200
6-15
200
Key:
6-15 Ωm
V.E=2.5
0
2KM

Fig.5.4g

PROFILE EW4

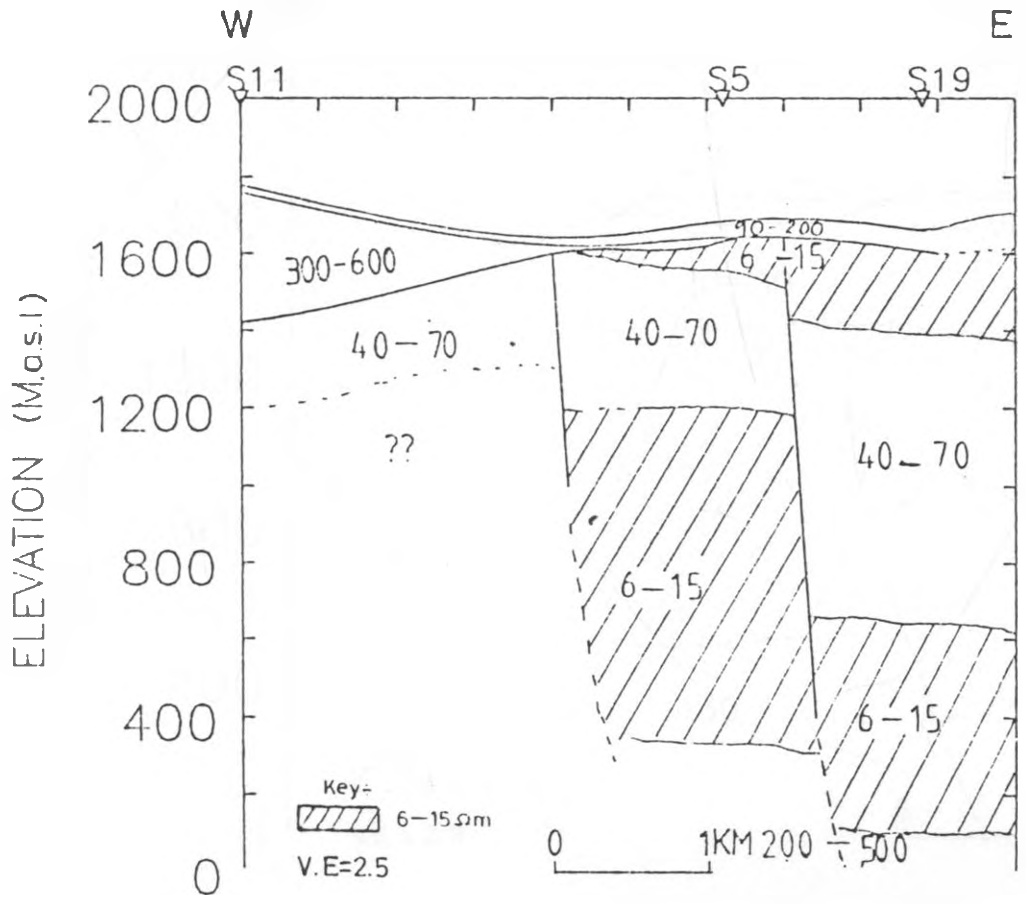

Fig. 5.4h

Profile EW5

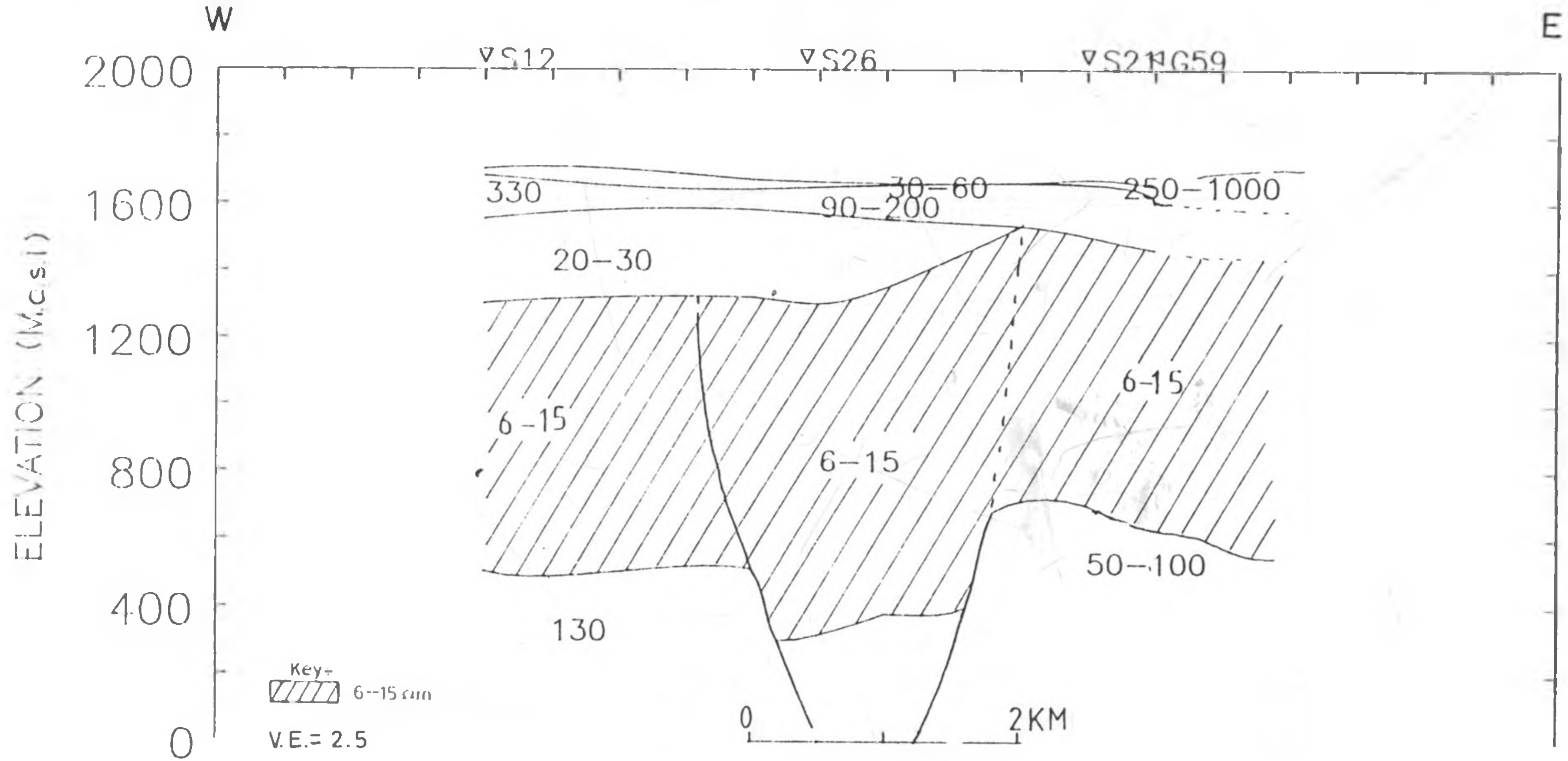

Fig. 5.4i

Profile EW6

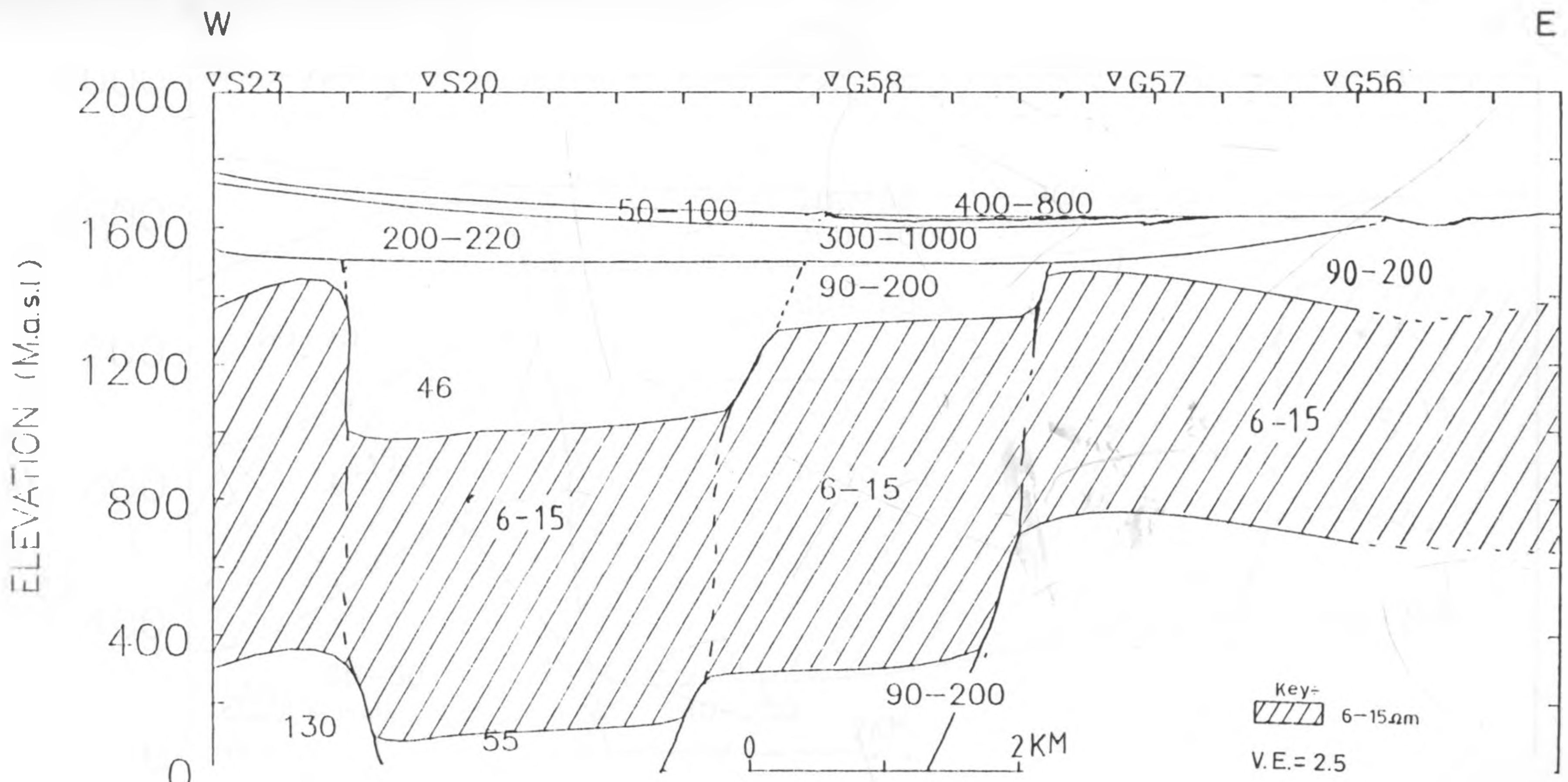

Fig. 5.4j

Profile EW7

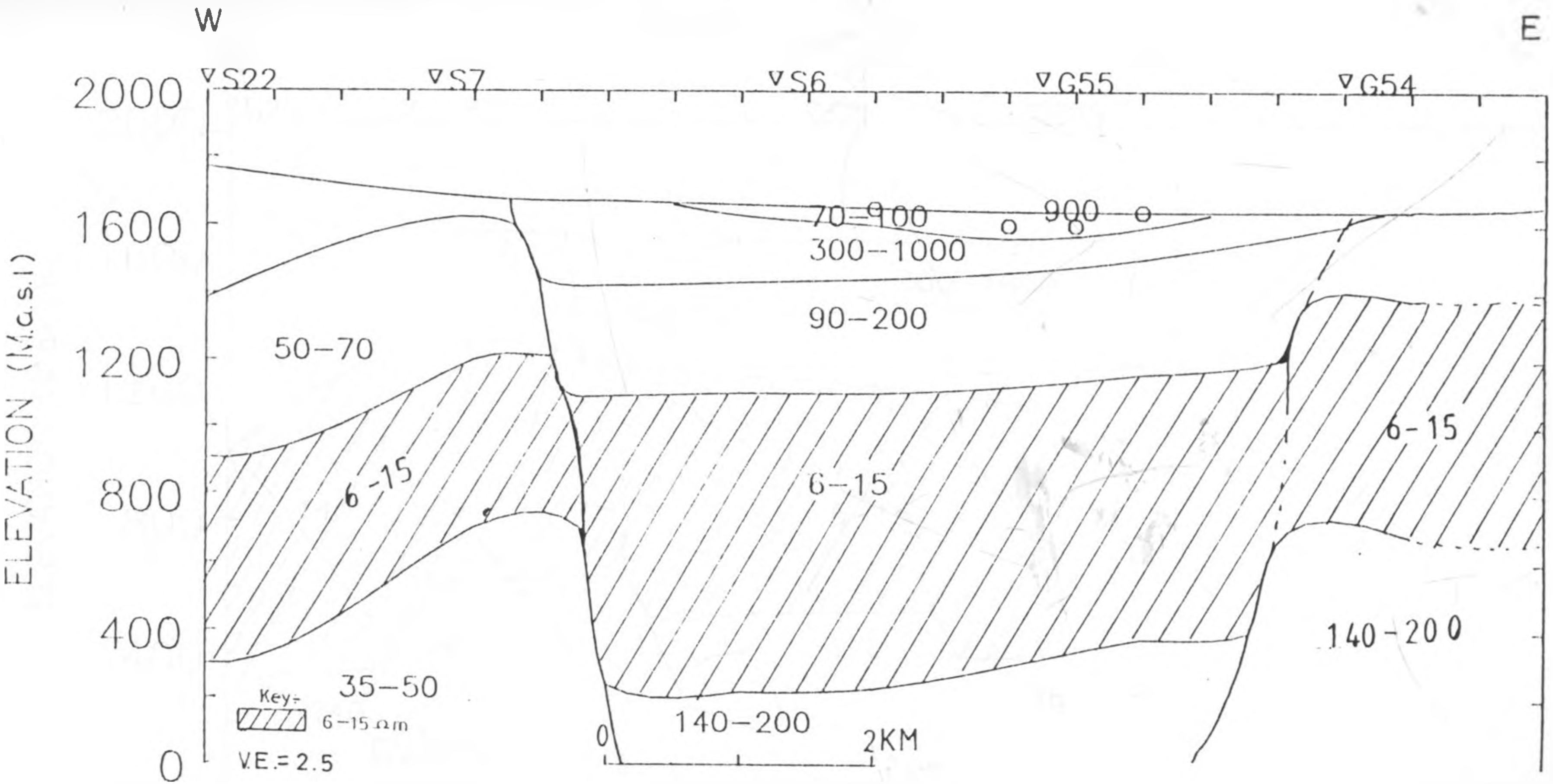

Fig. 5.4k

Profile EW9

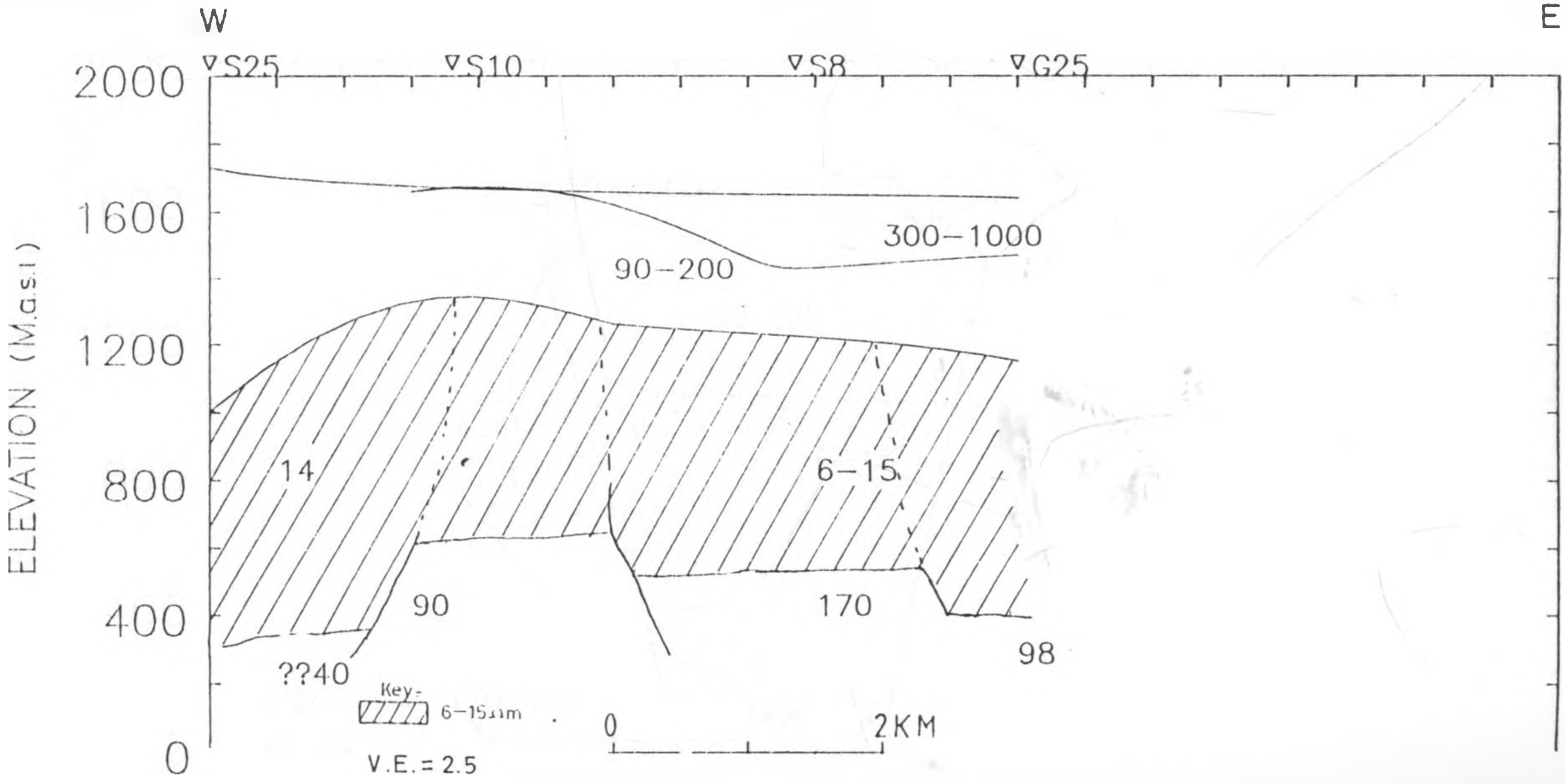

Fig 5.4l

Profile EW10

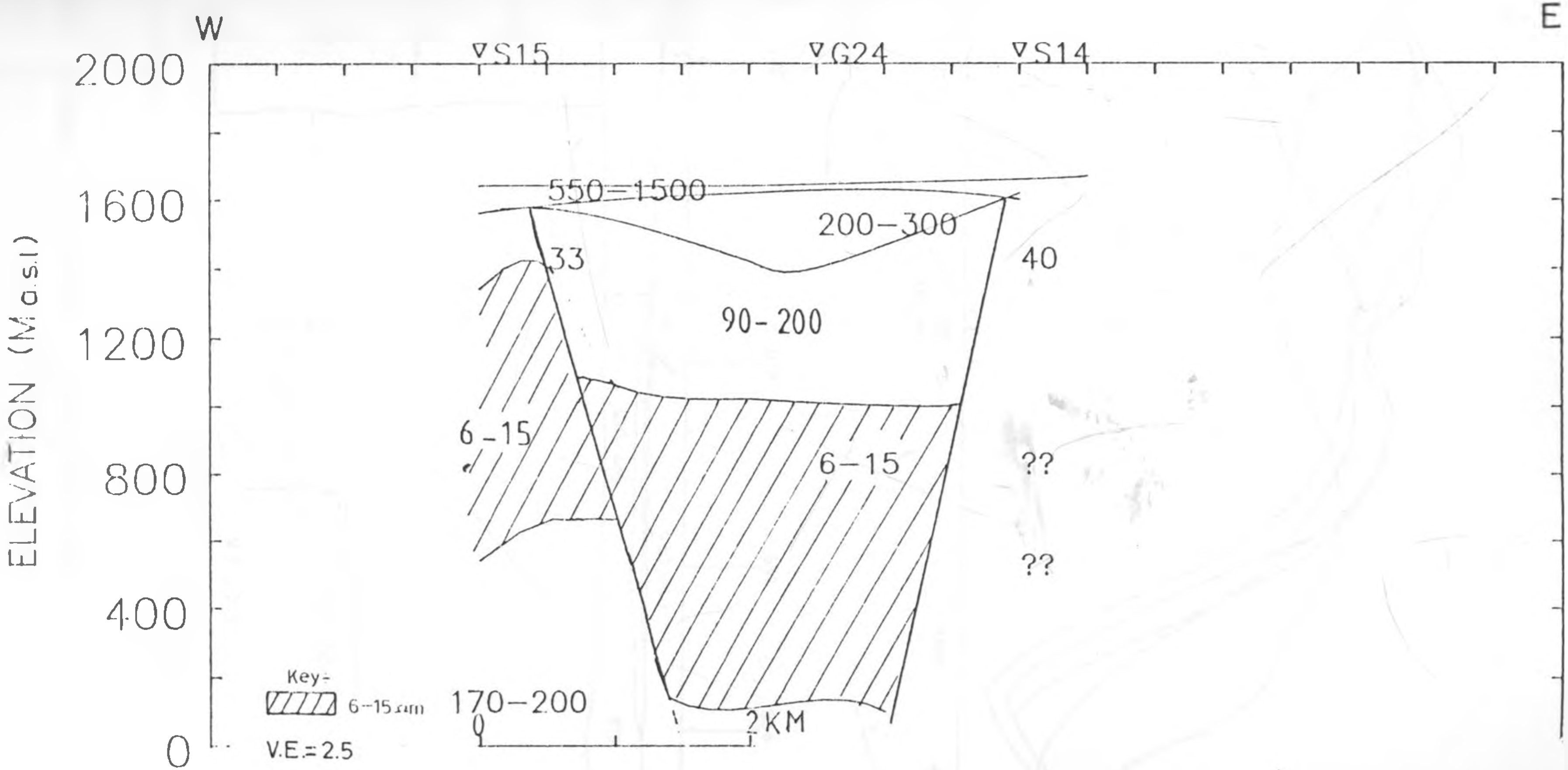

Fig. 5.4m

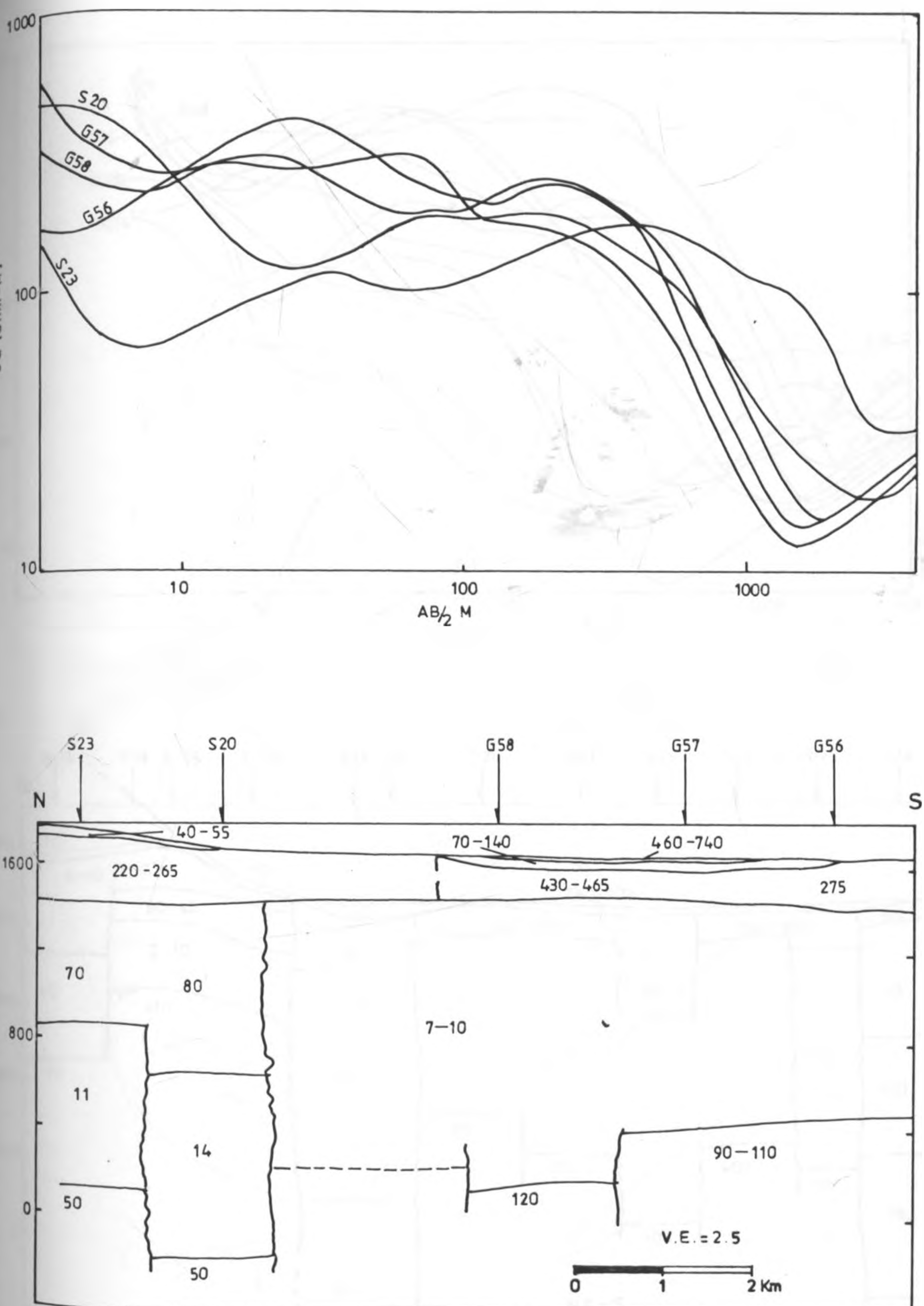

Fig.5.5a APPARENT RESISTIVITY CURVES AND THE GEOELECTRIC SECTION OF PROFILE EW-6 BASED ON MODELLING USING ONEILL CURVE FITTING

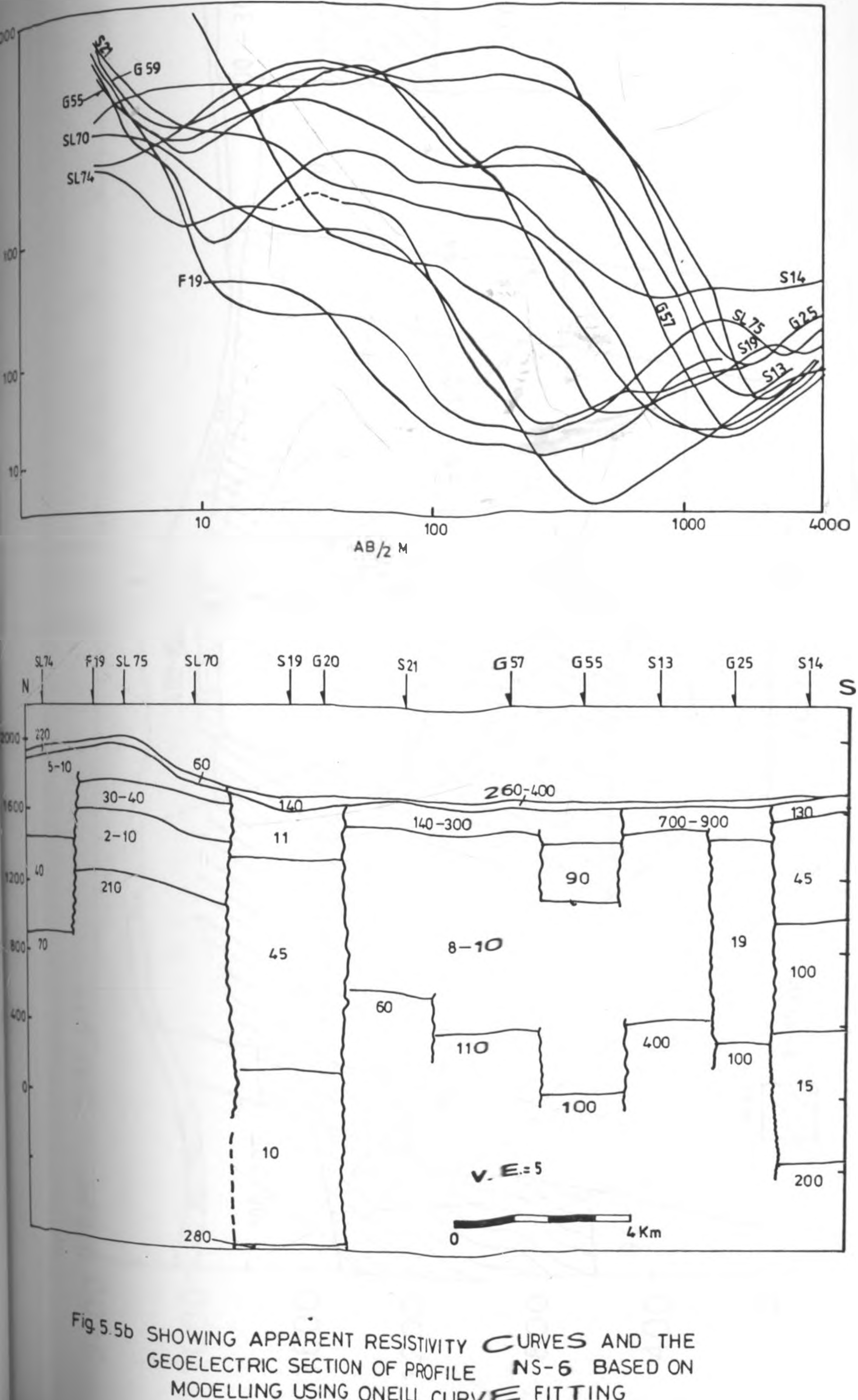

Fig. 5.5b SHOWING APPARENT RESISTIVITY CURVES AND THE GEOELECTRIC SECTION OF PROFILE NS-6 BASED ON MODELLING USING ONEILL CURVE FITTING

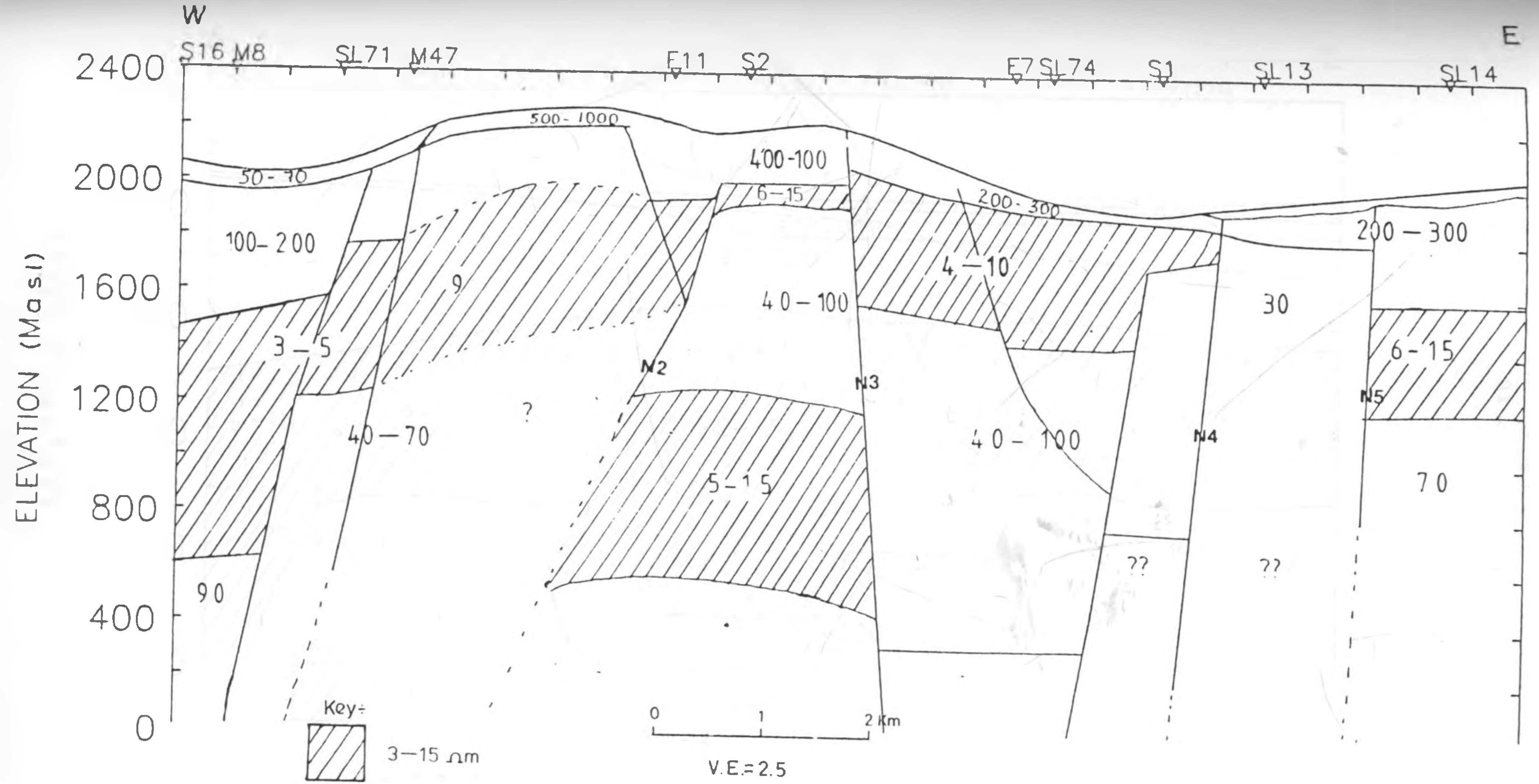

Fig. 5.6 Geoelectric section along profile, EW1 showing layer resistivities (ΩM)

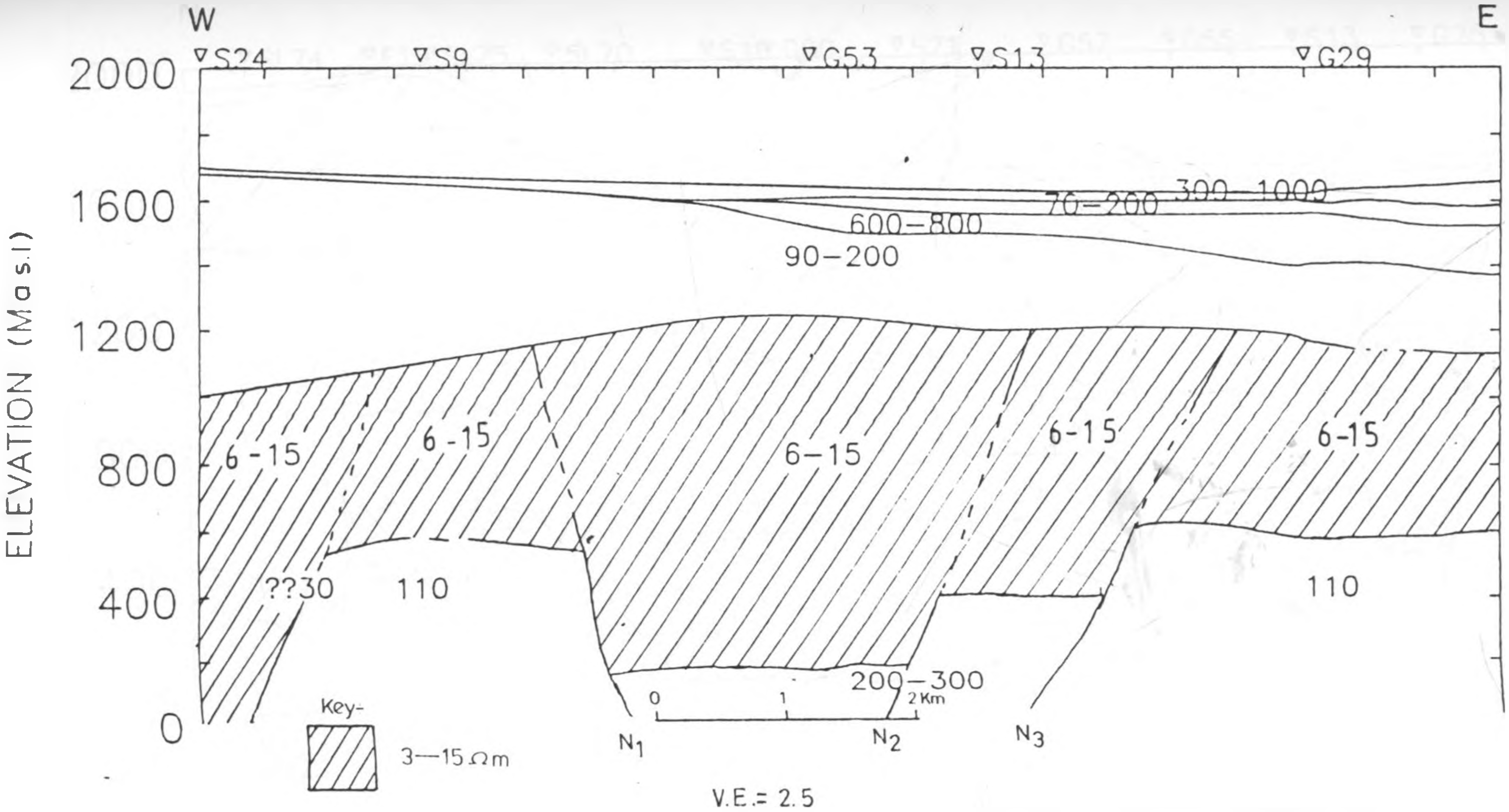

Fig. 5.7 Geoelectric section along profile EW8

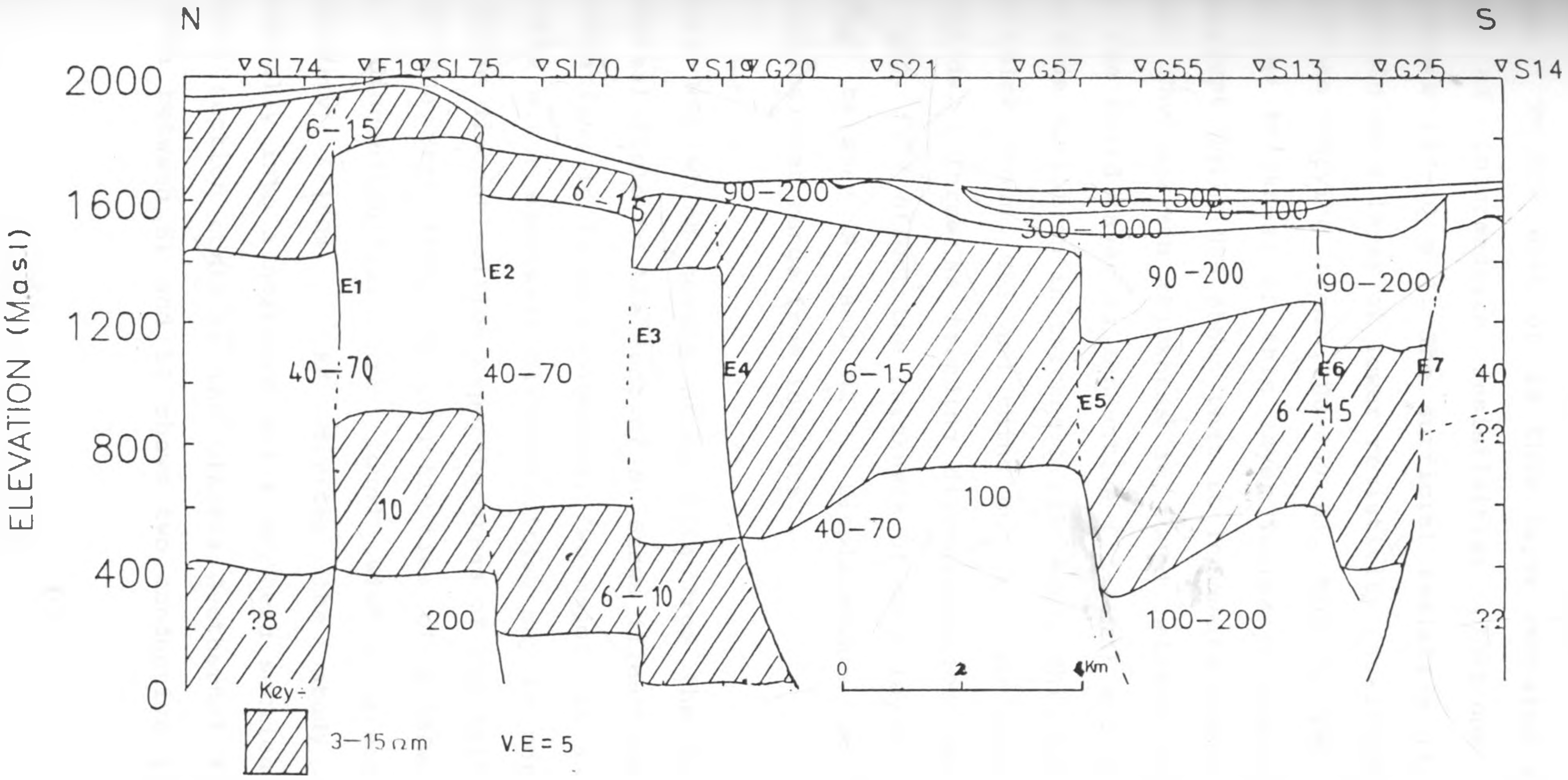

Fig. 5.8 Geoelectric section along profile NS6 from Olkaria geothermal field to the foot of mt. suswa

towards the Mau escarpments and thickens Eastwards (20-200m). To the east of S9 this layer contains a thin layer of intermediate resistivities (70-200Ωm) of thickness (20-40 m). The surficial resistive layer is underlain by a layer of lower resistivity (90-200Ωm) with thickness varying from (200-650 m). Profile EW8 shows that the thickness of this layer increases towards the escarpment while NS6 shows that it increases towards Mt. Suswa. The maximum thickness is found between G25 and G55. The third layer is conductive (3-16Ωm) and shows a very wide variation in thickness (350-800). This layer is very thick around G53 and thins out both westwards and eastwards. Three Ns trending discontinuities (N1, N2, N3) (Fig. 5.7) affect the thickness of this layer. It is thicker between N1 and N2 . Displacements on these discontinuities range from 100-300m.

Profile NS6 which covers about 21km from the Olkaria geothermal field to the foot of Mt Suswa illustrates the NS variations in layer parameters. Two major (E4 and E7) and five minor east-west discontinuities may be noticed. The major discontinuities separate areas of resistivities of 40-70Ωm from those of resistivities of 6-15Ωm. The minor discontinuities are found within areas of resistivity 6-15Ωm. E4 divides the study area electrically into a northern and a southern section. The northern section contains the Olkaria Geothermal field. The area between E1 and E2 shows two conductive layers especially around SL 75. The second conductive layer might be deeper at OW19 and absent between E4 and E7.

This means that the electric "basement" in the two sections is probably not the same rock formation. North of E4, the surficial conductive layer is underlain by a thick layer (600-900m) with intermediate resistivities (40-70Ωm) which could be attributed to fracturing and geothermal alteration of primary rocks to clay minerals. The thickness of this layer decreases towards the escarpment (profile EW2). To the south of E4, this layer is much deeper and shows higher resistivities (100-200Ωm) except in the region around G20 and S21. The displacement of this layer along E4 is about 860m. The minor discontinuities have displacements ranging from 100-300m.

Profiles EW1, EW2, EW3a and EW4 are difficult to interpret due to lack of closely spaced "deep" electrical resistivity soundings. However, all sections have four layered models showing similar properties to the sections south of E4. The differences in layer parameters involve the depths to the various interfaces. These are attributed to the effects of faulting. All the geolectric sections can be interpreted as representing a series of horst and graben structures extending eastwards from the flanks of the Mau escarpment. The horst structures are represented by the resistivity highs and from 1-D modelling may appear to be dome structures. The graben structures represent permeable areas. An anomalous resistive layer of limited extent is found around S11 and S18. This could represent rhyolite from the Oloserian dome that has not been altered. The N-S discontinuities in the northern section of the area are continuations from the southern section (with a slight offset on E4). N1 passes to the west of OW301 while N2 passes through the Olkaria volcano. N3 continues northwards into the Ololbutot fault. The discontinuities marked N4 and N5 on profile EW1 are not observed in the southern part of E4. This could be due to a displacement on E4.

The results from bore-holes in the Olkaria region indicate that the first decrease in resistivity corresponds to the top of the steam zone. For instance C1524 near S19 shows the top as 158 m while at X2 the top is at approximately 170m. Results from OW301 show that the first conductive layer corresponds to the surficial reservoir.

5.1.3 Gravity Interpretation

The gravity data used was obtained from the Ministry of Energy (Kenya). Since there is little data in the present study area , a simple qualitative and quantitative analysis was attempted. The Bouguer anomaly map (Fig. 5.9a) of the area between the southern end of Hell's Gate and the foot of Mt. Suswa shows a general negative anomaly with a north-south trend. If a regional gravity value of -175 mgals is assumed, three positive anomalies

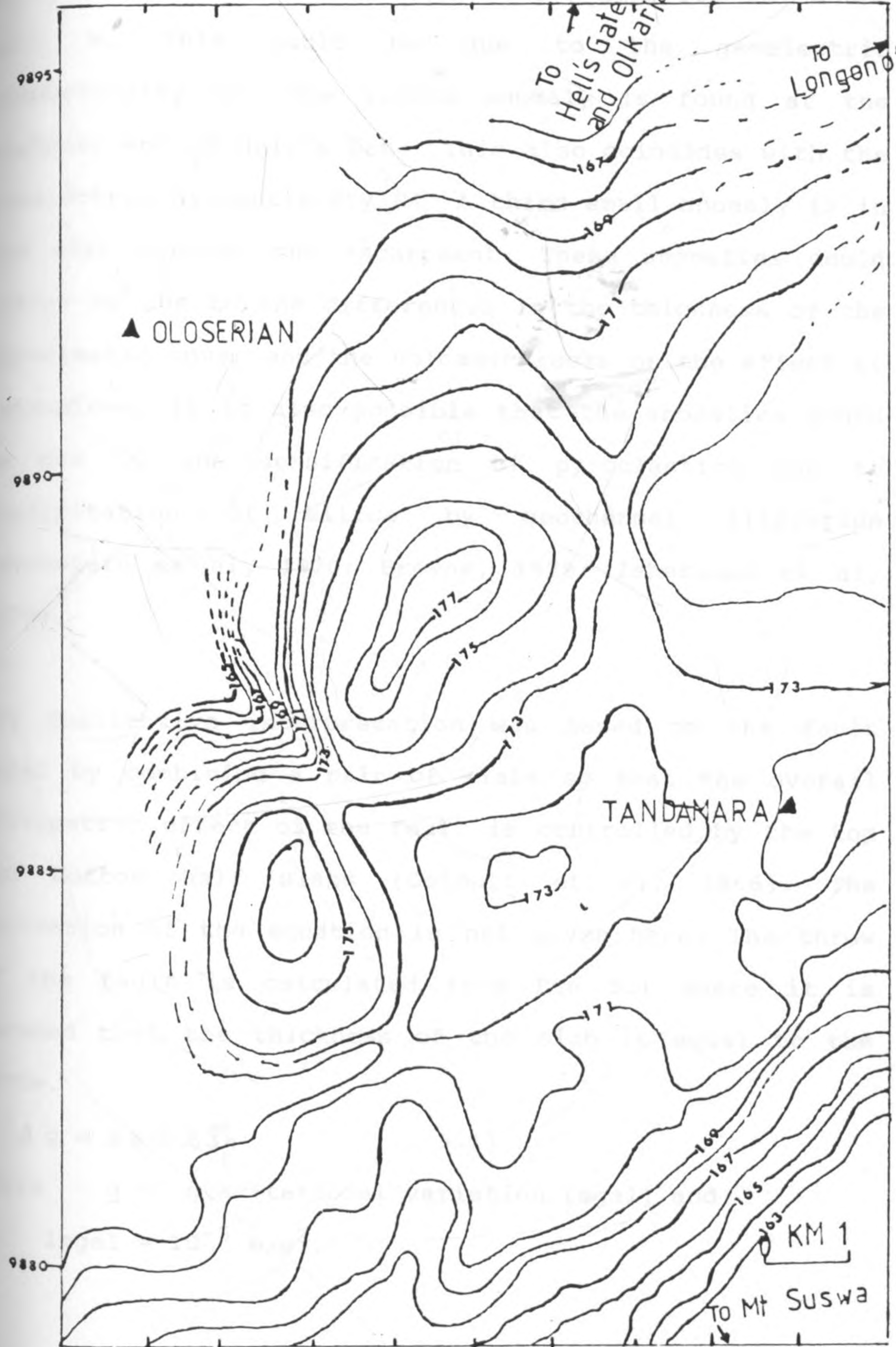

Fig. 5.9a. Bouguer anomaly map covering the southern part of the Suswa-Olkaria region

may be identified. The first anomaly is towards the foot of Mt. Suswa. The shape of gravity contours coincides with that observed on the resistivity maps for 750 m and 2000 m. This could be due to the geoelectric discontinuity E7. The second anomaly is found at the southern end of Hell's Gate. This also coincides with the geoelectric discontinuity E4. A third small anomaly is in the west towards the escarpment. These anomalies could either be due to the differences in the thickness of the pyroclastic cover and the volcanic rocks or the effect of intrusions. It is also possible that the anomalies could be due to the densification of pyroclastics due to precipitation of silica by geothermal alteration (Hochstein et al, 1970; Browne, 1978; Isherwood et al, 1978).

The qualitative interpretation was based on the fault model by combining a pair of slabs so that the overall gravimetric effect of the fault is controlled by the top and bottom half slabs (Geldart et al, 1966). The derivation of the equation is not given here. The throw of the fault is calculated from Eqn 5.1 where it is assumed that the thickness of the slab is equal to the throw.

$$\Delta g = 2\pi G \Delta\rho h \qquad 5.1)$$

where g = gravitational variation (mgal) and

1mgal = 10^{-5} m/s^2.

G = Universal gravitational constant ($m^3kg^{-1}S^{-1}$)

h = thickness of slab (m)

$\Delta\rho$ = density contrast (Kgm^{-3})

qn 5.1 can be written as

$$\Delta g = 419 \times 10^{-12} h$$

density contrast of 300kg/m^3 was used to represent the ontrast between the pyroclastics (intercalated with uffs) and the volcanic rocks. The density of 2,400 g./m^3 was assumed to represent the average density of he pyroclastics and the surficial volcanics. The density f 2,700 kg/m^3 represents arbitrary value of the effects f intrusives (2,900 kg/m^3) and the volcanic rocks of the lectrical "basement".

he gravity section (Fig. 5.9b) covers the region between 19 and S14 along the profile NS6. The discontinuities oincide with those obtained from the resistivity model Fig. 5.9c). From Eqn 5.2, the discontinuity E4 has a hrow of 795m (Δg = 10 mgal) with E5 and E6 both having a hrow of approximately 160m.

lthough there is some agreement between the gravity and lectrical resistivity data, a detailed model of gravity nterpretation would include the effects of intrusions. he available data is not enough for detailed modelling.

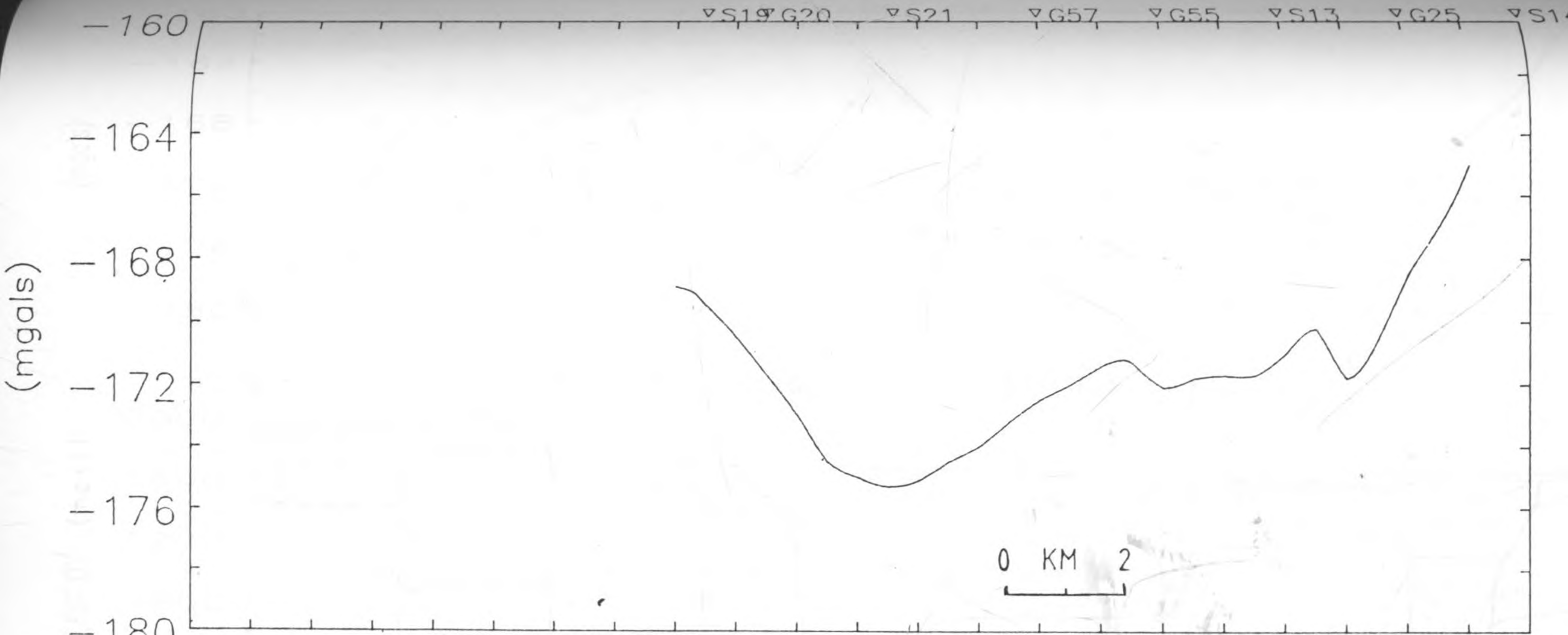

Fig. 5.9b Bouguer between S19 and S14 along profile NS 6

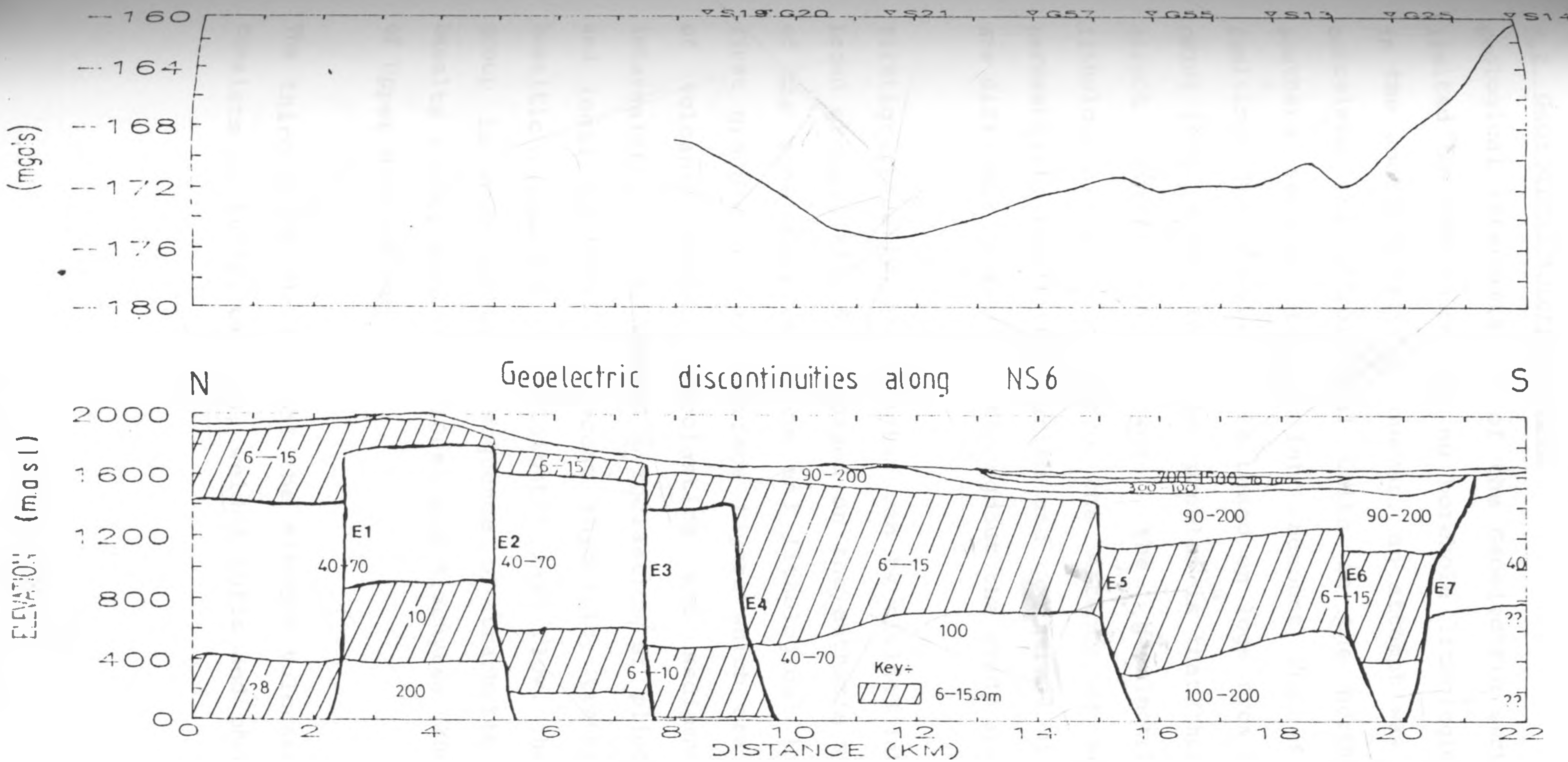

Fig. 5.9c.Correlation of the bouguer anomaly and the geoelectric discontinuities along NS6

5.2 Geological Interpretation

Geological interpretation of the Geoelectric sections is limited because there are no borehole lithological logs in the southern region. However, an attempt was made to correlate the lithological units in the northern and southern sections taking into account the effect of faulting. The correlation is based on logs from OW19 and OW301 (Fig. 5.10). The major problem is that there is no direct correlation between the geoelectric and lithological logs and also the effects of secondary permeability due to fracturing and geothermal alteration are difficult to evaluate throughout the study area.

Stratigraphically, this region can be divided into three broad groups (Fig. 5.11) based on the author's synthesis of the geoelectric sections and lithological logs. The first group covers the surface layers which are made up of volcanic soils, pyroclastics and sediments with intercalated tuffs, welded pyroclastics of pliocene age and local exposures of recent rhyolitic, trachytic and basaltic flows e.g. the Ololbutot lava flow. The second group is made up of a sequence of trachytes (300m), basalts (300m) rhyolites (100m) and trachytes (400m), all of Upper Miocene age.

The third group consists of the Miocene Volcanics which consists of tuffs, basalts, welded tuffs and phonolites.

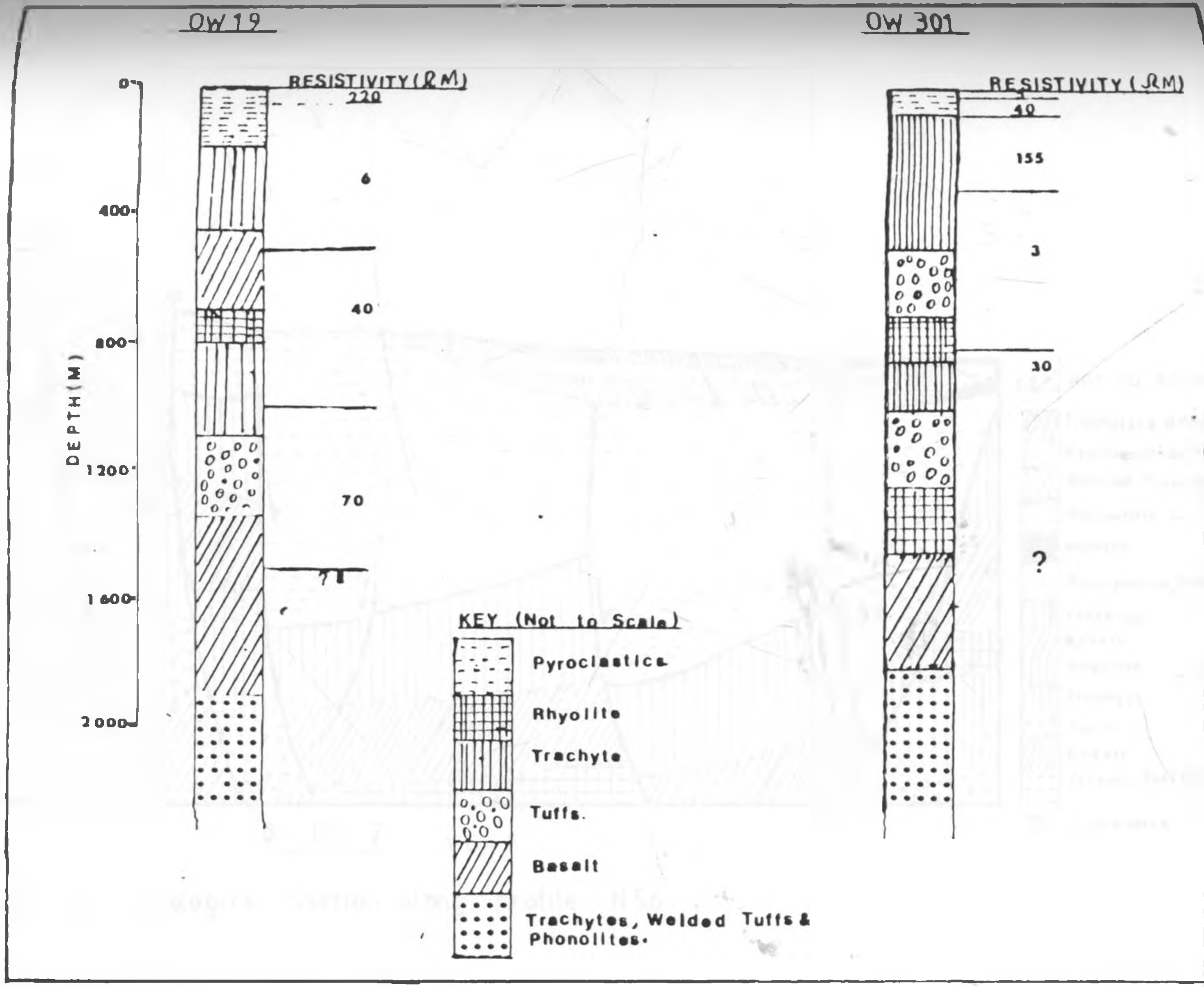

Fig 5.10 Lithological and Resistivity Logs for Wells OW 19 (Odongo 1981) and 301 (Muchemi 1984)

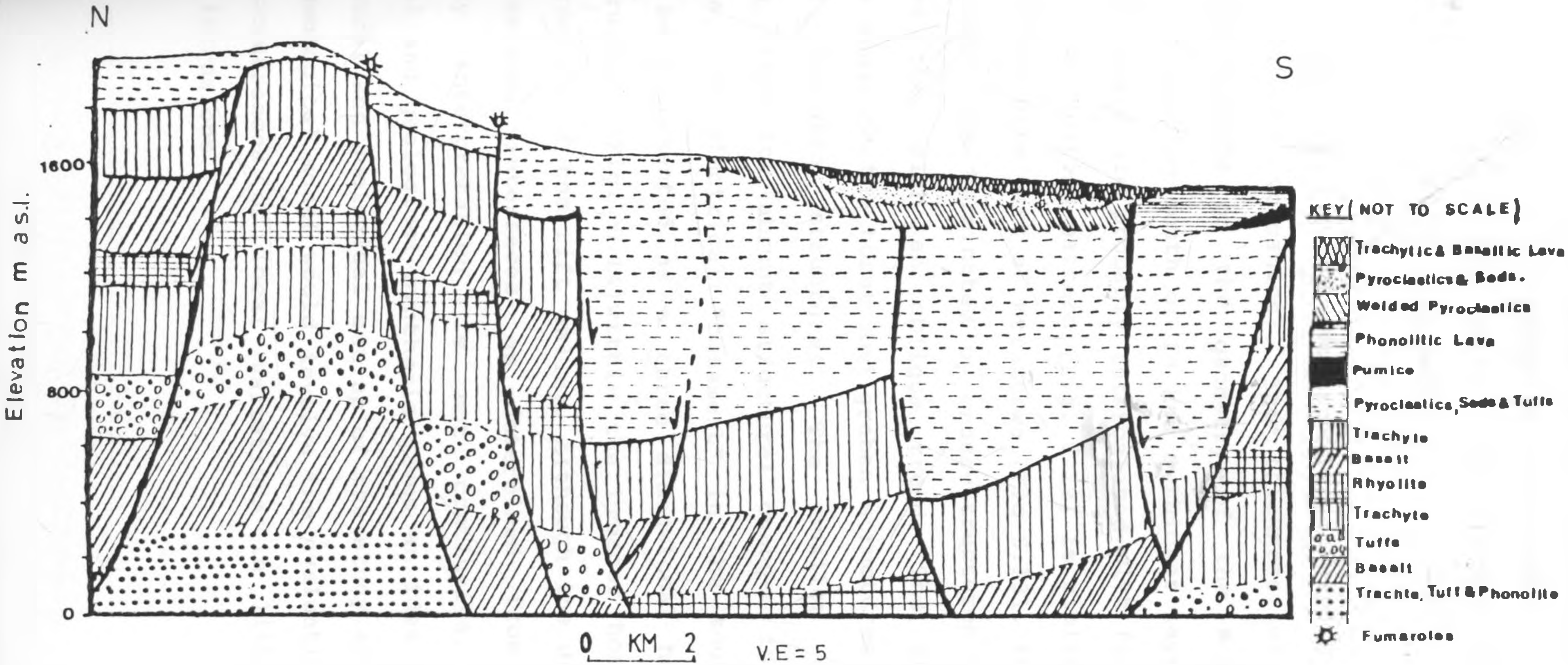

Fig. 5.11 Geological Section along profile NS6.

In the Olkaria region the third group constitutes the electrical "basement". This group is much deeper in the southern region so that here, the second group constitutes the electrical "basement".

Faulting has mainly affected the second and third groups (Miocene- Pliocene volcanics). The thickness of the pyroclastics depends on the geometry of the Miocene faulting. The section south of E4 has a thicker layer of pyroclastics which are probably intercalated with fluvial sediments. The faulting pattern (Fig. 5.12) is similar to that in the southern part of Mt. Suswa (Fig 5.13). The NS trending faults are terminated by cross-structures which cut across them with an oblique trend. The cross-structures separate the horst and graben structures into individual isolated structures. The smaller cross structures allow for abrupt structural changes in the study area. The electrical "basement" in the southern part may be represented as a three dimensional horst-graben structure (Fig. 5.14)within the broader horst - graben structure of the rift valley. Although the depths to the various interfaces as determined from the resistivity interpretation is not conclusive, the geophysical and geological synthesis gives an idea about the structural and geological set up of the study area. A detailed geological model would involve the evaluation of all the occurrences of local variations in lithology caused by intrusions.

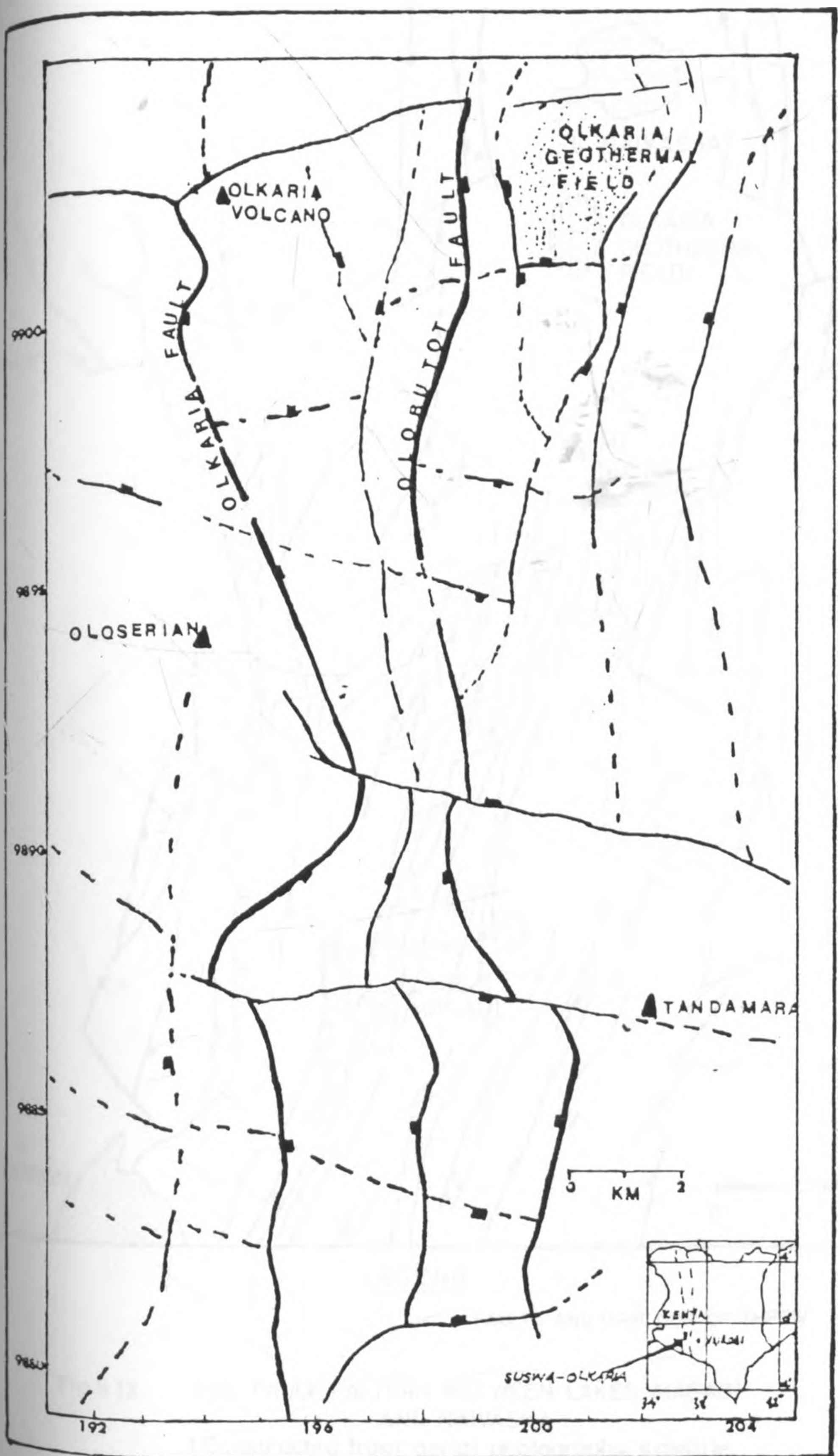

Direction of throw on faults,

Inferred Faults

Fig. 5.12 Faulting pattern beneath the pyroclastics in the Suswa-Olkaria region.

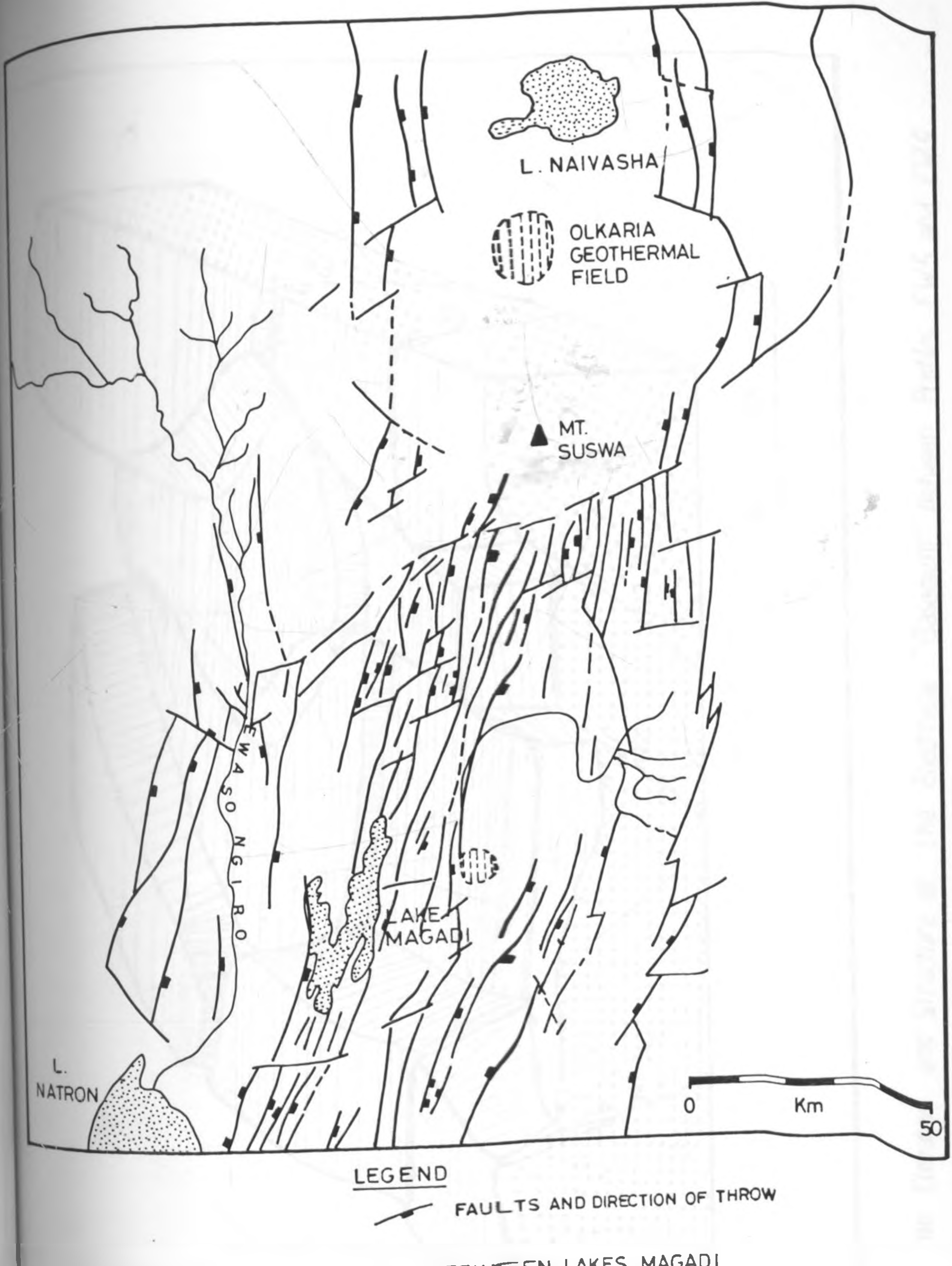

Fig.5.13 THE FAULT PATTERN BETWEEN LAKES MAGADI AND NAIVASHA
(Constructed from aerial photographs, satellite imagery and geological maps)

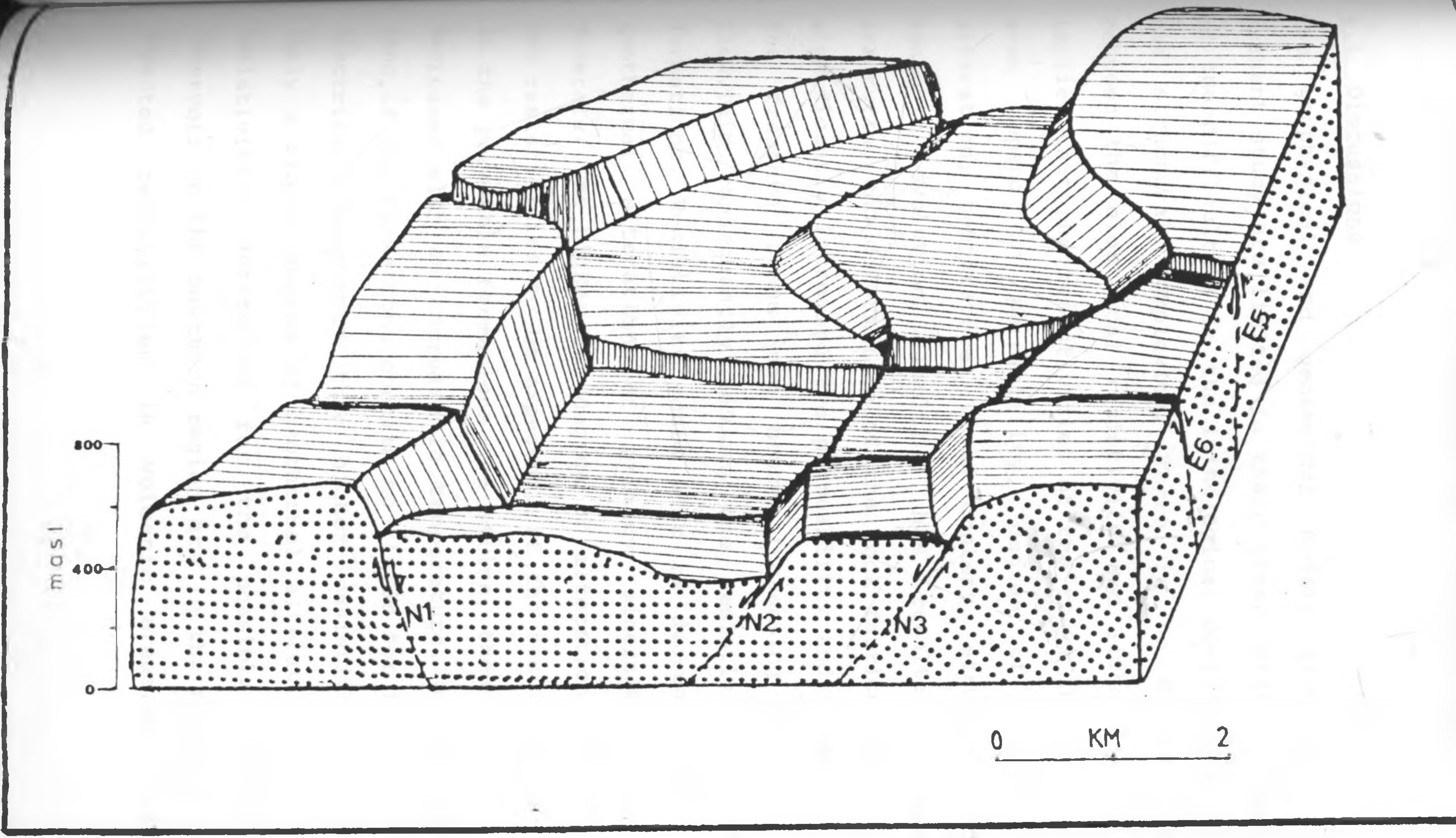

Fig. 5.14 Showing the Elevation and Structure of the Electrical "Basement" between Profiles EW5 and EW9

CHAPTER 6

DISCUSSIONS, CONCLUSIONS AND RECOMMENDATIONS

6.1 Discussions

The geophysical and geological models given in the present study are limited in their finer details because of the difficulties in the lithological correlations and the structural complexity. There is no direct link between the electrical resistivity and lithology. This implies that the resistivities of the rocks in the study area depend on permeability, degree of geothermal alteration, temperature, fluid content, structural and tectonic evolution. Faulting has resulted in the fracturing and deformation of the rock fabrics. This has significantly increased the permeability and porosity in the fracture zones and hence increasing the fluid flow.This consequently reduces the resistivity of the formations. Resistivity could also be decreased by the geothermal alteration of primary minerals to clay minerals. The higher the degree of alteration, the lower the resistivities to be expected. If the fluids contained in the permeable formations are saline, then resistivity decreases with an increase in temperature. On the other hand,if the formations contain no fluids for instance the electrical "basement" then higher resistivities might imply a higher degree of geothermal alteration. The low resistivities determined for the possible geothermal reservoir in the southern region are in the range of the expected resistivities in volcanic areas.The higher resistivities for the geothermal reservoir in the eastern part of Olkaria have been attributed to a lower degree of geothermal alteration than in the western part around OW301 (Mwangi 1986). If similar considerations apply to the present area of study then the higher resistivities of the conductive layer towards the escarpment in the southern region may be attributed to a lower degree of geothermal alteration. It is also possible that the low resistivity layer around OW301 extends both to the west and south of the present study area . This layer might represent the site of widespread fluvial and lacustrine sedimentation during the downwarping stage of the rift formation.

In Olkaria, the first near-surface reservoir found within the pyroclastics (intercalated with tuffs) and altered trachytes and basalts could be attributed to the interaction of meteoric water and steam flowing through the structures from the second deeper reservoir associated with tuffs and vesicular basalts. In terms of geothermal potential, the thick pyroclastic layer and altered trachyte in the southern region would constitute the geothermal reservoir. The latter can be modelled as a convective cell that is overpressurised (Etheridge et al 1983). The convective cell might be due to circulation of fluids in the faults and fractures within the conductive layer (reservoir). The closure of this system would be formed by the transfer faults E4 and E7 and the NS trending faults. The fault zones could also be areas of repetitive tectonic activity, surface erosion and deposition. This implies that they would be areas of complex fluid migration as well as recharge zones for the convective cell. The fumaroles and steam vents represent areas of vertical fluid migration to the surface.

From the structural point of view, the Olkaria geothermal field lies within a graben structure bound on all sides by horst structures. Difficulties arise from trying to fit the horst-graben structure into the ring structure suggested by Naylor (1972). The centers of volcanic eruptions seem to occur at fracture zones formed by the intersections of NS and oblique EW trending faults rather than on the rims of the ring structure. The major eruptive centres occur at the intersection of the major NS and EW trading faults. The fault geometry could either be described by the listric (Gibbs 1983, 1984a and b) or the linked fault models (Chapman and williams 1984) (Fig. 6.1a and b). The listric model implies that extensive internal deformation should occur within the listric fault block.

The main problem with this model is that rift blocks tend to rotate as coherent, relatively undeformed units. The model can be used to estimate the depth to the detachment by dividing the rift basin cross-section area by the surface extension (e). The linked fault model may incorporate rigidly rotating fault blocks. The displacement on the major fault (dt) is equal to the sum

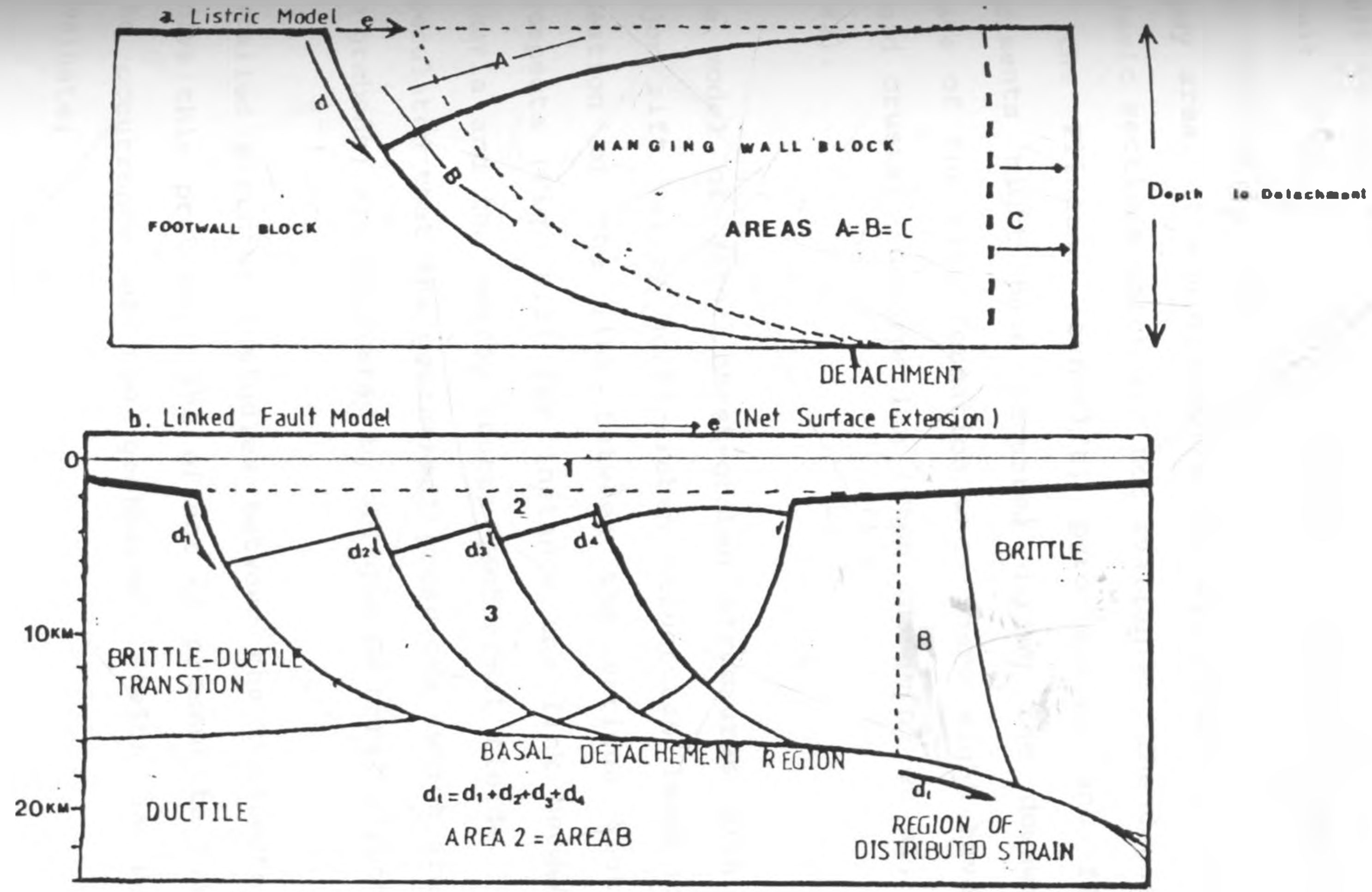

1 - Thermal Subsidence Phase.

2 - Syn-rift Volcanics and Sediments.

3 - Pre-rift Formations.

Fig 6.1 Listric and Linked Fault Models. (Gibbs 1983, 1984 and Chapman et al 1984) of the displacements on individual listrics (d1, d2 ...). This model implies that the displacement on the master fault is more than the net surface extension (e) and as a result of this, there is shearing in the rock units above the detachment. As to which model is applicable in the study area, it would require the evaluation of detailed seismic sections which are not available. The deposition of the Pliocene (syn-rift) pyroclastics and fluvial sediments might have occurred during the downwarping stage of the rift formation when there might have been broad crustal deformation (Chen Changming et al, 1981, 1982).

The model of minor horst-graben structures within the major rift valley horst-graben structures leads to the question of the link between the various geothermal prospects (Fig. 6.2) for instance the link between the Olkaria and the nearby Eburru geothermal fields. It is speculated that the geothermal prospects (which are found in grabens) are separated by oblique EW horst structures.

Detailed structural studies between the prospects might solve this problem. The effect of present tectonism on the occurrence of the geothermal fields is hard to evaluate.

Although the resistivity models give an indication of faults, alteration and the presence of fluids and the gravity model an indication of the structure and possible

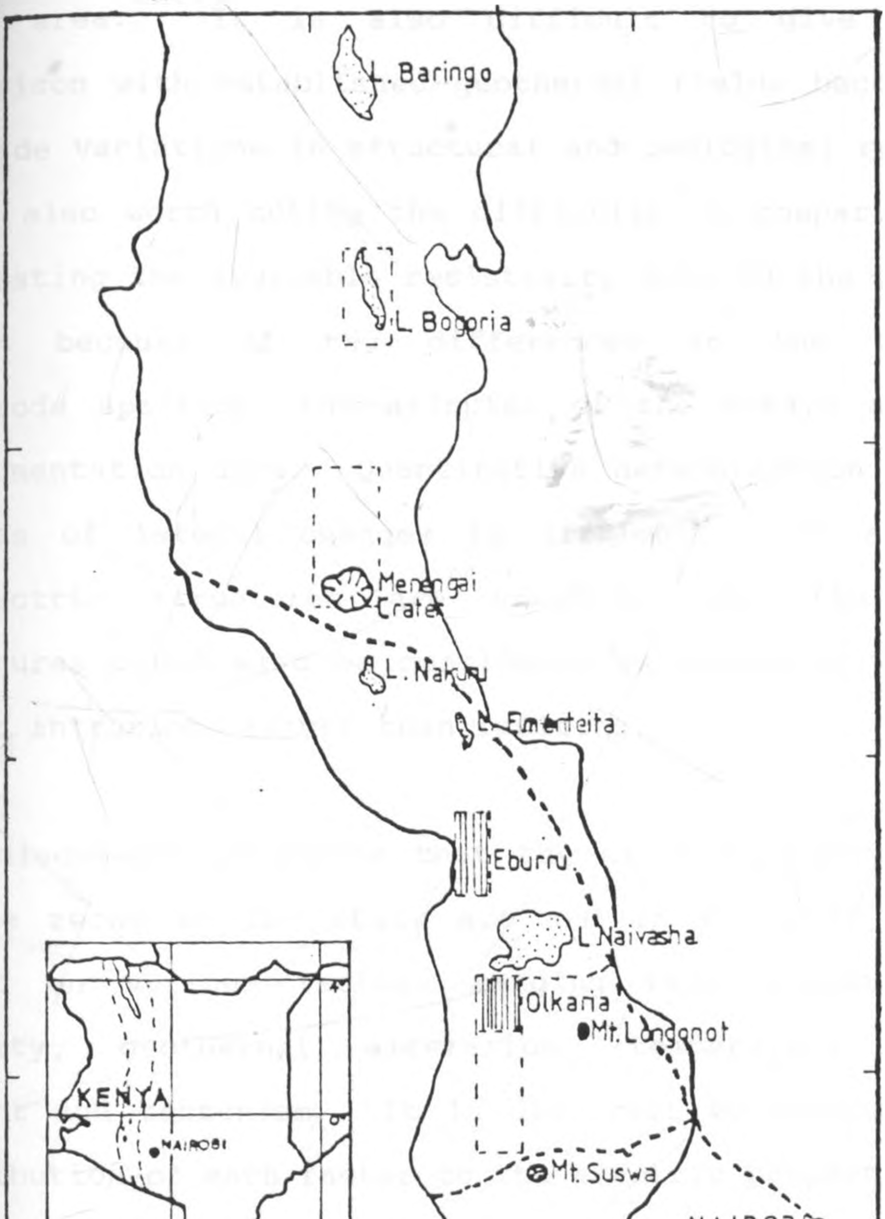

Fig. 6.2 Location of geothermal prospects in the Kenya Rift Valley. (Modified from Bhogal 1978)

effects of densification of rock formations, the data are not sufficient to give a detailed geothermal model in the study area. It is also difficult to give direct comparison with established geothermal fields because of the wide variations in structural and geological regimes. It is also worth noting the difficulty in comparing and contrasting the available resistivity data in the Olkaria region because of the differences in the current electrode spacings, the azimuths of the arrays and the instrumentation used. Quantitative determination of the effects of lateral changes is difficult. If all the geoelectric structures are smoothed out, the horst structures could also be considered as doming structures due to intrusions rather than faulting.

This discussion indicates that the electrical properties of the rocks in the study are and in the rift valley depend on various factors ranging from permeability, porosity, geothermal alteration, temperature, fluid content and tectonism. It is difficult to evaluate the contribution of each factor to the electric properties.

6.2 Conclusions

The electrical resistivity study has helped to throw some light onto the complex structural nature of the study area. Generalised models have been given to illustrate the variation in layer parameters. It is evident that the structural pattern of the rift floor cannot be considered to be uniform throughout.

The study has shown that;

a) The structural and tectonic evolution of the area has affected the resistivities of the rock formations.

b There are three broad electrical units in the study area i.e. the overburden (high resistivity), the potential reservoir (low resistivity) and the electrical "basement" (high resistivity).

c) The graben structures offer good prospects for potential geothermal fields. Three such areas are found around the Olkaria geothermal field, in the west around OW 301 and to the south of Njorowa gorge around Tandamara.

d) The discontinuities observed in the Olkaria region continue southwards and are occasionally interrupted by oblique E-W trending cross-structures. The discontinuities coincide with faults and act as either recharge zones or areas of complex fluid migration.

6.3 Recommendations

Further geophysical work should be carried out to determine the possible causes of the low resistivity layer extending towards the Mau-escarpment. This work should try to establish the exact locations of the discontinuities observed in the present study area. Teleseismic and Magnetotelluric studies should be carried out to establish the deep structure of this area. Micro-earthquake monitoring should be carried out to locate any areas of active faulting while induced polarisation (IP) should give an indication of the mineralisation and degree of geothermal alteration. It would also be worthwhile to carry out studies to determine the effect of faults, and lateral changes on the shape of apparent resistivity curves obtained from long electrode spacing.

It is imperative that any further geophysical work should be augmented by drilling exploratory wells especially between OW 19 and S19, to the west of Tandamara and on the horst-like structure around S9 or S7. These wells should be drilled to depth of about 1500m.

REFERENCES

Anderson, W. L. 1979. Numerical integration of related Hankel transforms of orders 0 and 1 by adaptive digital filtering, Geophysics Vol 44, 1287-2305

Baker, B. H. 1958. Geology of the Magadi area, Kenya Geological Survey, Report No. 42, p. 81.

Baker, B. H. 1963. Geology of the area south of Magadi, Kenya Geological Survey, Report No. 61, p. 27.

Baker, B. H. 1986. Tectonics and volcanism of the southern Rift Valley and its influence on rift sedimentation, Geol. Soc. Special publication No. 25, p. 45-53.

Baker, B. H. and Wohlenberg, J. 1971. Structure and evolution of Kenya Rift Valley. Nature (London) Phys. Sci. No. 229, p. 538-542.

Baker, B. H., Mohr. P. a., and Williams, L. A. J. 1972 Geology of the Eastern Rift System of Africa, Geol. Soc. Amer. Spc. Paper, No. 136, p. 67.

Balfour, Beatty and Co. 1968. Electrical Resistivity Survey in the Kenya Rift Valley, unpublished report to the then East African Power and Lighting Co. Ltd.

Banwell, C. J. and MacDonald, W. J. P. 1965. Resistivity surveying in New Zealand thermal areas. Eighth Commonwealth Mining and Metallurgical Congress, Australia and New Zealand, New Zealand section, No. 213, p. 7.

Banwell, C. J. 1972. Geothermal resources exploration project, Kenya - Immediate report on visit to project area, unpublished report.

Bhatachyrya, P. K. and Patra, H. P. 1968. Direct current geoelectric sounding 1; N. Y. Elsevier Publishing Co.

Bhogal, P. S. 1978. The electrical resistivity method of geophysical prospecting and its applications to geothermal exploration in the Rift Valley of Kenya (PhD) Thesis U.O.N.

Bichara, M. and Lakshmanan, J. 1976. Fast automatic processing of resistivity soundings, Geophysical Prospecting 26, p. 241-857.

Bostick, F. X. 1977. A simple and almost exact method of MT analysis (abstract). Workshop on Electrical methods in Geothermal Exploration, Snowbird, Utah.

Breusse, J. J. and Mathiez, J. P. 1956. Application of the electrical prospecting to tectonics in the search for natural steam at Larderello (Italy). Geophysical Case Histories, 2. P. 623-630.

Browne, P.R.L. 1978. Hydrothermal alteration in active geothermal fields. Annual Review, Earth and Plan. Sci.,6, p. 229-250.

Compagnie Generale de Geophysique, 1963. Abaques de Sondage electrique, The Hague, E.A.E.G.

Chapman, T. J. and Williams, G. D. 1984. Displacement-distance in th analysis of fold-thrust structures and linked-fault system, Jour. Geol. Soc. London, 141, p.121-128.

Chen, C., Chen, J., X., Chen, R. and Lili, 1981. Evolution of sedimentary tectonics of Bohai Rift System and its bearing on hydrocarbon accumulation Sci. Sin. Peking 24, p. 521-529.

Chen C., Huang, J., Chen, J. and Tian, X. 192. Depositional models of Tertiary rift basins. Eastern China and their application in oil and gas prediction, Ins. Geol. Acad, Sin. Res. Geol. p. 141-148.

Clarke, M. C. G. 1987. Compilation and interpretation of rock geochemical data for the Longonot and Greater Olkaria volcanic centres. British Geological Survey.

Davis, P. A. 1979. Development and application of resistivity inversion for several field arrays, Ms Thesis, University of Minnesota.

Davis, P. A., Greenhalgh, S. A. and Merrick, N. P. 1980. Resistivity sounding computations with any array using a single digital filter, Bulletin of the Australian Society of Exploration Geophysics 11, 54-62.

Duprat, A. 1970. Contribution de la geophisque a l'etude de la region geothermique de Denizli-Saraykoy (Turque), U. N. Symp. Development Geothermal Resources, Pisa.

Etheridge, M. A. Wall, V. J. and Vernon, R. H. 1983. The role of fluid phase during regional metamorphism and deformation, Journ, Met. Geol. 1, p. 205-226.

Foster, M. 1961. An application of the Wenner-Kolmogorov smoothing theory to matrix inversion, Journal of the Society for Industrial and Applied Mathematics 9, 387-392.

Furgerson, R. B. 1972. Electrical Resistivity Survey of the Olkaria Prospect, Kenya E. A. P. & L. Geothermal exploration project.

Geldart, L. P., Gill, D. E. and Sharma, B. 1966. Gravity anomalies of two-dimensional faults. Geophysics 31, p. 372-97.

Ghosh, D. P, 1971a. The application of filter theory to the direct interpretation of geoelectrical resistivity sounding measurements, Geophysical Prospecting 19. p. 192-217.

Ghosh, D. P. 1971b. Inverse filter coefficients for the computation of apparent resistivity standard curves for a horizontally stratified earth, Geophysical Prospecting 19, p. 769-775.

Gibbs, A. D. 1983. Balanced cross-section construction from seismic sections in areas of extensional tectonics. Journ. Struct. Geol. 5, . 253-260.

Gibbs, A. D, 1984a. Structural evolution of extensional basin Margins. Jour. Geol. Soc. London. 141, p. 609-620.

Gibbs, A. D, 1984b. Clyde Field growth fault secondary detachment above basement faults in North Sea. Amer. Ass. Pet. Geol. Bull., 68, p. 1029-1039.

Goldstein, N. E. and Razo, A. 1980. General overview of Geophysical studies at Cerro Prieto, Geothermics 9, no. 1/2. p. 1-5.

Grant, F. S. and West, G. F. 1965. Interpretation theory in applied geophysics, New York, McGraw-Hill.

Group Seven Inc. 1971. Electrical resistivity survey in the Rift Valley of Kenya; unpublished report to the UNDP/EAPL Project.

Hamilton, R. M., Smith B. E. and Knopp, F. 1973. Earthquakes in geothermal areas near Lakes Naivasha and Hannington, Kenya, unpublished report to UNDP/EAPL Project.

Hochstein M. P. and Hunt, T. M., 1970. Seismic, gravity and magnetic studies, Broadlands geothermal field, new Zealand. U. N. Symp. on Development and utilisation of Geothermal resources, Pisa.

Hochstein, M. P. 1971. Reinterpretation of a resistivity survey of the Kenya Rift Valley between Lakes Naivasha and Bogoria, Kenya; unpublished report to the UNDP/EAPL Project.

Hochstein, M. P. 1975a. Geophysical exploration of the El Tatio geothermal field (Northern Chile), Second U. N. sump on the development and use of geothermal resources, San Francisco.

Hochstein, M. P. 1976b. Geophysical exploration of the Kawah Kamojang geothermal field (West Java), Second U. N. Sump on the development and use of geothermal resources, San Francisco.

Hoel, A. E. and Kennard, R. W. 1970. Ridge regression: Biased estimation for non orthogonal problems, Technometrices, 12, p. 55 - 67.

Hoversten, G. M., Dey, A, A. and Morrison, H. F., 1982. Comparison of five least-squares inversion techniques in resistivity sounding, Geophys. Prosps. 30, 668-715.

Hummel, J. N. 1932. A theoretical study of apparent resistivity in surface potential methods, Geophys. Pros. Trans. Am. Inst. Mining Met. Eng. 97, p. 392 - 422.

Inman, J. R., Ryu, J. and Ward S. H., 1973. Resistivity inversion, Geophysics 38, p. 1088 - 1108.

Isherwood, W. F. and Mabey, D. R., 1978. Evaluation of Baltzor known geothermal resource area, Nevada. Geothermics 7, p. 221-229.

Johansen, H.K. 1977. A man computer interpretation system for resistivity soundings over a horizontally stratified earth. Geophys. prosp. 25, p.667-691

Johansen, H. K. and Sorensen, K. 1979. Fast Hankel transforms, Geophy. Pros 27, op. 376-901.

Keller, G. V. and Frischknecht, F. C. 1966. Electrical methods in geophysical prospecting, Pergammon Press, New York.

Keller, G. V., 1972. Electrical resistivity survey of the Kenya Rift Valley, unpublished report to the UNDP/EAPL Project.

Khan, M.A. and the Krisp Working Group; 1987. Structure of Kenya Rift from seismic refraction. Nature 26. No. 6101, p. 239-247.

Koefoed, O., 1965. Direct Methods of interpreting resistivity observation, Geophys. Pros. 13, p. 568-591.

Koefoed, O., 1968. The application of kernel function in interpreting geoelectric measurements, Geoexploration Monographs, Series 1, No. 2, Stuggart; Gebruder Borntraeger.

Koefoed, O., 1969. An analysis of equivalence in resistivity sounding, Geophys. Pros. 17 p. 327-335.

Koefoed, O., 1970. A fast method for determining the layer distribution from the raised kernel function in geoelectrical sounding, Geophys. pros 24, p. 617-632.

Koefoed, O., 1976. An approximate method of resistivity sounding interpretation, Geophys. pros. 24, p. 617-632.

Koefoed, O., 1976. Recent developments in the direct interpretation of resistivity soundings, Geoexploration 14, p. 243-250.

Kunetz, G. and Rocroi, J. P. 1970. Traitment automatique des sondages electriques, Geophys. pros 18, p. 157 - 198.

Levenberg, R. E., 1944. A method for the solution of certain nonlinear problems in least squares. Quart. Appl. Math. 12, p. 164 - 168.

Logatchev, N. A, Beloussou, V. V and Milanovsky, E. E. 1972 East African Rift development, Tectonophysics 15, p. 71-81.

Maillet, R., 1947. The fundamental equations of electrical prospecting. Geophysics 12, p. 529 - 556.

Marquardt, D. W. 1970. Generalised inverses, ridge regression, biased linear estimation, and non-linear estimation, Tectonomentrics 12, p. 591-612.

Marsden, D. 1973. The automatic fitting of a resistivity sounding by a geometrical progression of depths, Geophys. Pros. 21, p. 266 - 280.

McCall, G. J. H. 1967. Geology of the Nakuru-Thompson's falls-Lake Hannington area. Kenya Geol. Survey report No. 78.

McEuen, R. B. 1970. Delineation of geothermal deposits by means of long spacing resistivity and airborne magnetics. U. N. Sump. Development and Utilization of Geothermal Resources, Pisa.

Meidav, T. 1972. Further interpretation of resistivity data and recommendations for follow-up work, Kenya geothermal exploration project; unpublished report to the UNDP/EAPL project.

Meinardus, H. A. 1970, Numerical interpretation of resistivity soundings over horizontal beds, Geophys. pro. 18, p. 415-433.

Meju, A. M. 1988. The deep electrical structure of the great glen fault, Scotland. PhD Thesis, University of Edinburgh.

Merrick, N. P. 1977. A computer program for the inversion of Schlumberger sounding curves in the apparent resistivity domain.Hydrogeological Report 1977/5. New South Wales Water Resources Commission, Sydney, Australia.

Mooney, H. M. and Wetzel, W. W. 1956. The potential about a point electrode and apparent resistivity curves Minneapolis, University of Minnesota Press.

Muchemi, G. G. A Geological report of well OW-301 KPL Report No. G1/OW/301/017.

Murakami, Y., and Uchinda, T. 1982. Accuracy of the linear filter coefficients determined by the iteration of the least-squares methods, Geophysics 47, p. 244-256.

Mwangi, M. N. 1986. Interpretation of additional sounding data at Olkaria, kenya Power Company Ltd. geothermal project report No. GP/OW/010.

Naylor, W. 1. 1972. The geology of Eburru and Olkaria geothermal prospects. Unpublished report to the UNDP/EAPL Geothermal Exploration project.

Ndombi, J. M. 1981. The Structure of the shallow crust beneath the Olkaria geothermal field, Kenya deduced from gravity studies, Jour. Volcanol. Geotherm. Res. 9, p. 237-251.

Niwas, S. and Israil, M. A. 1987. A simple method of interpretation of resistivity sounding data using exponential approximation of the Kernel function. Geophys. pros, 35, p. 548-567.

Nyman, D. C. and Lindisman, M. 1977. Ves dipole-dipole filter coefficients, Geophysics, 42, p. 1037-1044.

Odongo M. E. O. 1981. A geological report of well OW-19 KPL. report no. GL/OW/19/010.

O'Neill, D. J. 1975. Improved linear filter coefficients for application in apparent computations, Bulletin of the Australian Society of Exploration Geophysics 6, p. 104-109.

O.Neill, D. J. and Merrick, N. P. 1984. a digital linear filter for resistivity sounding with a generalised electrode array, Geophys. Pros. 32, p. 105-123.

Orellana, E. and Mooney, H. H. 1966. Master tables and curves for vertical electrical sounding over layered structures, Interciencia, Madrid.

Parasnis, D. S. 1972. Principal of Applied Geophysics, Methuen & Co. Ltd.

Patrick, F. W. and Bostick, F. X. (Jr.) 1969. Magnetotelluric modelling techniques. Elec. Geophys. Res. Lab. Univ. of Texas, Tech. Report 59.

keris, C. K. 1940. Direct method of interpretation in resistivity prospecting, Geophysics 5, p. 31-42.

azo, A., Arellono, F. and Fonseca, H. 1980. Resistivity studies at Cerro Prieto, Geothermics 9 (1/2), p. 7 - 14.

ijo, L., Pelton, W. H., Feitosa E. C. and Ward, S. H. 1977. The interpretation of apparent resistivity data from Apodi Valley, Rio Grande de Norte, Brasil Geophysics 92, 9, p. 811-822.

ijkwaterstaat, 1979. standard graphs for resistivity prospecting, European Association of Exploration Geophysics.

isk, G. F., Macdonald, W. J. P., and Dawson, G. B. 1970. D. C. resistivity survey of the Broadlands geothermal region, New Zealand, Geothermics, special issue 2, 2, p. 287-294.

aggerson, E. P. 1970. The structural control and genesis of alkaline rocks in Central Kenya. Bull. Volcanic 34 (1), p. 38-76.

cot, J. 1953. The Great Rift Valley and its economic possibilities in the Press (Nairobi).

inner, N. J. 1977. Recent geophysical studies of the Kenya Rift Valley, Contemp. Phys., p. 455-470.

ichter, L.B. 1937. The interpretation of the resistivity prospecting methods for horizontal structures, Physics, 4, 307-322.

tanley, W. D., Jackson, D.B. and Zohdy A. A. R. 1976. the deep electrical investigations in the long Valley geothermal area, California. Journal of Geophysics Res. 81, p. 810-820.

Stefanesco, S. S., Schlumberger, C., and Schlumberger, M. 1930 Sur la distribution electrique potentielle autour d'une prix de terre ponctuelle dans un terrain a couches horizontals, homogenes, et isotropes, journal de physique et le Radium 1, p. 132-140.

Telford, W. M., Geldart, L. P., Sheriff, R. E., and Keys D. A. 1983. Applied Geophysics Cambridge University Press.

Thompson, A. D. and Dodson, R. G. 1963. Geology of Naivasha area, Kenya Geol. Survey, report no 55.

Torfason, H. 1987. Geothermal and geological survey of Mt. Suswa a UNDP technical report.

Tripp A. C., Ward S. H., Sill W. R., Swift C. M. and Petrick, W. R. 1978. Electromagnetic and schlumberger resistivity sounding in the Roosevelt Hot Spring Geophysics 43, No. 7, p. 1450-1469.

Van Nastrad, R. G. 1953, Limitation on resistivity methods as inferred from the buried sphere problem, Geophysics 18, p. 23-433.

Verdrintsev, G. A. 1963, Apparatus configuration for vertical electrical logging in Handbook of Geophysics, Tarkhov., A. G. editor Moscow, Gsotoptekhiadat.

William, L. A. F. 1969, Volcanic associations in the Great Rift Valley, East Africa. Nature (London) Phys. Sci. 224, p. 61-64.

Williams, L. A. J. 1970, The Volcanics of the Gregory Rift Valley, East Africa, Bull Volcanol 3, p. 439-465.

Woodhall, D. G. 1987, The geology of Longonot volcano, the Greater Olkaria Volcanic complex and adjacent areas. British Geological Survey.

Zohdy, A. A. R. 1965, the auxiliary point method of electrical sounding interpretation, and its relationship to the Dar Zarrouk parameters, Geophysics 30, p. 644-660.

Zohdy, A. A. R., Anderson, L. A. and Muffler, L. J. P. 1973, Resistivity, self-potential, and induced-polarisation surveys of a vapour-dominated geothermal system, Geophysics 38, p. 1130-1144.

APPENDIX A

Derivation of Filters

The choice of filters depends on the accuracy and economy of carrying out the analysis. Methods of filter design include the Wiener-Hopf least squares method which is preferable for low sampling rate filters (Koefoed 1979). It uses less computer memory and time than the Fourier transform method which is successful in producing filters with high sampling rates (long filters). Iteration on least squares method used in the program Resinv 88 improves the accuracy due to a reduction of oscillations in the filter tails and minimization of round-off errors (Murakami and Uchinda 1982). Other methods of filter design include the direct integration technique (Bichara and Lakshmanan 1976)and the modified Fourier transform method using a "Sinsh" interpolating function that removes the high frequency components of the filter (Johansen and Sorensen 1979).

Since the mathematical manipulations of filter designs are beyond the scope of the present study, an outline of the derivation of digital linear filters that map composite resistivity transforms to apparent resistivities assuming horizontal layering is given. Methods of filter designs depend on the Input functions (Eqn A1 and A2) that satisfy Eqn 2.8 (Chapter 2). The rapidly decaying Input Output functions (Anderson 1979) are inappropriate for the least square method since the calculated filter depends on the sampling interval chosen. For the O'Neill coefficients (O'Neill et al 1984) used in the present study, the Input-Output functions are based on those by Davis (1979). The filter length was truncated when the digital coefficients fell below 10^{-3} , 10^{-4} and 10^{-5}.

The input function I(y) is given as:

$$I(y) = [\exp(1-y) + \exp(-2y) /[15 \exp(\exp(-y)] \qquad A1$$

and the output function O(x) as:

$$O(x) = \exp(x) /15 (1+\exp(2x))^{2.5}] \qquad A2$$

From Eqn (2.8)

$r = \exp(x)$ and $d=\exp(-y)$

so that (2.8) becomes

$$V_{(r)} = 1/2\pi \quad r \int_{-\infty}^{\infty} T(y) f(x-y)\, dy$$

The filter function then has the form of

$$f(x-y) = \exp(x-y)\, J_0 [\exp(x-y)] \qquad A3$$

The above expressions can be manipulated mathematically so that Eqn. 2.8 is expressed as a convolution integral in a discrete form (Rijo et al 1977).

$$V_{(r)} = \frac{1}{2\pi r} \sum_{j=n_1}^{n_2} T(\ln r - nj) \cdot C(nj) \qquad A4$$

Where nj = filter coefficient abscissae

C(nj) = digital filter coefficients.

n_1 = number of coefficients to the left of the filter origin.

n_2 = number of coefficients to the right of the filter origin.

When the potential difference between potential electrodes is considered A4 becomes

$$\Delta V^i = \frac{1}{2\pi} \sum_{j=n_1}^{n_2} T_{ij} \cdot C_j \qquad A5$$

For the configuration used in the present study,

$$T_{ij} = T\left[\ln \frac{(AM)-nj}{(AM)^i}\right] - T\left[\ln \frac{(AN)^i - nj}{(AN)^i}\right] -$$

$$T\left[\ln \frac{(BM)^i - nj}{(BM)^i}\right] + T\left[\ln \frac{(BN)^i - nj}{(BN)^i}\right] \qquad A6$$

Where Tij is the composite transform function and C_j = C(nj).

These manipulations imply that apparent resistivity (Eqn 2.9) can be expressed as a linear function of resistivities obtained by a convolution of the filter with resistivity transforms. The resistivity transforms are divided by the inter-electrode distance before convolution with the filter to give an electric potential. The potentials for each electrode pairs are then added up to give a total potential difference which is converted to apparent resistivity by means of geometric factor.

A sampling interval of In 10/6 was used. For models with large resistivity contrasts, a sampling interval of ln 10/12 would be appropriate. This increases the computation time but it has a higher accuracy. The length of the filter is minimized when the coefficients coincide with the nodes at which the filter oscillates. For large negative and positive abscissae, the nodes are equally spaced at half the filter interval. The optimal abscissae are shifted relative to the origin by

$$X = [n - \phi(fn)/\pi] . \Delta x$$

where n = 0, 1, 2, ..., Δx = sampling interval, (fn) =phase of the filter at Nyquist frequency ($1/\Delta x$). In the program Resinv 88 (Appendix B) the shift used was 0.13069.

APPENDIX B

Program resinv 88

The details of the main programme and the sub-routines are found in the sub-titles in the listing below. The programme can be used for Schlumberger, Wenner or Bipole-Bipole arrays. The maximum number of iterations is set to fifteen but may be increased.

```
C    *****************************************************************
C
C          INVERSION AND MODELLING PROGRAM FOR USE WITH
C                        AMDAHL
C
C        ONLY 15 LAYERS  AND 29 DATA POINTS I.E. 5 DECADES
C    *****************************************************************

           INTEGER E,CHECK
             CHARACTER*50 TXT
           COMMON /Z1/E,M,N/Z2/DELX,SPAC/Z3/N3/Z4/I1,RMS,RMSC/Z5/IX
           COMMON /ZA1/ Q(65,30)/ZA2/Q1(32,30)/ZA4/R(31),R2(31)
           COMMON /ZA3/P(29)/ZA5/ R1(31),P1(29) /ZA6/SN(30)
           DIMENSION NF(29),X(29),XIN(31),YIN(31)

C    *****************************************************************
C
C           READ IN MODEL PARAMETERS AND DATA
C
C    *****************************************************************
          CALL EMAG3('DEFINE','7,RESINVOUT,,C',IFLAG)
           DELX = ALOG(10.)/6
  1030 FORMAT (I1)
  1031 FORMAT (I2)
  1032 FORMAT (F8.3)
    34 FORMAT(A60)
  2020   CONTINUE
           WRITE(*,34)('PROFILE 1=SCHLUM,2=WENNER,3=BI-BI
       1' FORMAT (I1)')
           READ (5,*) INDEX
           IF (INDEX.LE.0) STOP2
             READ(40,1080)TXT
1080           FORMAT(A50)
             READ(40,*)M
             M=MIN(M,31)
             WRITE(6,*)M
             DO 1081,I=1,M
             READ(40,*)XIN(I),YIN(I)
1081            WRITE(6,*)XIN(I),YIN(I)

C           WRITE(*,34) ('NO. OF ELECTRODE SPACINGS FORMAT (I2) ')
C           READ (*,1031) M
          M=MIN(M,31)
C          WRITE(*,34)(' TYPE IN ELECTRODE SPACINGS FORMAT (F8.3)')
C          READ(*,1032) (XIN(I),I=1,M)
C          WRITE(*,34)(' TYPE IN RESISTANCES FORMAT (F8.0) ')
C          READ(*,1032) (YIN(I),I=1,M)
         CALL SPLINE(M,XIN,YIN)
  2010     WRITE(*,34) ('NO. OF LAYERS FORMAT (I1) ')
           READ (5,*) E
          E=MIN(E,15)
           WRITE(*,34) ('NUMBER  OF FIXED PARMS FORMAT (I1) ')
           READ (5,*) NN
           IF (INDEX-2) 12,12,6
     6     WRITE(*,34) ('N-SPACING=1A=0 FORMAT (I1)')
           READ (5,*) IX
           IF (IX.EQ.1) GO TO 9
           J = 1
           GO TO 11
     9     J = M
    11     WRITE(*,34)('N-VALUE FORMAT (F8.3)')
           READ (*,1032) (SN(I),I=1,J)
           GO TO 512
    12     IX = -1
   512     N = 2*E-1
C            SPAC = ALOG (SPAC)
           WRITE(*,34)(' TYPE IN THICKNESSES OF',
       1' GUESSED STRUCTURE FORMAT (F8.3)')
             READ(5,*)(P(I),I=1,E-1)
C            READ (*,1032) (P(I),I=1,E-1)
         WRITE(*,34) (' TYPE IN RESISTIVITIES FORMAT (F8.0) ')
C          READ(*,1032) (P(I),I=E,N)
           READ(5,*)(P(I),I=E,N)
            IF ( NN.LE.0) GOTO 40
         WRITE(*,34)('POSN IN LAYER PARMS LIST OF ANY FIXED PARMS',
       1' FORMAT (I2)')
           READ(5,*)(NF(I),I=1,NN)
C            READ (*,1031) (NF(I),I=1,NN)
    40     WRITE(*,34) ('%RMS CUTOFF FORMAT (F8.3)')
           READ(5,*)RMSC
C            READ (*,1032) RMSC
           IF (INDEX-2) 43,45,47
    43     WRITE (*,44)
    44     FORMAT (/,10X,' *SCHLUMBERGER ARRAY*')
           GO TO 52
    45     WRITE (*,46)
    46     FORMAT (/,10X,' *WENNER ARRAY*')
           GO TO 52
    47     WRITE (*,48)
    48     FORMAT (/,10X,' *BIPOLE-BIPOLE ARRAY*')
           IF (IX.NE.1)GOTO 50
           SP = EXP(SPAC)
           WRITE (*,49) SP
    49     FORMAT (/,15X,' BIPOLE A-SPACING = ',F6.2)
           GOTO 52
    50     WRITE (*,51) SN(1)
    51     FORMAT (/,15X,' BIPOLE N-SPACING',F6.2)
```

```
C
C       SET UP INITIAL VALUES FOR EPSILON INCREMENTS AND
C       DECREMENTS AND MAXIMUM NO. OF ITERATIONS.
C
C ******************************************************************
  52    I1 = 0
        U = 10.
        V = 1.5
  53    I1MAX = 15
        JMAX = 15
  60    K1 = 0
        J1 = 0
        IF (INDEX-2) 70,80,80
  70    CALL SCHLUM (K1)
        GO TO 100
  80    CALL WENBIP (K1,INDEX)
        IF (NN.LE.0) GO TO 100
        DO 90 I=1,NN
           K =NF(I)
           DO 90 J=1,M
  90       Q(J,K) = 0
 100    DO 120,I=1,M
           R(I) = Q(I,N+1)
           R1(I) = ALOG(R2(I)/R(I))
           DO 110 J = 1,N
 110          Q(I,J) =Q(I,J)/R(I)
 120    CONTINUE
        IF ( I1.GT.0) GOTO 170
C ******************************************************************
C
C                    COMPUTE SUM OF SQUARES
C
C ******************************************************************
        PHI = 0
        DO 130 I=1,M
           PHI = PHI+R1(I)**2
 130    CONTINUE
C ******************************************************************
C
C                    COMPUTE RMS %-AGE ERROR
C
C ******************************************************************
        RMS = 0
        DO 140 I = 1,M
 140    RMS = RMS+(1-R(I)/R2(I))**2
        RMS = 100.*SQRT(RMS/M)
        CALL OUTPUT
        IF (RMS.LE.RMSC) GOTO 1000
C ******************************************************************
C
C                    COMPUTE INITIAL EPSILON
C
C ******************************************************************
        E1 = 0
        DO 160 I = 1,M
           DO 150 J = 1,N
 150       E1 = E1 + Q(I,J)**2
 160    CONTINUE
        E1 = SQRT(E1/(M*N))
C ******************************************************************
C
C                    ORTHOGANAL FACTORISATION
C
C ******************************************************************
 170    CALL ORTH1
 180    CALL ORTH2(E1)
        CALL BAKSUB
        IF (NN.LE.0) GOTO200
        DO 190 I=1,NN
           J = NF(I)
           P1(J) = 0
 190    CONTINUE
 200    DO 210 I=1,N
           X(I) = P(I)
           P(I) = P(I) + P1(I)
           IF (P(I).LE.0) P(I) = 0.001
 210    CONTINUE
        K1 = 1
C ******************************************************************
C
C                    COMPUTE NEW MODEL APP. RESIS.
C
C ******************************************************************
        IF (INDEX-2) 220,230,230
 220    CALL SCHLUM (K1)
        GOTO 250
 230    CALL WENBIP(K1,INDEX)
C ******************************************************************
C
C                    COMPUTE NEW SUM OF SQUARES
C
C ******************************************************************
 250    PHI1 = 0
        DO 260 I = 1,M
           R(I) = Q(I,N+1)
           IF (R(I).LE.0) R(I) =0.001
           A = ALOG(R2(I)/R(I))
           PHI1 = PHI1+A**2
 260    CONTINUE
```

```
C  ***********************************************************
C
C                     COMPARE NEW AND OLD SUM OF SQUARES.
C                          AND INCREASE EPSILON
C
C  ***********************************************************
      IF (PHI1.LE.PHI) GO TO 280
      DO 275 I = 1,N
  275 P(I) = X(I)
      E1 = V*E1
      J1 = J1 + 1
      IF ( J1.LT.JMAX ) GOTO 180
      WRITE (*,277)
  277 FORMAT (/,' *J1 = JMAX...TRIAL MODEL WILL NOT CONVERGE* )
      CALL OUTPUT
      GO TO 1000
  280 PHI = PHI1
C  ***********************************************************
C
C                      COMPUTE NEW %-AGE RMS ERROR
C
C  ***********************************************************
      RMS = 0
      DO 290 I = 1,M
  290 RMS = RMS + (1-R(I)/R2(I))**2
      RMS = 100.*SQRT(RMS/M)
      I1 = I1 + 1
     WRITE(*,1002) I1,RMS
 1002 FORMAT (' ITERATION ',I4,' RMS ',F8.3)
      IF (RMS.LE.RMSC) GO TO320
      IF (I1.GE.I1MAX) GOTO 320
C  ***********************************************************
C
C                      COMPUTE NEW EPSILON
C
C  ***********************************************************
      IF (J1) 300,300,310
  300 E1 = E1/U
  310 GO TO 60
  320 CALL OUTPUT
C  ***********************************************************
C
C                 CHECKS INPUT FILE FOR MORE DATA
C                 IF THERE IS NONE IT STOPS.
C
C  ***********************************************************
 1000 WRITE(*,34)('0=STOP,1=NEWMODEL,2=NEW DATA SET,3=PRINTER',
     1' OUTPUT,4=NEW RMS FORMAT(I1)')
      READ (5,*) CHECK
      IF(CHECK.LE.0) STOP 3
      IF(CHECK.EQ.1) GOTO 2010
     IF(CHECK.EQ.2) GOTO 2020
     IF(CHECK.EQ.3) CALL PRNTER(TXT)
     IF(CHECK.EQ.3) GOTO 1000
     IF(CHECK.EQ.4) GOTO 40
      STOP4
      END
C  ***********************************************************
C
C            ********END OF MAIN PROGRAM********
C
C  ***********************************************************
      SUBROUTINE SCHLUM (K1)
      INTEGER E
      COMMON /Z1/E,M,N/Z2/DELX,SPAC
      COMMON /ZA1/Q(65,30)/ZA3/P(29)

      DIMENSION FLTR(29)
      DATA (FLTR(I),I=1,29)/.00046256,-.0010907,.0017122,
     2 -.0020687,.0043048,-.0021236,.015995,.017065,.098105,
     3 .21918,.64722,1.1415,.47819,-3.515,2.7743,-1.201,.4544,
     4 -.19427,.097364,-.054099,.031729,-.019109,.011656,
     5 -.0071544,.0044042,-.002715,.0016749,-.0010335,.00040124/
      Y = SPAC-19.*DELX-0.13069
      DO 20 I = 1,M+29
      CALL TRNSFM (Y,I,K1)
   20 Y = Y + DELX
      J = 1
      IF (K1.GT.0) J=N+1
      DO 30 I=J,N+1
   30 CALL FILTER (FLTR,29,I)
      RETURN
      END
      SUBROUTINE TRNSFM (Y,I,K1)
      INTEGER E
      COMMON /Z1/E,M,N
      COMMON /ZA1/Q(65,30)/ZA3/P(29)

      DIMENSION T(15)
      U = 1./EXP(Y)
      T(1) = P(N)
      IF(K1.LE.0) Q(I,N) = 1.
      DO 30 J=2,E
      A = -2.*U*P(E+1-J)
      IF (A.GT.40..OR.A.LT.-40.) THEN
         A = 0.
      ELSE
         A = EXP(A)
```

```
      ENDIF
      B = (1.-A)/(1.+A)
      RB = P(N+1-J)
      TPR = RS*B
      T(J) = (TPR+T(J-1))/(1.+TPR*T(J-1)/RS**2)
      IF(K1.GT.0) GOTO 30
      C = T(J-1)/RS
      D = (1.+B*C)**2
      Q(I,N+1-J) = (B*(1.-C*C)+2.*B*T(J-1)*(T(J-1)+TPR)/(RS**2))/D
      Q(I,E+1-J) = ((4.*U*RS*A/((1.+A)**2))*(1.-C*C))/D
      AA = (1.-B*B)/D
      DO 20 K = (E+2-J),E
         IF(K.GE.E) GOTO 20
         Q(I,K) = Q(I,K)*AA
20       Q(I,K+E-1) = Q(I,K+E-1)*AA
30    CONTINUE
      Q(I,N+1) = T(E)
      RETURN
      END
      SUBROUTINE FILTER(FLTR,K,L)
      INTEGER E
      COMMON /Z1/ E,M,N
      COMMON /ZA1/Q(65,30)

      DIMENSION RES(31),FLTR(K)
      DO 20 I = 1,M
      RE = 0
      DO 10 J = 1,K
      R = FLTR(J) * Q(I +K-J,L)
10    RE = RE + R
20    RES(I) = RE
      DO 30 I = 1,M
30    Q(I,L) = RES(I)
      RETURN
      END
      SUBROUTINE ORTH1

      INTEGER E

      COMMON /Z1/ E,M,N/Z3/N3..
      COMMON /ZA1/ Q(65,30)

      N3 = N
      IF (M.EQ.N) N3 = N-1
      DO 60 I = 1,N3
      I2 = I + 1
      S3 = 0
      DO 10 J = I,M
10    S3 = S3 + Q(J,I)**2
      IF (S3.EQ.0) GO TO 60
      S3 = SQRT(S3)
      IF (Q(I,I).GT.0) S3 = -S3
      S4 = 1/SQRT(2*S3*(S3-Q(I,I)))
      DO 20 J = I2,M
20    Q(J,I) = -S4*Q(J,I)
      Q(M+1,I) = S4*(S3-Q(I,I))
      Q(I,I) = S3
      IF (I.EQ.N) GO TO 60
      DO 50 J = I2,N
      S1 = Q(I,J)*Q(M+1,I)
      DO 30 K = I2,M
30    S1 = S1 + Q(K,J)*Q(K,I)
      S1 = -2*S1
      Q(I,J) = Q(I,J) + S1*Q(M+1,I)
      DO 40 K = I2,M
40    Q(K,J) = Q(K,J) + S1*Q(K,I)
50    CONTINUE
60     IF (S3.EQ.0.) Q(M+1,I)=0.
      RETURN
      END
      SUBROUTINE ORTH2 (E1)

      INTEGER E
      COMMON /Z1/E,M,N
      COMMON /ZA1/ Q(65,30)/ZA2/Q1(32,30)
      DO 80 I = 1,N
      I2 = I + 1
      IF (I.EQ.N) GOTO 20
      DO 10 J = I2,N
10    Q1(I,J) = 0
20    Q1(I,I) = E1
      S3 = Q(I,I)**2
      DO 30 J = 1,I
30    S3 = S3 + Q1(J,I)**2
      S3 = SQRT(S3)
      IF (Q(I,I).GT.0) S3 = -S3
          S4 = 1./SQRT(2.*S3*(S3-Q(I,I)))
      Q1(N+2,I) = S4 *(S3-Q(I,I))
      DO 40 J = 1,I
40    Q1(J,I) = -S4*Q1(J,I)
      Q1(I2,I) = S3
      IF (I.EQ.N) GOTO 80
      DO 70 J = I2,N
      S1 = Q(I,J)*Q1(N+2,I)
      DO 50 K = 1,I
50    S1 = S1+Q1(K,J)*Q1(K,I)
      S1 = -2*S1
      DO 60 K = 1,I
60    Q1(K,J) = Q1(K,J)+S1*Q1(K,I)
70    Q1(J+1,I) = Q(I,J)+S1*Q1(N+2,I)
80    CONTINUE
      RETURN
      END
```

```
      SUBROUTINE BAKSUB

      INTEGER E

      COMMON /Z1/ E,M,N/Z3/N3
      COMMON /ZA1/ Q(65,30)/ZA2/Q1(32,30)
      COMMON /ZA5/ R1(31),P1(29)
      DIMENSION C(60)

      DO 10 I = 1,M
 10   C(I) = R1(I)
      N2 = N + 2
      DO 40 I = 1,N3
      S1 = C(I)*Q(M+1,I)
      DO 20 J = I+1,M
 20   S1 = S1 + C(J)*Q(J,I)
      S1 = -2*S1
      C(I) = C(I)+S1*Q(M+1,I)
      DO 30 J = I+1,M
 30   C(J) = C(J) + S1*Q(J,I)
 40   CONTINUE
      DO 50 I = 1,N
 50   C(M+I) = 0
      DO 80 I=1,N
      S1 = Q1(N+2,I)*C(I)
      DO 60 J = 1,I
 60   S1 = S1 + C(M+J)*Q1(J,I)
      S1 = -2*S1
      C(I) = C(I)+S1*Q1(N+2,I)

      DO 70 J = 1,I
 70 C(M+J) = C(M+J) + S1 * Q1(J,I)
 80   CONTINUE
C       DELTA-P MODEL CORRECTIONS
      DO 85 I = 1,N
 85   P1(I) = 0
        P1(N) = C(N)/Q1(N+1,N)
        P1(N-1) = (C(N-1)-Q1(N+1,N-1)*P1(N))/Q1(N,N-1)
      DO 100 K = 3,N
      I = N-K+1
      S1 = 0
      DO 90 J = I+1 ,N
 90   S1 = S1 + Q1(J+1,I)*P1(J)
      P1(I) = (C(I)-S1)/Q1(I+1,I)
 100  CONTINUE
      RETURN
      END
      SUBROUTINE OUTPUT
      INTEGER E
      COMMON /Z1/E,M,N/Z2/DELX,SPAC/Z4/I1,RMS,RMSC/Z5/IX
      COMMON /ZA4/R(31),R2(31)/ZA3/P(29)/ZA6/SN(30)

      WRITE (*,10)I1
 10   FORMAT (/,'   *ITERATION NO.*',1X,I2)
      WRITE (*,20)
 20   FORMAT (/,'  LAYER NO.',6X,'THICKNESS',3X,'RESISTIVITY',5X,
     1         'THICK*RES',4X,'THICK/RES')
     DO 40 I = 1,E-1
      J = I
      D1 = P(I)*P(I+E-1)
      D2 = P(I)/P(I+E-1)
      WRITE (*,30) J,P(I),P(I+E-1),D1,D2
 30   FORMAT (4X,I2,10X,F8.2,5X,F8.3,7X,F9.3,4X,F8.3)
 40   CONTINUE

      WRITE (*,50) E,P(N)
 50   FORMAT (4X,I2,22X,F9.3)
      IF (IX.NE.1) GOTO 56
      WRITE (*,53)
 53   FORMAT (/,18X,' N',7X,'MODEL RHO',6X,'FIELD RHO')
      GO TO 75
 56   X = SPAC
      DO 60 I = 1,M
      SN(I) = EXP(X)
 60   X = X + DELX

      WRITE (*,70)
 70   FORMAT (/,15X,' SPACING',2X,'MODEL RHO',1X,'FIELD RHO')
 75   DO 90 I = 1,M
      WRITE (*,80) SN(I),R(I),R2(I)
 80   FORMAT (14X,F8.3,2X,F8.3,1X,F8.3)
 90   CONTINUE
      WRITE (*,100) RMS
 100  FORMAT (/,10X,'   RMS %-AGE ERROR =',F8.3,///)
      RETURN
      END
      SUBROUTINE SPLINE (M,X,Y)
      COMMON /Z2/ DELX,SPAC
      COMMON /ZA4/ R(31),R2(31)
      DIMENSION B(30),C(30),DELY(30),DELSQY(30),H(30),H2(30)
      DIMENSION S2(30),X(30),S3(30),SS2(31),T(31),Y(31)

      N = M
      WRITE (*,126)
 126  FORMAT (//,6X,'INPUT SPACINGS       CALCULATED APP.RESIS.',/)
C     DO 11 I=1,N
C 11   Y(I)=6.283*Y(I)*X(I)
      DO 128 I = 1,M
 128  WRITE (*,127) X(I),Y(I)
 127  FORMAT (10X,F8.3,11X,F8.3)
      DO 150 I = 1,N
 150  X(I) = ALOG(X(I))
      SPAC = X(1)
      M = INT((X(M)-SPAC)/DELX)+1
```

```
C  MAX NO POINTS 31
      M=MIN(31,M)
        A = SPAC
        DO 300 I = 1,M
        T(I) = A
  300   A = A+ DELX
        EPSLN = 0.00001
        N1 = N-1
        DO 51 I= 1,N1
        H(I) = X(I+1)-X(I)
   51   DELY(I) = (Y(I+1)-Y(I))/H(I)
        DO 52 I = 2,N1
        H2(I) = H(I-1)+H(I)
        B(I) = 0.5*H(I-1)/H2(I)
        DELSQY(I) = (DELY(I)-DELY(I-1))/H2(I)
        S2(I) = 2.*DELSQY(I)
   52   C(I) = 3.*DELSQY(I)
        S2(1), = 0.
        S2(N) = 0.
        OMEGA = 1.071797
    5   ETA = 0.
        DO 10 I = 2,N1
        W = (C(I)-B(I)*S2(I-1)-(.5-B(I))*S2(I+1)-S2(I))*OMEGA
        IF (ABS(W)-ETA) 10,10,9
    9   ETA = ABS (W)
   10   S2(I) = S2(I) + W
C        IF (ETA-EPSLN) 14,5,5
   14   DO 53 I = 1,N1
   53   S3(I) = (S2(I+1)-S2(I))/H(I)
        DO 61 J = 1,M
        I = 1
        IF (T(J) - X(1)) 58,17,55
   55   IF(T(J)-X(N)) 57,59,58
   56   IF (T(J)-X(I)) 60,17,57
   57   I = I+1
        GO TO 56
   58   WRITE (*,44) J
   44   FORMAT (/,I3,' *ARGUMENT OUT OF RANGE* ')
        GO TO 61
   59   I = N
   60   I = I-1
   17   HT1 = T(J)-X(I)
        HT2 = T(J) -X(I+1)
        PROD = HT1*HT2
        SS2(J) = S2(I) +HT1*S3(I)
        DELSQS = (S2(I) +S2(I+1)+SS2(J))/6.
        R2(J) = Y(I) + HT1 *DELY(I)+PROD*DELSQS
   61   CONTINUE
        RETURN
        END
        SUBROUTINE WENBIP (K1,INDEX)

        INTEGER E
        COMMON /Z1/E,M,N/Z2/DELX,SPAC/Z5/IX
        COMMON /ZA1/Q(65,30)/ZA3/P(29)/ZA6/SN(30)

        DIMENSION FLTR(34),T(65)

        DATA (FLTR(I),I=1,34)/.000238935,.00011557,.00017034,
     1 .00024935,.00036665,.00053753,.0007896,.0011584,.0017008,
     2 .0024959,.003664,.0053773,.007893,.011583,.016998,.024934,
     3 .036558,.053507,.078121,.11319,.16192,.22363,.28821,.30276,
     4 .15523,-.32026,-.53557,.51787,-.196,.054394,-.015747,.0053941,
     5 -.0021446,.000665125/

        S=ALOG(2.)
        IF (INDEX-2) 10,10,60
   10   Y = SPAC-10.87925*DELX
        DO 55 I = 1,M+33
        CALL TRNSFM (Y,I,K1)
        IF (K1.GT.0) GO TO 30
        DO 20 J = 1,N
   20   T(J) = Q(I,J)
   30   T(N+1) = Q(I,N+1)
        Y1 = Y +S
        CALL TRNSFM (Y1,I,K1)
        IF (K1.GT.0) GO TO 50
        DO 40 J = 1,N
   40   Q(I,J) = 2.*T(J)-Q(I,J)
   50   Q(I,N+1) = 2.*T(N+1)-Q(I,N+1)
   55   Y = Y + DELX
        GO TO 160

   60   M1 = 1
        IF ( IX.NE.1) GO TO 70
        M1 = M
        M = 1
   70   DO 150 I = 1,M1
        Y = SPAC - 10.87925*DELX
        A = SN(I)
        B = 1.
        IF (A.LT.1.) B = A*A+A-1
        A1 = ABS(A-1)
        S1 = ALOG(A1)
        IF (A.LT.1.) Y = Y-ALOG(A)
        S2 = ALOG(A)
        S3 = ALOG (A+1)
        DO 80 K = 1,N
   80   T(K) = Q(J,K)/A1
   90   T(N+1) = Q(J,N+1) /A1
        Y1 = Y + S2
```

```
      CALL TRNSFM (Y1,J,K1)
      IF (K1.GT.0) GO TO 110
      DO 100 K = 1,N
100   T(K) = T(K)-2.*Q(J,K)/A
110   T(N+1) = T(N+1)-2.*Q(J,N+1)/A
      Y1 = Y + S3
      CALL TRNSFM (Y1,J,K1)
      IF (K1.GT.0) GO TO 130
      DO 120 K = 1,N
120   Q(J,K) = (T(K)+Q(J,K)/(A+1.))*A*(A+1.)*A1/(2.*B)
130   Q(J,N+1) = (T(N+1)+Q(J,N+1)/(A+1.))*A*(A+1.)*A1/(2.*B)
140   Y = Y*DELX
      IF (IX.NE.1) GO TO 150
      J = 1
      IF (K1.GT.0) J = N+1
      DO 145 K = J,N+1
      CALL FILTER (FLTR,34,K)
145   Q(I+34,K) = Q(1,K)
150   CONTINUE .
      IF (IX.NE.1.) GO TO 160
      M = M1
      DO 154 I = 1,M
      IF (K1.GT.0) GO TO 154
      DO 152 J = 1,N
152   Q(I,J) = Q(I+34,J)
154   Q(I,N+1) = Q(I+34,N+1)
      GO TO 180
160   J = 1
      IF (K1.GT.0) J = N+1
      DO 170 I = J,N+1
170   CALL FILTER (FLTR,34,I)
180   RETURN
      END
      SUBROUTINE PRNTER(TXT)
      INTEGER E
      COMMON /Z1/E,M,N/Z2/DELX,SPAC/Z4/I1,RMS,RMSC/Z5/IX
      COMMON /ZA4/R(31),R2(31)/ZA3/P(29)/ZA6/SN(30)

      CHARACTER*50 TXT


      WRITE(7,48)TXT
48    FORMAT(A50)

      WRITE (7,10)I1
   10 FORMAT (/,'  *ITERATION NO.*',1X,I2)
      WRITE (7,20)
   20 FORMAT (/,'  LAYER NO.',6X,'THICKNESS',3X,'RESISTIVITY',5X,
     1        'THICK*RES',4X,'THICK/RES')
      DO 40 I = 1,E-1
      J = I
      D1 = P(I)*P(I+E-1)
      D2 = P(I)/P(I+E-1)
      WRITE (7,30) J,P(I),P(I+E-1),D1,D2
   30 FORMAT (4X,I2,12X,F6.2,5X,F8.3,8X,F8.3,4X,F8.3)
   40 CONTINUE

      WRITE (7,50) E,P(N)
   50 FORMAT (4X,I2,23X,F8.3)
      IF (IX.NE.1) GOTO 56
      WRITE (7,53)
   53 FORMAT (/,18X,' N',7X,'MODEL RHO',6X,'FIELD RHO')
      GO TO 75
   56 X = SPAC
      DO 60 I = 1,M
      SN(I) = EXP(X)
   60 X = X + DELX

      WRITE (7,70)
   70 FORMAT (/,15X,' SPACING',2X,'MODEL RHO',1X,'FIELD RHO')
   75 DO 90 I = 1,M
      WRITE (7,80) SN(I),R(I),R2(I)
   80 FORMAT (14X,F8.3,2X,F8.3,1X,F8.3)
   90 CONTINUE
      WRITE (7,100) RMS
  100 FORMAT (/,10X,'   RMS %-AGE ERROR =',F8.3,///)
      RETURN
      END
**end**
```

APPENDIX C

Tabulation of model results from data analysis using Resinv 88.

ERATION NO.* 15 S1

ER NO.	THICKNESS	RESISTIVITY	THICK*RES	THICK/RES
1	2.45	9.565	23.431	0.256
2	0.69	1.226	0.844	0.561
3	10.23	80.834	826.553	0.126
4	205.92	4.036	831.043	51.022
5	1614.75	130.414	*********	12.382
6	1700.07	12.430	21131.508	136.774
7		119.713		

SPACING	MODEL RHO	FIELD RHO
3.000	8.644	8.600
4.403	8.108	8.056
6.463	8.374	8.359
9.487	10.254	10.132
13.925	13.498	12.093
20.439	17.184	18.041
30.000	20.120	22.300
44.034	20.737	20.727
64.633	17.908	17.778
94.868	12.560	11.485
139.247	7.760	8.443
204.386	5.747	5.756
299.997	6.162	6.000
440.335	8.133	7.877
646.323	11.420	10.586
948.671	16.034	17.377
1392.458	22.070	22.453
2043.847	29.405	32.920
2999.956	37.266	33.200
4403.324	44.070	45.286

RMS %-AGE ERROR = 6.414

ERATION NO.* 15

S 2

ER NO.	THICKNESS	RESISTIVITY	THICK*RES	THICK/RES
1	2.56	6097.051	15624.820	0.000
2	32.53	761.102	24761.219	0.043
3	188.03	420.359	79041.000	0.447
4	41.49	2.186	90.684	18.984
5	769.97	72.961	56177.187	10.553
6	944.32	13.110	12379.801	72.032
7		2004.380		

SPACING	MODEL RHO	FIELD RHO
3.000	5007.012	4830.000
4.403	3835.075	3971.024
6.463	2404.935	2576.703
9.487	1347.970	1278.801
13.925	909.659	840.550
20.439	794.730	810.581
30.000	748.890	794.000
44.034	696.741	694.001
64.633	621.195	646.300
94.868	534.023	528.614
139.247	457.058	438.023
204.386	386.248	368.335
299.997	295.199	288.501
440.335	179.025	208.450
646.323	81.245	78.776
948.671	40.159	35.924
1392.458	36.362	40.407
2043.847	39.486	40.437
2999.956	42.202	38.600
4403.324	48.219	50.057

RMS %-AGE ERROR = 6.408

S3

ITERATION NO. 1

LAYER NO.	THICKNESS	RESISTIVITY	THICK*RES	THICK/RES
1	2.96	1150.002	3409.452	0.003
2	41.06	115.280	4733.508	0.356
3	204.92	29.883	6123.777	6.857
4	199.90	64.699	12932.926	3.090
5	1500.00	7.568	11351.289	198.215
6		100.005		

SPACING	MODEL RHO	FIELD RHO
3.000	995.280	1000.000
4.403	803.227	835.829
6.463	529.001	518.137
9.487	283.384	270.675
13.925	159.242	165.392
20.439	124.272	134.844
30.000	114.137	135.000
44.034	104.136	108.339
64.633	87.807	80.896
94.868	65.916	56.247
139.247	46.691	46.454
204.386	36.746	37.554
299.997	34.185	34.000
440.335	34.133	35.548
646.323	32.490	35.016
948.671	26.827	23.643
1392.458	19.022	17.629
2043.847	13.931	13.948
2999.956	14.043	15.000
4403.324	18.143	17.816

RMS %-AGE ERROR = 7.418

ITERATION NO. 2

S4

LAYER NO.	THICKNESS	RESISTIVITY	THICK*RES	THICK/RES
1	1.01	499.991	505.722	0.002
2	7.13	33.743	240.461	0.211
3	20.07	74.442	1494.014	0.270
4	100.97	10.345	1044.575	9.760
5	650.07	47.436	30836.363	13.704
6	500.02	3.241	1620.582	154.278
7		79.801		

SPACING	MODEL RHO	FIELD RHO
3.000	122.269	123.000
4.403	57.324	55.776
6.463	39.937	41.970
9.487	39.227	40.504
13.925	42.686	41.444
20.439	47.224	43.972
30.000	49.488	52.500
44.034	45.994	46.141
64.633	35.973	34.034
94.868	24.103	23.529
139.247	17.094	18.678
204.386	16.623	17.587
299.997	19.882	20.000
440.335	24.273	23.488
646.323	28.216	25.537
948.671	30.130	28.902
1392.458	28.471	28.532
2043.847	23.712	23.964
2999.956	19.832	22.000
4403.324	20.846	19.730

RMS %-AGE ERROR = 5.237

ITERATION NO.* 9

S5

LAYER NO.	THICKNESS	RESISTIVITY	THICK*RES	THICK/RES
1	2.83	1727.755	4874.848	0.002
2	21.41	58.239	1246.858	0.368
3	40.44	410.803	16612.445	0.098
4	91.77	7.881	723.249	11.644
5	445.91	52.441	23383.809	8.503
6	987.47	6.398	6317.508	154.347
7		501.714		

SPACING	MODEL RHO	FIELD RHO
3.000	1436.721	1454.000
4.403	1092.924	1122.573
6.463	631.869	628.982
9.487	257.593	254.889
13.925	98.692	98.039
20.439	71.172	75.843
30.000	77.603	73.000
44.034	94.584	85.957
64.633	116.370	110.713
94.868	133.073	132.798
139.247	132.449	145.796
204.386	107.682	123.599
299.977	68.692	71.001
440.335	38.917	32.014
646.323	29.088	30.179
948.671	28.243	30.344
1392.458	26.017	27.280
2043.847	21.921	19.283
2999.956	20.368	22.000
4403.324	24.767	24.335

RMS %-AGE ERROR = 7.962

ITERATION NO. 2

S6

LAYER NO.	THICKNESS	RESISTIVITY	THICK*RES	THICK/RES
1	3.94	952.667	3757.109	0.004
2	7.31	88.323	645.393	0.083
3	200.53	327.501	65673.437	0.612
4	297.47	76.809	22847.918	3.873
5	900.02	7.993	7193.844	112.602
6		149.739		

SPACING	MODEL RHO	FIELD RHO
3.000	889.047	864.000
4.403	791.544	846.748
6.463	611.260	637.119
9.487	384.729	377.977
13.925	220.305	212.610
20.439	172.915	177.637
30.000	192.229	200.000
44.034	225.330	215.391
64.633	256.029	249.266
94.868	279.431	282.946
139.247	291.418	279.835
204.386	286.064	272.358
299.997	254.794	273.000
440.335	193.985	203.951
646.323	119.045	108.705
948.671	57.740	55.366
1392.458	25.514	27.025
2043.847	18.161	17.331
2999.956	22.536	23.200
4403.324	30.920	30.606

RMS %-AGE ERROR = 4.578

ITERATION NO. 3 S7

LAYER NO.	THICKNESS	RESISTIVITY	THICK*RES	THICK/RES
1	0.98	996.856	978.351	0.001
2	6.10	35.714	217.856	0.171
3	97.73	275.989	26972.809	0.354
4	429.74	64.282	27624.418	6.685
5	498.25	20.260	10094.387	24.593
6		38.925		

SPACING	MODEL RHO	FIELD RHO
3.000	192.062	180.000
4.403	72.531	76.666
6.463	47.123	43.438
9.487	52.094	50.675
13.925	66.667	61.248
20.439	87.901	87.366
30.000	113.912	112.000
44.034	142.656	147.977
64.633	170.762	184.234
94.868	192.365	195.905
139.247	198.786	182.858
204.386	181.650	169.009
299.997	142.825	145.001
440.335	99.838	112.183
646.323	69.225	69.435
948.671	50.509	46.513
1392.458	38.648	27.596
2043.847	33.798	38.036
2999.956	34.079	35.000
4403.324	35.719	36.028

RMS %-AGE ERROR = 6.264

ITERATION NO. 2 S8

LAYER NO.	THICKNESS	RESISTIVITY	THICK*RES	THICK/RES
1	1.00	150.453	150.392	0.007
2	1.78	28.854	51.280	0.062
3	0.00	269.835	0.270	0.000
4	11.10	138.885	1542.051	0.080
5	194.00	601.311	*********	0.323
6	190.16	127.105	24170.105	1.496
7	699.67	8.583	6004.902	81.522
8		170.224		

SPACING	MODEL RHO	FIELD RHO
3.000	64.610	67.200
4.403	56.238	55.483
6.463	64.310	65.730
9.487	80.340	85.124
13.925	100.938	97.528
20.439	128.066	123.555
30.000	165.411	165.299
44.034	214.676	215.433
64.633	273.537	271.596
94.868	336.402	336.984
139.247	393.776	396.578
204.386	427.879	437.415
299.997	421.733	446.501
440.335	349.073	361.440
646.323	222.925	233.684
948.671	100.218	75.415
1392.458	35.649	30.048
2043.847	23.768	24.357
2999.956	30.484	29.900
4403.324	41.603	42.366

RMS %-AGE ERROR = 8.912

S9

ITERATION NO. 15

LAYER NO.	THICKNESS	RESISTIVITY	THICK*RES	THICK/RES
1	0.76	1539.383	1170.491	0.000
2	9.32	22.652	211.208	0.412
3	13.97	911.192	12725.879	0.015
4	534.47	63.139	33745.953	8.465
5	413.53	4.469	1848.098	92.533
6		125.558		

SPACING	MODEL RHO	FIELD RHO
3.000	109.869	110.000
4.403	34.032	33.920
6.463	25.744	26.126
9.487	27.913	27.942
13.925	34.365	32.974
20.439	46.347	46.325
30.000	63.846	62.799
44.034	85.503	87.877
64.633	108.300	113.196
94.868	126.364	125.234
139.247	131.907	128.004
204.386	120.622	124.182
299.997	97.941	96.901
440.335	75.699	74.656
646.323	58.960	60.055
948.671	43.694	43.193
1392.458	29.347	29.999
2043.847	22.419	21.690
2999.956	25.242	26.000
4403.324	33.539	33.183

RMS %-AGE ERROR = 2.243

S10

ITERATION NO. 0

LAYER NO.	THICKNESS	RESISTIVITY	THICK*RES	THICK/RES
1	1.30	930.000	1209.000	0.001
2	4.00	43.000	172.000	0.093
3	75.00	175.000	13125.000	0.429
4	245.00	125.000	30625.000	1.960
5	675.00	9.000	6075.000	75.000
6		90.000		

SPACING	MODEL RHO	FIELD RHO
3.000	346.609	323.300
4.403	153.650	168.670
6.463	77.523	87.645
9.487	73.841	74.856
13.925	89.452	93.627
20.439	108.213	106.530
30.000	126.436	123.000
44.034	141.938	139.864
64.633	152.820	150.204
94.868	157.421	157.895
139.247	154.334	167.459
204.386	143.212	152.849
299.997	124.685	139.201
440.335	97.750	94.269
646.323	63.963	54.711
948.671	33.997	35.555
1392.458	20.774	23.020
2043.847	21.914	23.021
2999.956	28.595	30.000
4403.324	37.169	34.786

RMS %-AGE ERROR = 7.139

ITERATION NO. 3

S12

LAYER NO.	THICKNESS	RESISTIVITY	THICK*RES	THICK/RES
1	1.41	999.754	1410.725	0.001
2	8.98	35.543	319.226	0.253
3	176.45	337.004	59464.676	0.524
4	1995.37	18.969	37849.590	105.193
5		119.192		

SPACING	MODEL RHO	FIELD RHO
3.000	416.843	420.000
4.403	182.428	179.632
6.463	69.274	68.624
9.487	46.801	46.094
13.925	52.662	50.633
20.439	68.319	69.366
30.000	91.431	96.100
44.034	120.547	120.021
64.633	154.049	150.818
94.868	188.789	185.346
139.247	218.496	216.966
204.386	232.361	239.437
299.997	216.073	224.608
440.335	163.043	192.372
646.323	93.028	86.233
948.671	42.863	41.885
1392.458	24.774	25.786
2043.847	22.978	20.809
2999.956	26.370	26.500
4403.324	33.304	34.987

RMS %-AGE ERROR = 5.136

ITERATION NO. 15

S 1[illegible]

LAYER/NO.	THICKNESS	RESISTIVITY	THICK*RES	THICK/RES
1	1.76	270.608	475.124	0.006
2	0.67	39.399	26.583	0.017
3	13.70	1404.632	19241.375	0.010
4	3.16	6.422	20.293	0.492
5	50.72	817.068	41438.551	0.062
6	314.71	73.448	23114.863	4.285
7	581.38	5.732	3332.357	101.432
8		235.356		

SPACING	MODEL RHO	FIELD RHO
3.000	219.743	220.000
4.403	211.001	210.027
6.463	242.826	246.167
9.487	315.613	307.301
13.925	408.704	414.261
20.439	497.890	493.866
30.000	547.392	535.331
44.034	516.633	548.026
64.633	402.225	395.359
94.868	271.915	271.093
139.247	207.064	203.470
204.386	202.055	201.273
299.997	195.996	203.889
440.335	160.295	160.369
646.323	104.229	99.171
948.671	52.846	54.880
1392.458	24.684	24.490
2043.847	19.536	19.071
2999.956	25.586	26.600
4403.324	35.816	35.214

RMS %-AGE ERROR = 2.597

ITERATION NO. 15 S14

LAYER NO.	THICKNESS	RESISTIVITY	THICK*RES	THICK/RES
1	2.03	806.364	1640.279	0.003
2	4.54	45.520	206.530	0.100
3	9.90	668.011	6613.148	0.015
4	119.11	147.633	17584.395	0.807
5	389.48	38.708	15075.980	10.062
6	539.75	98.279	53046.234	5.492
7	690.26	17.117	11815.273	40.326
8		254.173		

SPACING	MODEL RHO	FIELD RHO
3.000	549.074	640.000
4.403	347.595	254.659
6.463	174.865	218.396
9.487	105.471	96.546
13.925	113.673	105.070
20.439	145.905	140.165
30.000	179.456	201.623
44.034	203.487	231.384
64.633	208.919	192.794
94.868	193.729	175.033
139.247	165.185	172.039
204.386	131.391	135.890
299.997	96.242	95.623
440.335	67.554	67.483
646.323	53.992	52.647
948.671	52.964	54.411
1392.458	55.500	56.138
2043.847	56.331	55.014
2999.956	57.702	58.000
4403.324	66.040	66.212

RMS %-AGE ERROR = 11.399

ITERATION NO. 3 S15

LAYER NO.	THICKNESS	RESISTIVITY	THICK*RES	THICK/RES
1	1.33	54.268	72.101	0.024
2	2.83	17.949	50.820	0.158
3	93.58	574.901	53798.332	0.163
4	222.42	33.428	7434.895	6.654
5	803.52	8.801	7071.453	91.303
6		169.296		

SPACING	MODEL RHO	FIELD RHO
3.000	36.639	42.500
4.403	32.459	37.980
6.463	36.140	33.280
9.487	48.534	55.336
13.925	68.277	70.378
20.439	95.322	92.525
30.000	130.638	132.709
44.034	174.397	183.947
64.633	224.192	237.011
94.868	272.276	303.462
139.247	302.305	320.416
204.386	291.050	307.185
299.997	225.912	213.567
440.335	130.543	118.414
646.323	54.660	48.363
948.671	21.668	21.036
1392.458	15.709	17.137
2043.847	19.216	17.859
2999.956	26.451	28.200
4403.324	36.424	39.238

RMS %-AGE ERROR = 8.374

ITERATION NO. 2 S 16

LAYER NO.	THICKNESS	RESISTIVITY	THICK*RES	THICK/RES
1	1.35	1400.128	1895.352	0.001
2	7.40	297.327	2199.828	0.025
3	85.10	59.942	5101.109	1.420
4	529.71	106.927	56640.027	4.954
5	899.99	3.405	3064.575	264.304
6		80.283		

SPACING	MODEL RHO	FIELD RHO
3.000	763.089	790.000
4.403	501.843	493.218
6.463	348.414	346.016
9.487	270.755	261.660
13.925	204.180	209.793
20.439	136.278	120.590
30.000	88.836	102.000
44.034	69.213	79.349
64.633	64.424	65.230
94.868	65.025	60.557
139.247	69.086	65.227
204.386	75.910	72.968
299.997	83.122	83.000
440.335	87.186	90.816
646.323	83.976	84.775
948.671	69.538	67.195
1392.458	45.266	45.166
2043.847	22.705	23.764
2999.956	13.052	12.000
4403.324	14.119	14.823

RMS %-AGE ERROR = 6.281

ITERATION NO. 5 S18

LAYER NO.	THICKNESS	RESISTIVITY	THICK*RES	THICK/RES
1	2.60	985.313	2565.285	0.003
2	85.21	92.503	7881.863	0.921
3	209.17	673.260	*********	0.311
4	902.08	3.339	3011.824	270.185
5		44.695		

SPACING	MODEL RHO	FIELD RHO
3.000	805.299	872.300
4.403	609.115	571.044
6.463	367.044	349.638
9.487	187.393	201.053
13.925	114.807	123.438
20.439	98.571	88.691
30.000	95.555	91.300
44.034	95.885	99.852
64.633	99.793	103.722
94.868	110.601	110.024
139.247	133.089	129.967
204.386	168.335	154.155
299.997	208.436	211.499
440.335	236.841	244.135
646.323	231.862	265.044
948.671	180.387	182.272
1392.458	100.539	87.257
2043.847	37.244	40.873
2999.956	13.698	13.400
4403.324	12.680	12.787

RMS %-AGE ERROR = 6.982

ITERATION NO. 1 S 19

LAYER NO.	THICKNESS	RESISTIVITY	THICK*RES	THICK/RES
1	4.46	2099.964	9362.762	0.002
2	77.26	93.716	7240.742	0.824
3	300.08	11.133	3340.910	26.953
4	899.99	49.517	44565.238	18.175
5	700.00	9.579	6705.031	73.080
6		279.999		

SPACING	MODEL RHO	FIELD RHO
3.000	1988.209	1950.000
4.403	1804.877	1649.491
6.463	1432.315	1338.038
9.487	891.904	776.221
13.925	403.448	386.465
20.439	162.524	212.325
30.000	104.183	118.859
44.034	94.314	86.308
64.633	87.610	78.621
94.868	75.850	76.348
139.247	56.563	57.283
204.386	34.620	40.183
299.997	20.091	22.182
440.335	16.002	16.468
646.323	17.796	17.223
948.671	21.699	20.526
1392.458	25.911	23.458
2043.847	29.423	28.571
2999.956	32.493	30.000
4403.324	37.565	39.321

RMS %-AGE ERROR = 9.603

ITERATION NO. 2 S 20

LAYER NO.	THICKNESS	RESISTIVITY	THICK*RES	THICK/RES
1	1.86	558.621	1036.277	0.003
2	3.48	375.369	1306.095	0.009
3	6.65	55.367	368.322	0.120
4	184.33	213.915	39431.633	0.862
5	492.79	46.655	22991.191	10.562
6	999.64	8.859	8855.664	112.840
7		55.442		

SPACING	MODEL RHO	FIELD RHO
3.000	494.332	479.200
4.403	433.203	440.376
6.463	348.286	354.917
9.487	247.734	243.928
13.925	160.348	159.886
20.439	121.924	123.334
30.000	127.628	126.000
44.034	147.826	145.934
64.633	167.481	176.972
94.868	182.250	179.800
139.247	189.048	179.800
204.386	183.523	186.801
299.997	160.424	148.501
440.335	120.437	129.535
646.323	77.373	89.031
948.671	46.123	44.025
1392.458	27.794	28.129
2043.847	19.278	19.386
2999.956	19.136	19.200
4403.324	23.558	24.561

RMS %-AGE ERROR = 4.527

ITERATION NO. 2 S 21

LAYER NO.	THICKNESS	RESISTIVITY	THICK*RES	THICK/RES
1	1.83	902.418	1648.867	0.002
2	13.14	253.473	3330.698	0.052
3	184.90	120.952	22363.555	1.529
4	800.94	8.323	6666.355	96.231
5		54.083		

SPACING	MODEL RHO	FIELD RHO
3.000	669.757	764.000
4.403	504.989	491.669
6.463	364.623	337.561
9.487	288.172	282.805
13.925	252.624	263.809
20.439	223.991	239.475
30.000	190.288	166.001
44.034	158.066	151.879
64.633	136.666	140.729
94.868	125.202	134.035
139.247	116.412	123.069
204.386	102.934	105.196
299.997	79.370	85.001
440.335	48.423	45.082
646.323	23.472	22.368
948.671	13.281	15.052
1392.458	12.962	13.537
2043.847	16.241	15.176
2999.956	21.037	20.000
4403.324	26.672	27.427

RMS %-AGE ERROR = 6.953

ITERATION NO. 3 S22

LAYER NO.	THICKNESS	RESISTIVITY	THICK*RES	THICK/RES
1	1.21	599.511	728.103	0.002
2	2.26	10.225	23.116	0.221
3	11.88	61.550	731.392	0.193
4	14.38	25.848	371.776	0.556
5	204.88	461.079	94466.750	0.444
6	496.82	51.857	25763.723	9.580
7	599.92	4.359	2614.921	137.636
8		43.124		

SPACING	MODEL RHO	FIELD RHO
3.000	178.313	177.000
4.403	64.350	63.806
6.463	27.563	26.298
9.487	27.427	26.568
13.925	33.301	32.516
20.439	39.051	39.189
30.000	44.211	42.000
44.034	50.596	50.413
64.633	62.357	63.916
94.868	82.580	85.647
139.247	110.641	111.960
204.386	143.543	144.068
299.997	175.269	172.000
440.335	194.145	176.582
646.323	185.396	192.104
948.671	143.227	140.836
1392.458	83.780	91.898
2043.847	37.417	38.487
2999.956	19.469	19.000
4403.324	19.391	22.622

RMS %-AGE ERROR = 5.012

ITERATION NO. 6

S 23

LAYER NO.	THICKNESS	RESISTIVITY	THICK*RES	THICK/RES
1	1.33	398.484	529.510	0.003
2	3.28	31.033	101.784	0.106
3	11.51	239.843	2759.916	0.048
4	3.69	7.518	27.752	0.491
5	206.15	205.311	42325.547	1.004
6	644.14	135.238	87112.375	4.763
7	600.72	5.241	3148.512	114.614
8		129.740		

SPACING	MODEL RHO	FIELD RHO
3.000	168.853	169.000
4.403	89.741	89.513
6.463	60.746	61.053
9.487	66.878	66.686
13.925	83.340	80.930
20.439	98.752	97.246
30.000	106.766	115.000
44.034	104.745	105.389
64.633	99.179	95.478
94.868	102.192	99.090
139.247	117.170	119.467
204.386	136.320	134.761
299.997	151.642	165.000
440.335	157.776	155.716
646.323	151.235	148.671
948.671	131.048	116.181
1392.458	98.354	107.005
2043.847	60.770	64.330
2999.956	35.541	33.000
4403.324	31.490	32.595

RMS %-AGE ERROR = 4.970

ITERATION NO. 15

S 25

LAYER NO.	THICKNESS	RESISTIVITY	THICK*RES	THICK/RES
1	1.07	439.101	470.942	0.002
2	6.70	31.458	210.794	0.213
3	25.65	899.149	23064.012	0.029
4	2.66	1.781	4.738	1.494
5	157.54	521.971	82233.000	0.302
6	472.92	16.732	7912.797	28.264
7	796.22	36.837	29330.082	21.615
8		25.939		

SPACING	MODEL RHO	FIELD RHO
3.000	123.438	123.000
4.403	59.326	60.028
6.463	42.120	40.761
9.487	46.533	48.783
13.925	61.282	61.085
20.439	85.023	82.201
30.000	116.775	107.200
44.034	154.305	143.538
64.633	191.281	199.332
94.868	215.678	249.852
139.247	214.885	252.838
204.386	189.606	153.185
299.997	161.853	158.000
440.335	151.394	158.198
646.323	145.709	151.279
948.671	121.707	123.319
1392.458	81.531	76.293
2043.847	47.640	50.256
2999.956	32.892	32.400
4403.324	29.222	29.477

RMS %-AGE ERROR = 8.040

ITERATION NO. 2

S 25

LAYER NO.	THICKNESS	RESISTIVITY	THICK*RES	THICK/RES
1	4.17	347.557	1448.398	0.012
2	10.43	59.303	618.784	0.176
3	144.23	184.823	26657.242	0.780
4	604.30	114.697	69311.687	5.269
5	700.29	14.622	10239.434	47.893
6		42.705		

SPACING	MODEL RHO	FIELD RHO
3.000	330.163	321.000
4.403	302.543	297.692
6.463	248.854	248.512
9.487	175.828	179.905
13.925	115.799	111.266
20.439	93.692	83.062
30.000	100.858	80.000
44.034	118.362	109.714
64.633	136.522	138.665
94.868	151.622	162.857
139.247	161.208	170.905
204.386	162.987	144.076
299.997	155.481	140.000
440.335	140.172	121.747
646.323	120.839	120.483
948.671	98.191	105.613
1392.458	71.124	77.741
2043.847	46.342	48.334
2999.956	34.313	33.000
4403.324	33.725	33.793

RMS %-AGE ERROR = 9.216

ITERATION NO. 3

S 26

LAYER NO.	THICKNESS	RESISTIVITY	THICK*RES	THICK/RES
1	4.86	816.478	3964.341	0.006
2	30.03	62.979	1891.111	0.477
3	66.61	163.512	10891.234	0.407
4	250.43	21.040	5269.055	11.902
5	1007.69	11.716	11806.160	86.009
6		108.220		

SPACING	MODEL RHO	FIELD RHO
3.000	783.948	735.000
4.403	728.370	724.125
6.463	608.583	592.423
9.487	418.276	428.844
13.925	223.026	197.829
20.439	109.181	127.686
30.000	76.796	73.300
44.034	76.499	71.071
64.633	84.653	81.079
94.868	93.262	98.800
139.247	94.115	109.721
204.386	81.162	78.158
299.997	57.328	55.001
440.335	34.613	31.941
646.323	21.623	24.172
948.671	16.691	20.085
1392.458	16.194	15.645
2043.847	19.058	19.113
2999.956	24.931	21.600
4403.324	33.218	39.152

RMS %-AGE ERROR = 9.338

ITERATION NO. 3

G 24

LAYER NO.	THICKNESS	RESISTIVITY	THICK*RES	THICK/RES
1	1.22	655.626	801.931	0.002
2	2.90	71.016	206.035	0.041
3	10.66	181.737	1937.770	0.059
4	5.77	56.080	323.844	0.103
5	103.45	248.109	25667.988	0.417
6	403.38	105.051	42375.125	3.840
7	1017.01	15.243	15502.398	66.719
8		238.894		

SPACING	MODEL RHO	FIELD RHO
3.000	263.167	260.000
4.403	150.016	153.036
6.463	112.423	110.658
9.487	117.418	118.159
13.925	130.226	128.422
20.439	138.909	135.039
30.000	143.139	130.000
44.034	149.733	129.266
64.633	164.169	139.183
94.868	181.643	156.235
139.247	192.134	190.128
204.386	187.519	199.994
299.997	165.579	185.001
440.335	133.342	128.134
646.323	99.917	85.142
948.671	68.165	59.387
1392.458	42.788	42.358
2043.847	32.676	31.741
2999.956	37.648	35.000
4403.324	50.773	51.652

RMS %-AGE ERROR = 9.258

ITERATION NO. 2

G 25

LAYER NO.	THICKNESS	RESISTIVITY	THICK*RES	THICK/RES
1	0.85	144.920	122.511	0.006
2	2.38	800.055	1900.269	0.003
3	18.09	349.686	6327.055	0.052
4	143.56	839.136	*********	0.171
5	201.49	194.738	39238.602	1.035
6	700.33	13.157	9214.484	53.228
7		98.334		

SPACING	MODEL RHO	FIELD RHO
3.000	326.034	310.000
4.403	391.072	420.550
6.463	437.158	443.436
9.487	451.227	429.560
13.925	437.868	446.117
20.439	421.972	418.882
30.000	431.682	439.999
44.034	478.158	487.577
64.633	548.896	554.689
94.868	618.212	594.058
139.247	659.608	661.702
204.386	643.962	577.005
299.997	545.229	525.004
440.335	372.735	313.981
646.323	191.012	185.315
948.671	72.132	68.932
1392.458	30.900	34.141
2043.847	29.615	28.238
2999.956	37.843	37.500
4403.324	48.039	49.026

RMS %-AGE ERROR = 6.252

G29

LAYER NO.	THICKNESS	RESISTIVITY	THICK*RES	THICK/RES
1	2.84	196.257	557.267	0.014
2	18.03	356.281	6422.687	0.051
3	37.52	179.065	6718.926	0.210
4	174.81	322.568	56388.824	0.542
5	202.45	114.983	23278.320	1.761
6	600.17	6.674	4005.350	89.931
7		109.349		

SPACING	MODEL RHO	FIELD RHO
3.000	208.384	215.000
4.403	223.938	209.704
6.463	248.299	240.223
9.487	276.119	285.241
13.925	299.167	307.806
20.439	310.297	314.932
30.000	303.900	310.000
44.034	280.136	297.818
64.633	252.275	258.354
94.868	239.434	221.727
139.247	245.132	235.255
204.386	253.279	250.891
299.997	243.883	250.001
440.335	203.789	199.003
646.323	136.280	143.796
948.671	67.598	70.451
1392.458	28.237	27.994
2043.847	20.527	21.017
2999.956	25.974	25.000
4403.324	34.705	35.997

RMS %-AGE ERROR = 3.898

ITERATION NO. 4

G53

LAYER NO.	THICKNESS	RESISTIVITY	THICK*RES	THICK/RES
1	2.03	722.990	1465.362	0.003
2	15.68	169.975	2665.619	0.092
3	20.41	938.383	19147.910	0.022
4	8.33	96.609	804.427	0.086
5	141.49	800.387	*********	0.177
6	138.17	99.910	13804.434	1.383
7	781.93	6.202	4849.609	126.074
8		224.931		

SPACING	MODEL RHO	FIELD RHO
3.000	554.098	600.000
4.403	416.598	411.917
6.463	287.238	279.710
9.487	215.862	204.110
13.925	198.399	211.900
20.439	212.770	215.599
30.000	251.770	249.999
44.034	308.219	307.616
64.633	366.530	360.163
94.868	415.200	420.441
139.247	453.408	479.061
204.386	477.123	448.979
299.997	459.448	450.000
440.335	367.500	367.996
646.323	216.927	225.064
948.671	83.988	85.062
1392.458	24.424	23.599
2043.847	16.061	15.175
2999.956	21.517	23.000

RMS %-AGE ERROR = 4.121

ITERATION NO. 3

G 54

LAYER NO.	THICKNESS	RESISTIVITY	THICK*RES	THICK/RES
1	1.62	1008.116	1634.469	0.002
2	2.42	64.142	154.942	0.038
3	23.65	318.580	7533.660	0.074
4	303.76	148.821	45205.980	2.041
5	699.45	6.411	4484.129	109.103
6		149.437		

SPACING	MODEL RHO	FIELD RHO
3.000	550.932	670.000
4.403	311.532	307.613
6.463	176.483	141.279
9.487	158.727	135.243
13.925	185.828	181.956
20.439	216.014	211.515
30.000	237.315	240.000
44.034	241.813	265.322
64.633	226.127	217.423
94.868	198.072	179.134
139.247	171.846	175.995
204.386	153.176	169.330
299.997	135.515	150.001
440.335	108.844	110.261
646.323	70.767	63.414
948.671	34.893	33.463
1392.458	17.657	18.833
2043.847	17.218	17.872
2999.956	23.358	22.000
4403.324	32.169	32.244

RMS %-AGE ERROR = 9.724

ITERATION NO. 0

G 55

LAYER NO.	THICKNESS	RESISTIVITY	THICK*RES	THICK/RES
1	2.50	589.272	1474.318	0.004
2	2.43	77.429	187.917	0.031
3	23.04	941.825	21701.930	0.024
4	11.10	96.398	1070.322	0.115
5	94.26	793.940	74838.312	0.119
6	342.00	178.468	61035.492	1.916
7	803.06	7.054	5664.621	113.848
8		140.266		

SPACING	MODEL RHO	FIELD RHO
3.000	488.690	640.000
4.403	389.549	382.516
6.463	288.109	246.140
9.487	251.199	229.340
13.925	291.868	305.569
20.439	368.004	364.754
30.000	445.408	474.999
44.034	499.870	522.819
64.633	512.655	488.306
94.868	492.095	469.656
139.247	472.282	476.307
204.386	460.540	492.657
299.997	418.303	428.003
440.335	324.354	297.479
646.323	206.561	192.579
948.671	104.382	112.056
1392.458	41.401	42.470
2043.847	20.655	19.342
2999.956	22.627	23.000
4403.324	30.783	31.435

RMS %-AGE ERROR = 8.245

ITERATION NO. 2 G 56

LAYER NO.	THICKNESS	RESISTIVITY	THICK*RES	THICK/RES
1	5.82	167.271	973.727	0.035
2	21.88	410.447	8981.582	0.053
3	252.94	152.157	38485.844	1.662
4	750.80	5.803	4356.574	129.392
5		91.967		

SPACING	MODEL RHO	FIELD RHO
3.000	169.563	170.000
4.403	173.834	166.620
6.463	184.351	186.886
9.487	205.461	233:084
13.925	237.295	274.889
20.439	271.610	248.481
30.000	295.200	250.000
44.034	294.968	281.061
64.633	265.797	303.587
94.868	220.505	217.451
139.247	180.968	168.883
204.386	154.203	150.058
299.997	129.066	150.001
440.335	93.854	96.163
646.323	52.085	51.461
948.671	21.998	22.403
1392.458	12.250	13.250
2043.847	13.865	14.166
2999.956	18.879	18.000
4403.324	25.556	25.426

RMS %-AGE ERROR = 8.040

ITERATION NO. 6 G57

LAYER NO.	THICKNESS	RESISTIVITY	THICK*RES	THICK/RES
1	1.26	1507.683	1898.493	0.001
2	4.61	174.433	803.328	0.026
3	12.11	752.246	9109.895	0.016
4	25.18	78.704	1981.447	0.320
5	113.32	530.584	60123.363	0.214
6	55.83	34.658	1934.799	1.611
7	687.87	6.015	4137.246	114.367
8		103.447		

SPACING	MODEL RHO	FIELD RHO
3.000	637.410	620.000
4.403	361.721	370.939
6.463	257.815	260.992
9.487	268.354	255.887
13.925	317.004	308.250
20.439	360.953	380.640
30.000	369.257	380.000
44.034	327.222	318.969
64.633	259.958	262.481
94.868	221.126	213.308
139.247	229.028	224.254
204.386	246.452	241.189
299.997	232.156	209.002
440.335	172.167	191.509
646.323	90.556	115.866
948.671	32.759	25.172
1392.458	14.418	16.167
2043.847	15.576	15.298
2999.956	21.250	20.500
4403.324	28.763	29.213

RMS %-AGE ERROR = 9.641

ITERATION NO. 2 G 58

LAYER NO.	THICKNESS	RESISTIVITY	THICK*RES	THICK/RES
1	1.18	679.968	802.274	0.002
2	3.60	169.538	610.045	0.021
3	11.03	460.428	5077.738	0.024
4	19.55	69.735	1362.990	0.280
5	108.44	417.382	45262.461	0.260
6	199.17	107.552	21421.297	1.852
7	1000.37	8.405	8408.090	119.021
8		119.337		

SPACING	MODEL RHO	FIELD RHO
3.000	351.716	350.000
4.403	260.192	262.488
6.463	234.029	234.825
9.487	252.038	239.287
13.925	279.427	280.860
20.439	288.316	309.121
30.000	263.230	260.000
44.034	215.305	212.477
64.633	182.954	183.658
94.868	189.735	186.359
139.247	216.900	230.808
204.386	234.221	244.703
299.997	221.639	222.501
440.335	172.757	157.411
646.323	103.358	86.994
948.671	45.426	45.590
1392.458	19.254	21.054
2043.847	16.247	15.616
2999.956	21.169	20.500
4403.324	28.815	29.217

RMS %-AGE ERROR = 5.863

ITERATION NO. 2 G59

LAYER NO.	THICKNESS	RESISTIVITY	THICK*RES	THICK/RES
1	1.46	1216.362	1778.787	0.001
2	3.96	206.638	817.604	0.019
3	44.39	603.656	26798.207	0.074
4	148.98	64.399	9594.250	2.313
5	946.80	11.155	10561.965	84.873
6		53.638		

SPACING	MODEL RHO	FIELD RHO
3.000	683.379	770.000
4.403	445.010	421.135
6.463	324.578	302.147
9.487	321.578	300.343
13.925	370.351	372.706
20.439	426.937	448.920
30.000	471.158	500.000
44.034	485.963	498.255
64.633	450.115	475.025
94.868	350.953	360.552
139.247	216.478	214.364
204.386	109.000	110.337
299.997	54.391	50.001
440.335	29.494	28.638
646.323	17.542	19.328
948.671	14.103	14.759
1392.458	14.978	14.653
2043.847	18.166	17.151
2999.956	22.963	22.000
4403.324	28.634	29.419

RMS %-AGE ERROR = 5.577

ITERATION NO. 1 SL70

LAYER NO.	THICKNESS	RESISTIVITY	THICK*RES	THICK/RES
1	3.53	300.193	1059.767	0.012
2	52.19	102.163	5331.598	0.511
3	180.01	7.726	1390.754	23.299
4	999.97	43.052	43050.551	23.227
5	700.03	7.731	5411.879	90.548
6		199.984		

SPACING	MODEL RHO	FIELD RHO
3.000	283.656	288.000
4.403	259.727	276.286
6.463	218.206	246.090
9.487	168.768	178.202
13.925	131.067	129.274
20.439	112.097	103.057
30.000	103.351	100.000
44.034	95.369	103.915
64.633	81.718	89.556
94.868	59.306	67.011
139.247	33.778	36.357
204.386	17.005	15.504
299.997	12.424	15.500
440.335	14.169	18.131
646.323	17.840	20.236
948.671	21.933	22.764
1392.458	25.567	24.721
2043.847	27.961	27.154
2999.956	29.435	32.000

RMS %-AGE ERROR = 9.773

ITERATION NO. 4 SL71

LAYER NO.	THICKNESS	RESISTIVITY	THICK*RES	THICK/RES
1	4.42	131.396	580.166	0.034
2	65.07	7.676	499.431	8.477
3	288.40	98.691	28462.672	2.922
4	300.00	1.445	433.395	207.663
5		98.669		

SPACING	MODEL RHO	FIELD RHO
3.000	124.399	115.000
4.403	112.968	109.998
6.463	89.877	101.362
9.487	56.643	61.384
13.925	26.841	23.429
20.439	12.191	12.857
30.000	8.679	9.075
44.034	8.432	7.535
64.633	9.135	9.407
94.868	10.988	12.388
139.247	14.425	15.550
204.386	19.423	20.808
299.997	25.478	25.108
440.335	31.503	26.500
646.323	35.352	31.861
948.671	34.280	40.063
1392.458	27.495	30.122
2043.847	18.961	18.027
2999.956	15.005	15.500
4403.324	17.394	17.001

RMS %-AGE ERROR = 9.220

ITERATION NO. 1

SL70

LAYER NO.	THICKNESS	RESISTIVITY	THICK*RES	THICK/RES
1	3.53	300.193	1059.767	0.012
2	52.19	102.163	5331.598	0.511
3	180.01	7.726	1390.754	23.299
4	999.97	43.052	43050.551	23.227
5	700.03	7.731	5411.879	90.548
6		199.984		

SPACING	MODEL RHO	FIELD RHO
3.000	283.656	288.000
4.403	259.727	276.286
6.463	218.206	246.090
9.487	168.768	178.202
13.925	131.067	129.274
20.439	112.097	103.057
30.000	103.351	100.000
44.034	95.369	103.915
64.633	81.718	89.556
94.868	59.306	67.011
139.247	33.778	36.357
204.386	17.005	15.504
299.997	12.424	15.500
440.335	14.169	18.131
646.323	17.840	20.236
948.671	21.933	22.764
1392.458	25.567	24.721
2043.847	27.961	27.154
2999.956	29.435	32.000

RMS %-AGE ERROR = 9.773

ITERATION NO. 4

SL71

LAYER NO.	THICKNESS	RESISTIVITY	THICK*RES	THICK/RES
1	4.42	131.396	580.166	0.034
2	65.07	7.676	499.431	8.477
3	288.40	98.691	28462.672	2.922
4	300.00	1.445	433.395	207.663
5		98.669		

SPACING	MODEL RHO	FIELD RHO
3.000	124.399	115.000
4.403	112.968	109.998
6.463	89.877	101.362
9.487	56.643	61.384
13.925	26.841	23.429
20.439	12.191	12.857
30.000	8.679	9.075
44.034	8.432	7.535
64.633	9.135	9.407
94.868	10.988	12.388
139.247	14.425	15.550
204.386	19.423	20.808
299.997	25.478	25.108
440.335	31.503	26.500
646.323	35.352	31.861
948.671	34.280	40.063
1392.458	27.495	30.122
2043.847	18.961	18.027
2999.956	15.005	15.500
4403.324	17.394	17.001

RMS %-AGE ERROR = 9.220

APPENDIX D

Tabulation of some results of the Most-Square Method.

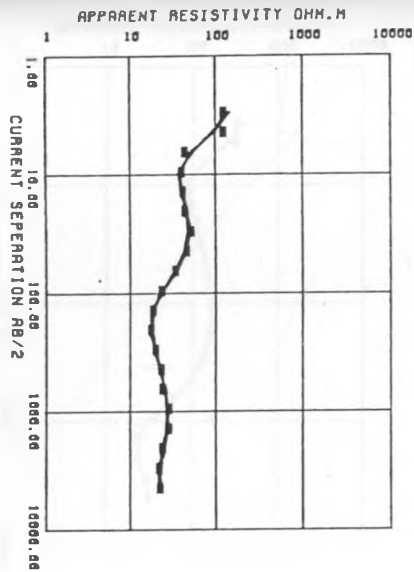
APPARENT RESISTIVITY OHM.M
1
10
100
1000
10000
CURRENT SEPERATION AB/2
1.00
10.00
100.00
1000.00
10000.00

54

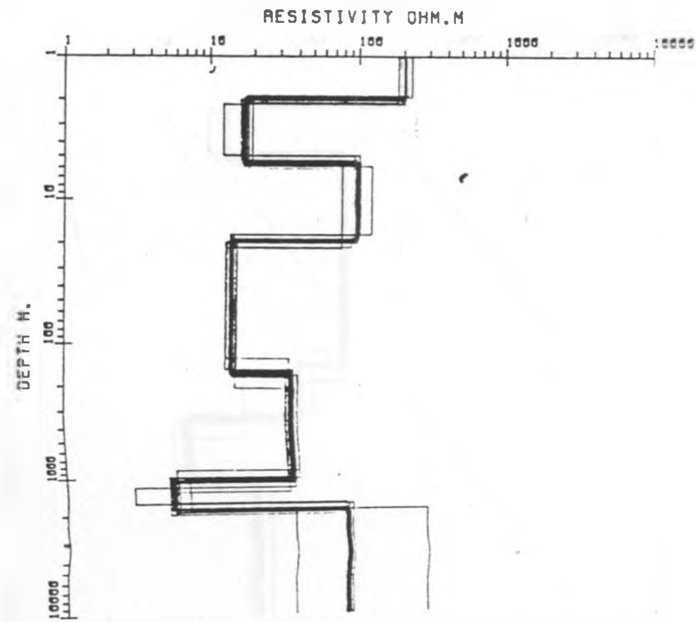
RESISTIVITY OHM.M
1
10
100
1000
10000
DEPTH M.
1
10
100
1000
10000

MOST-SQUARES SM DC MODELS FOR SITE SUS-OLK S2

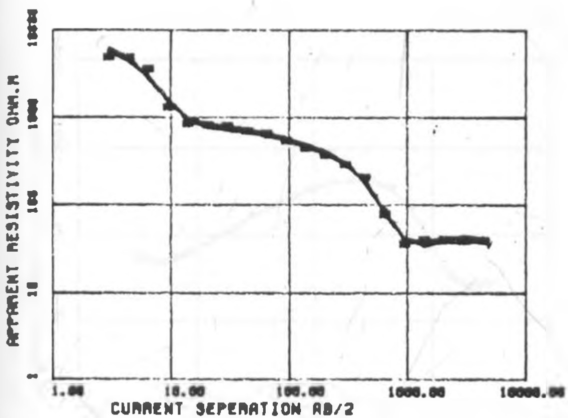

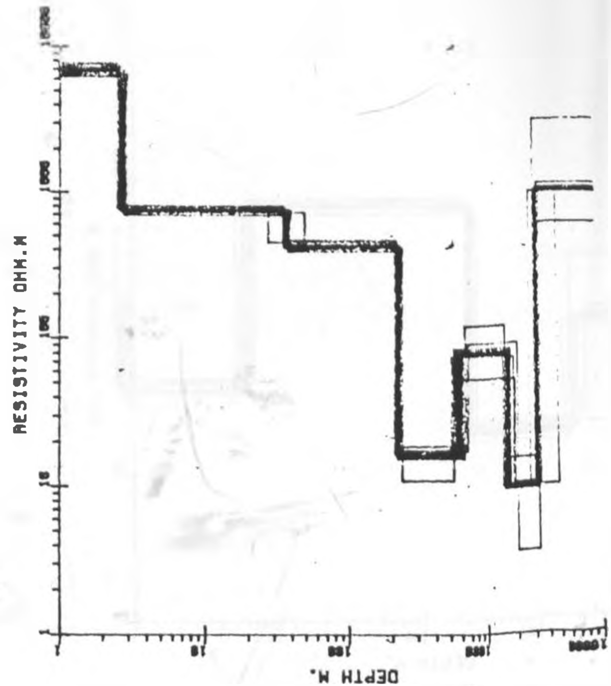

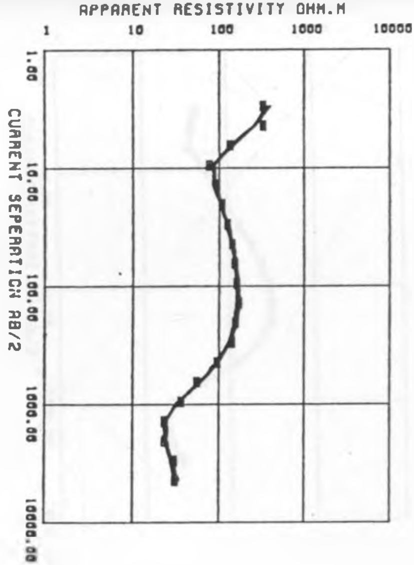
APPARENT RESISTIVITY OHM.M
1
10
100
1000
10000
CURRENT SEPERATION AB/2
1.00
10.00
100.00
1000.00
10000.00

S 10

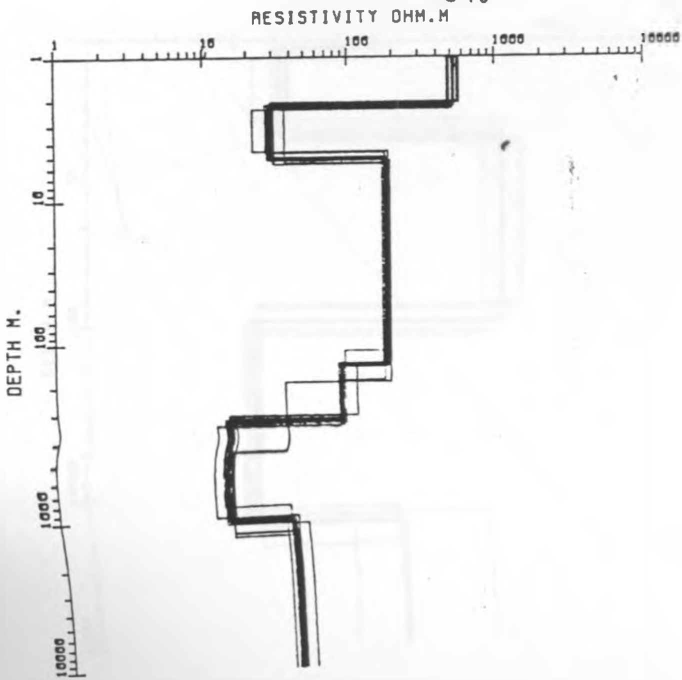
RESISTIVITY OHM.M
1
10
100
1000
10000
DEPTH M.
10
100
1000
10000

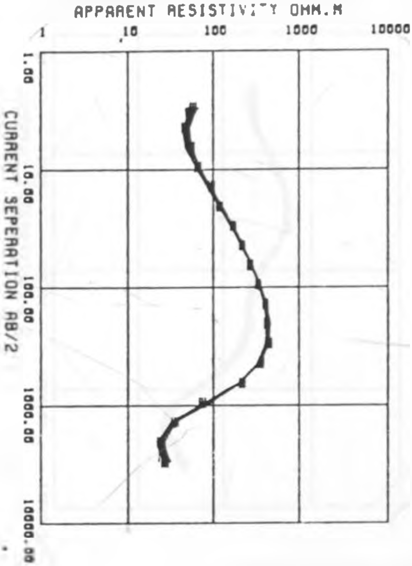
APPARENT RESISTIVITY OHM.M
1
10
100
1000
10000
CURRENT SEPERATION AB/2
1.00
10.00
100.00
1000.00
10000.00

S6

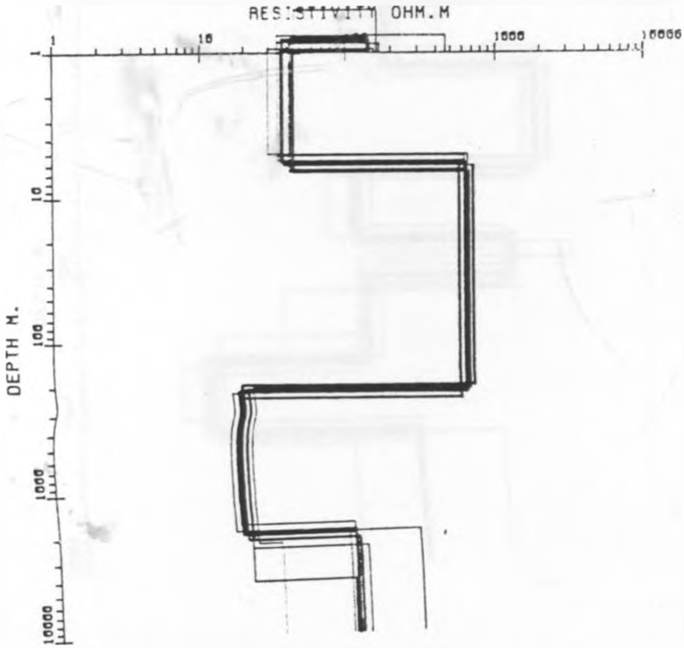
RESISTIVITY OHM.M
1
10
1000
10000
DEPTH M.
10
100
1000
10000

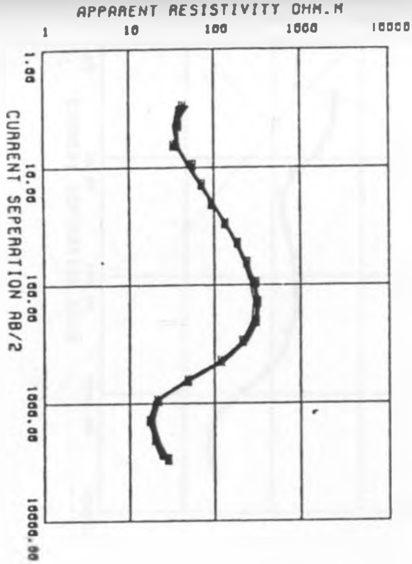
APPARENT RESISTIVITY OHM.M
1
10
100
1000
10000
CURRENT SEPERATION AB/2
1.00
10.00
100.00
1000.00
10000.00

S15

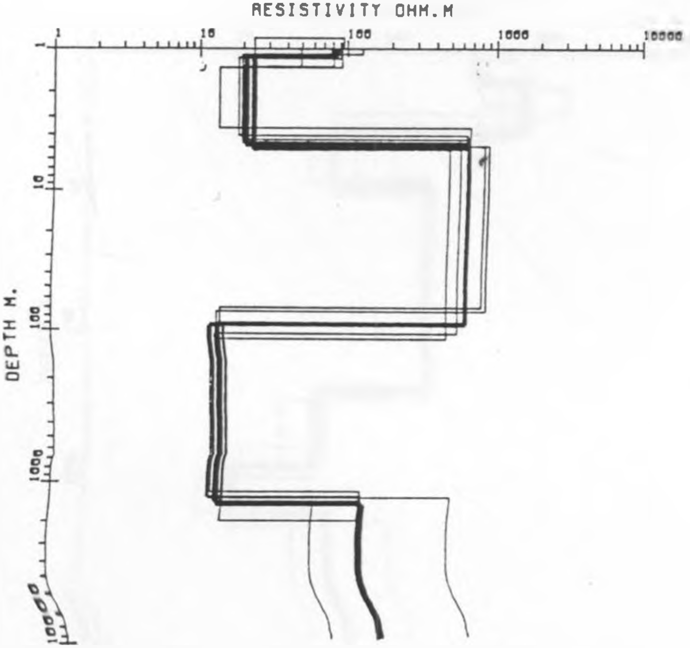
RESISTIVITY OHM.M
1
10
100
1000
10000
DEPTH M.
10
100
1000
10000

MOST-SQUARES SM DC MODELS FOR SITE SUS-OLK S13

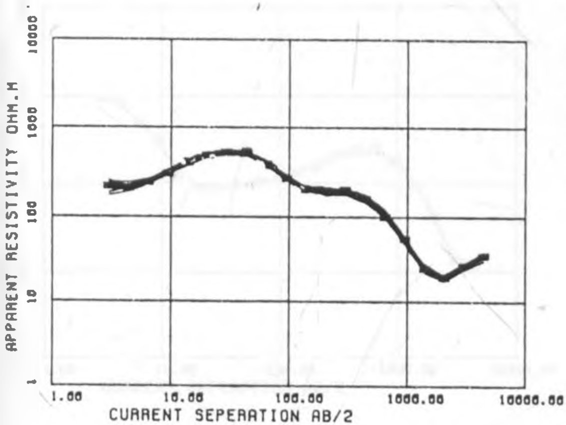

MOST-SQUARES SM DC MODELS FOR SITE SUS-OLK S18

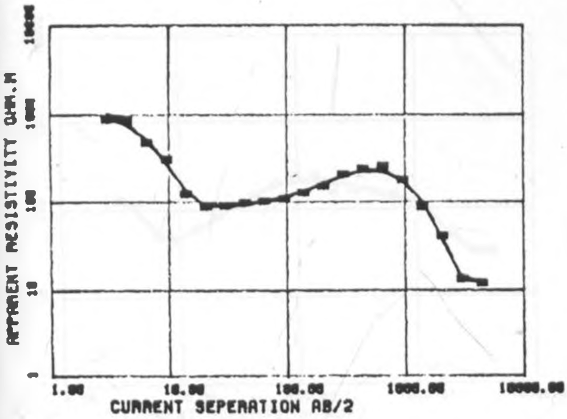

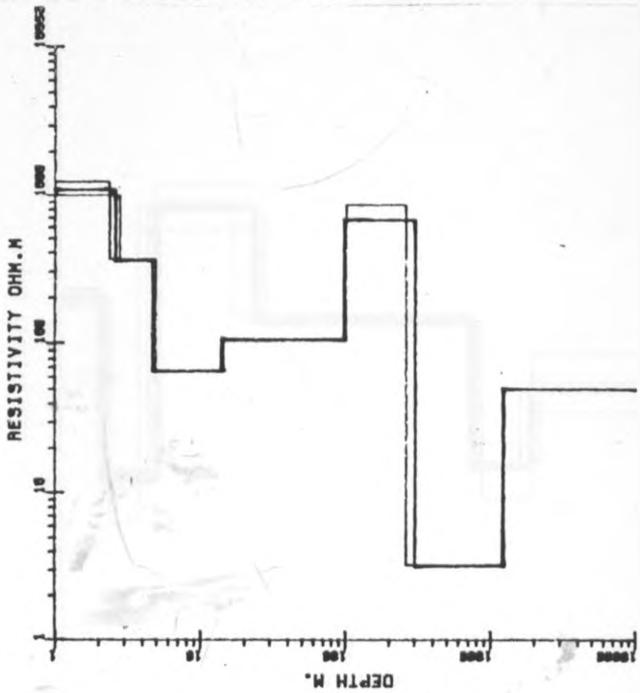

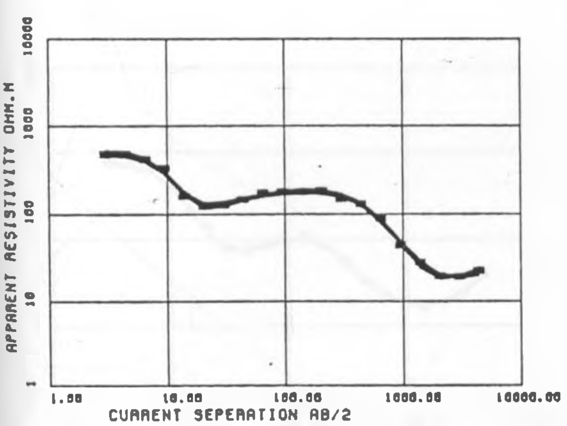

S 20

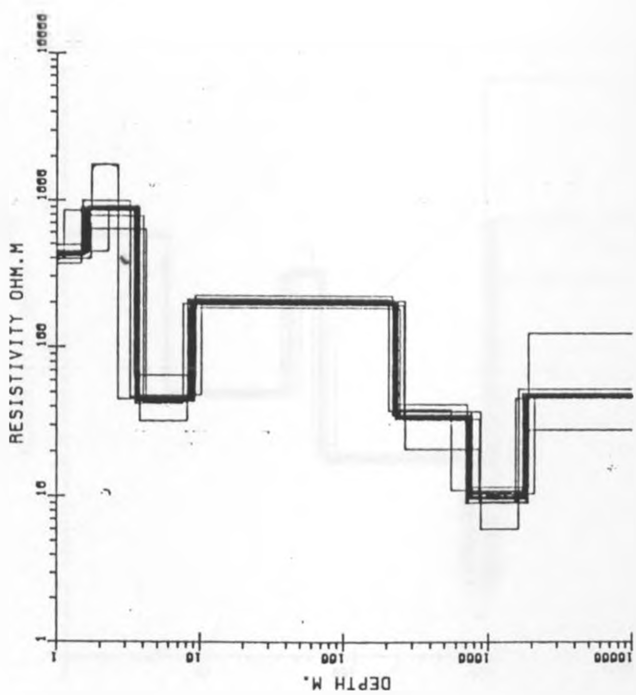

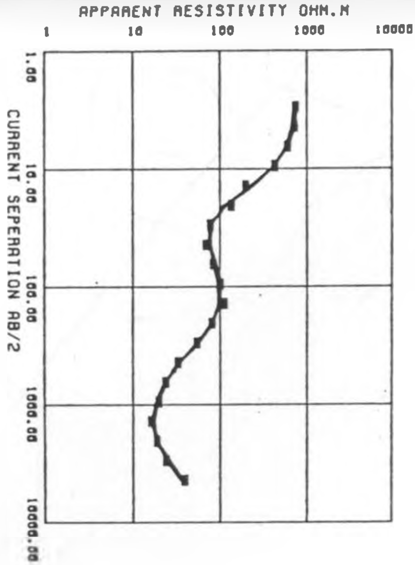
APPARENT RESISTIVITY OHM.M
1
10
100
1000
10000
CURRENT SEPERATION AB/2
1.00
10.00
100.00
1000.00
10000.00

S 26

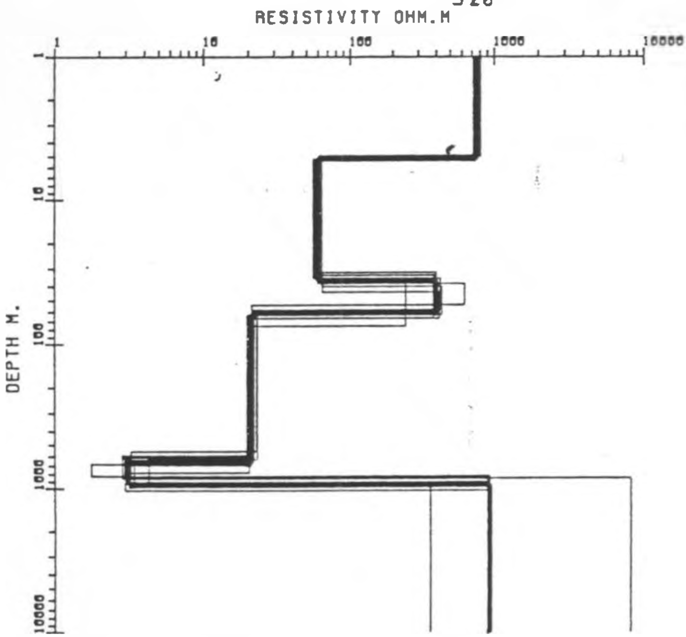
RESISTIVITY OHM.M
1
10
100
1000
10000
DEPTH M.
10
100
1000
10000

MOST-SQUARES SM DC MODELS FOR SITE SUS-OLK S24

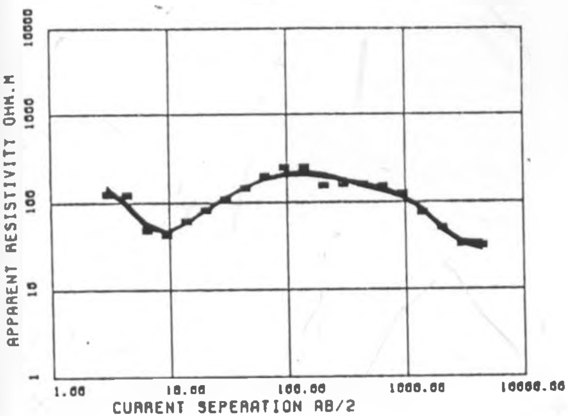

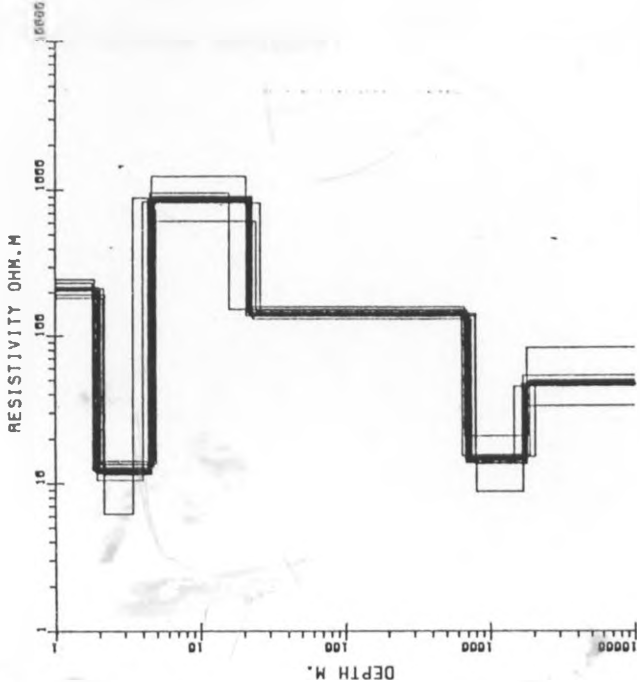

APPENDIX E

Tabulation of some results of the Occam method.

MOST-SQUARES SM DC MODELS FOR SITE SUS-OLK G58

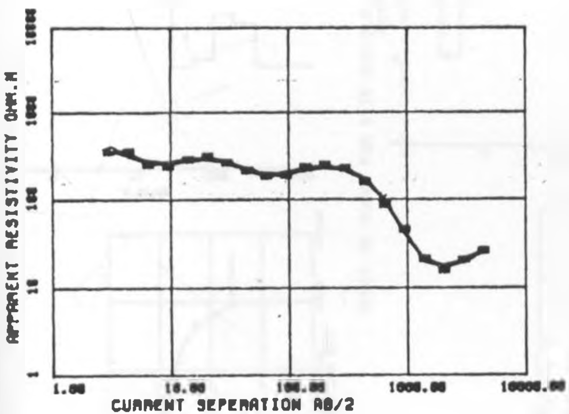

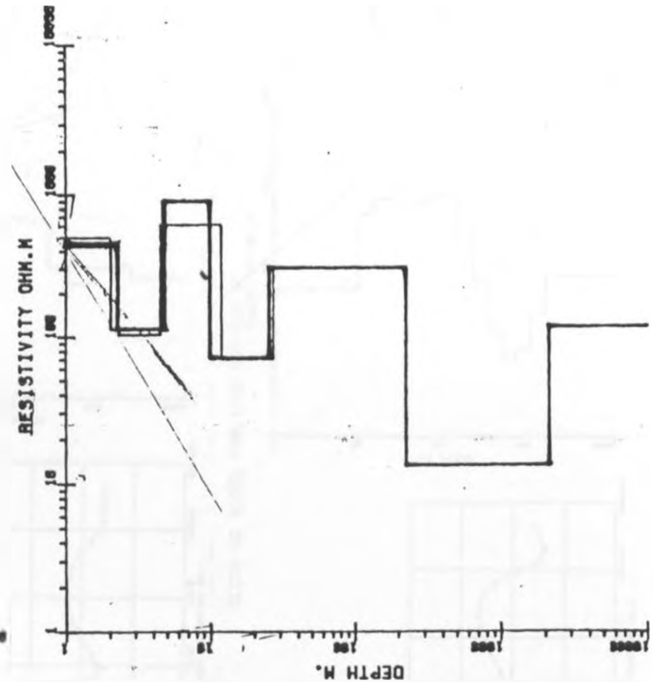

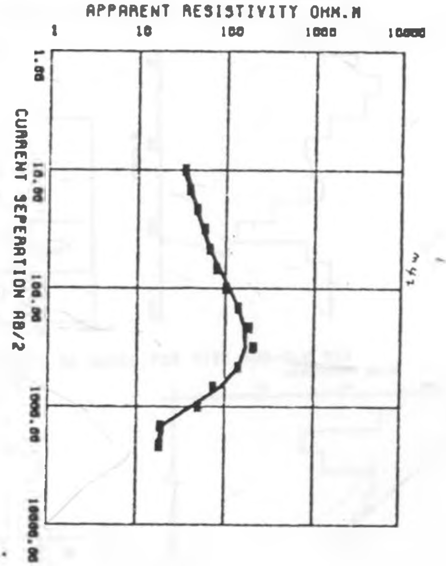

APPARENT RESISTIVITY OHM.M
1
10
100
1000
10000
1.00
10.00
100.00
1000.00
10000.00
CURRENT SEPERATION AB/2
M47

M47

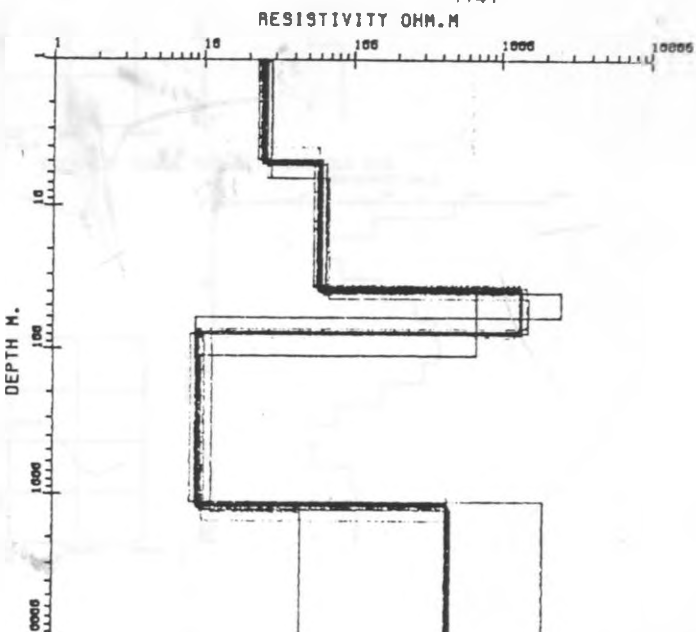

RESISTIVITY OHM.M
1
10
100
1000
10000
DEPTH M.
10
100
1000
10000

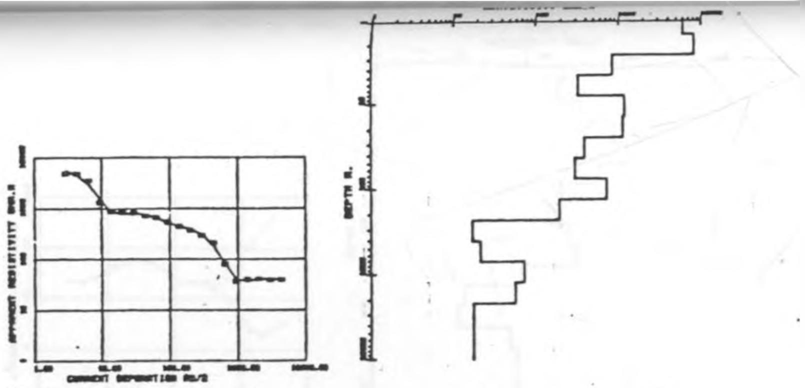

OCCAM DC MODEL FOR SITE SUS-OLK S7

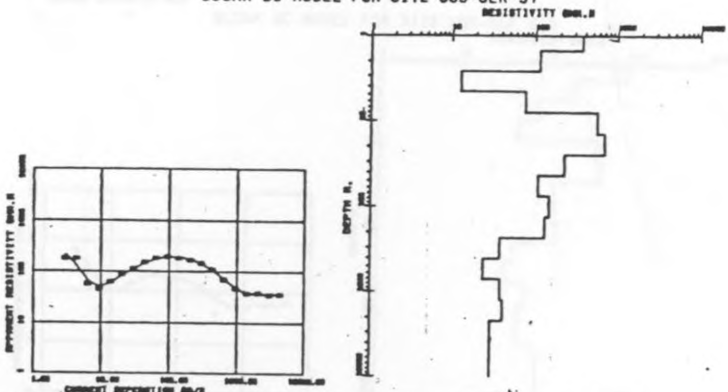

OCCAM DC MODEL FOR SITE SUS-OLK S8

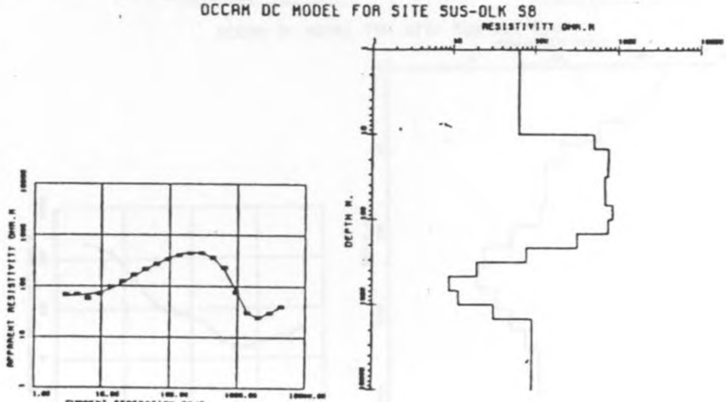

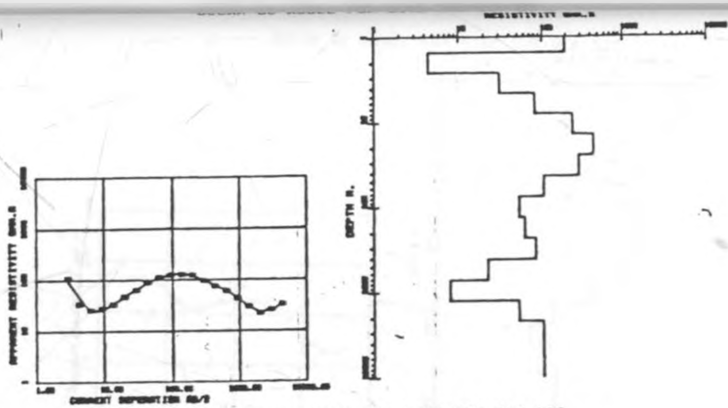

OCCAM DC MODEL FOR SITE SUS-OLK S10

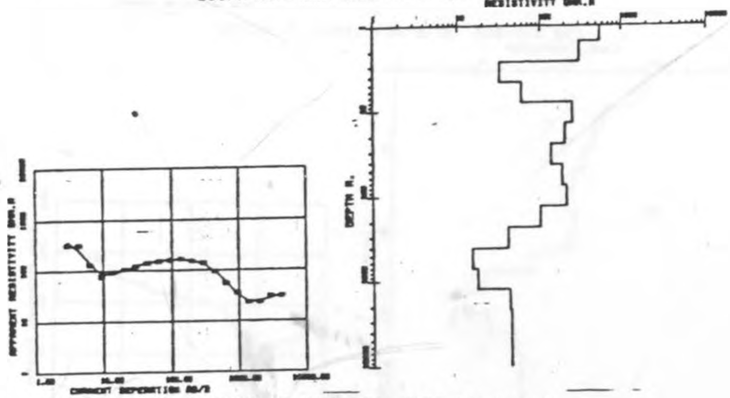

OCCAM DC MODEL FOR SITE SUS-OLK S12

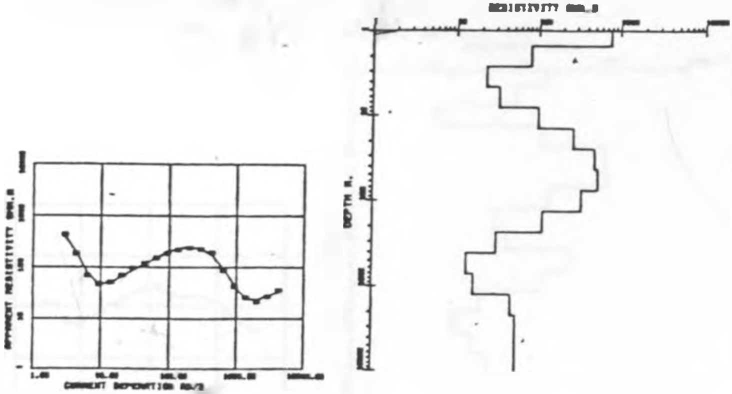

OCCAM DC MODEL FOR SITE SUS-OLK 513

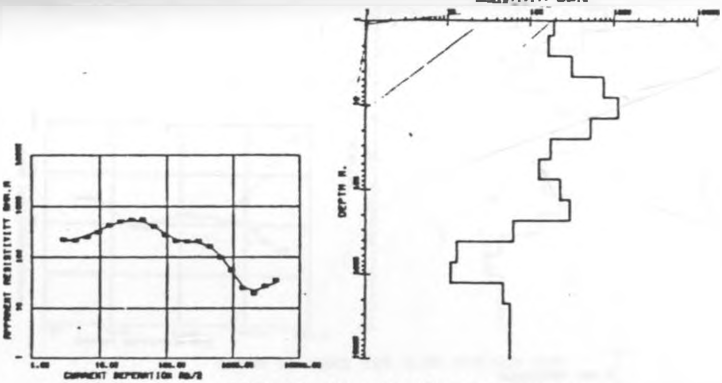

OCCAM DC MODEL FOR SITE SUS-OLK 514

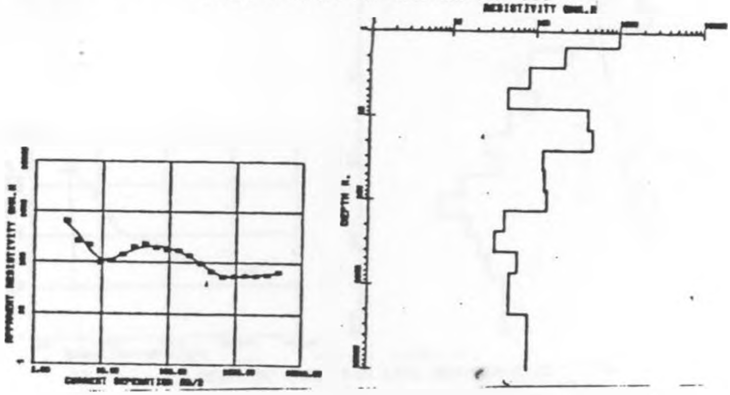

OCCAM DC MODEL FOR SITE SUS-OLK 519

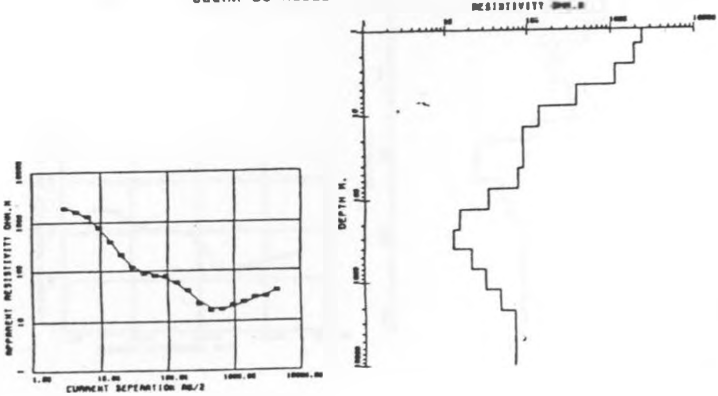

OCCAM DC MODEL FOR SITE SUS-OLK S20

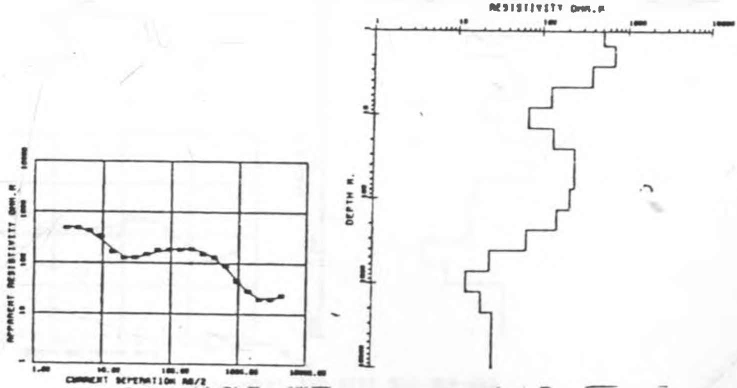

OCCAM DC MODEL FOR SITE SUS-OLK S21

OCCAM DC MODEL FOR SITE SUS-OLK S24

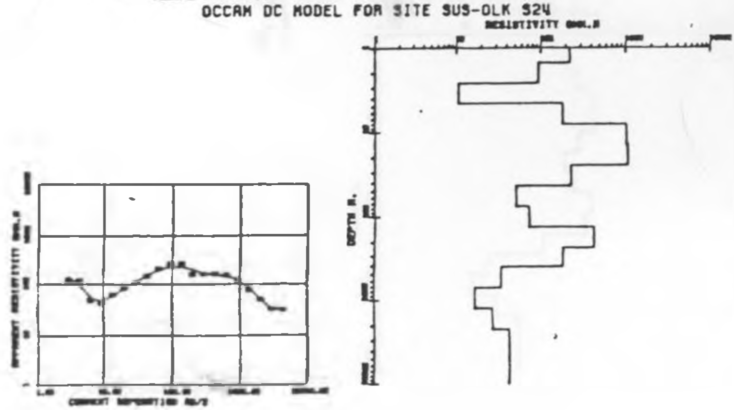

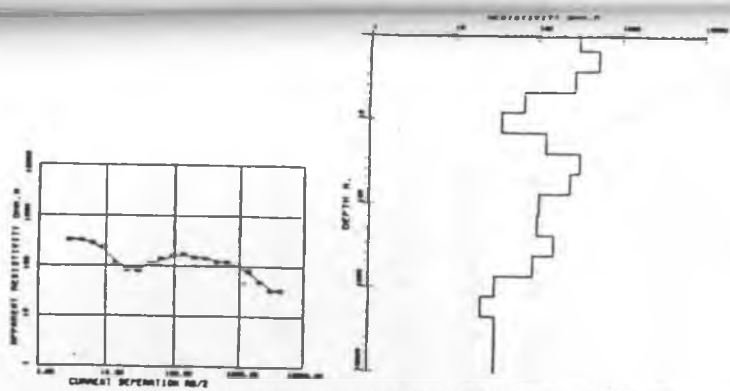

OCCAM DC MODEL FOR SITE SUS-OLK G20

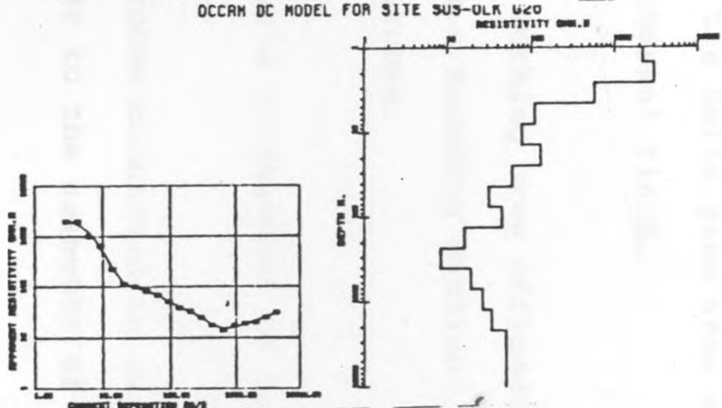

OCCAM DC MODEL FOR SITE SUS-OLK-SL70

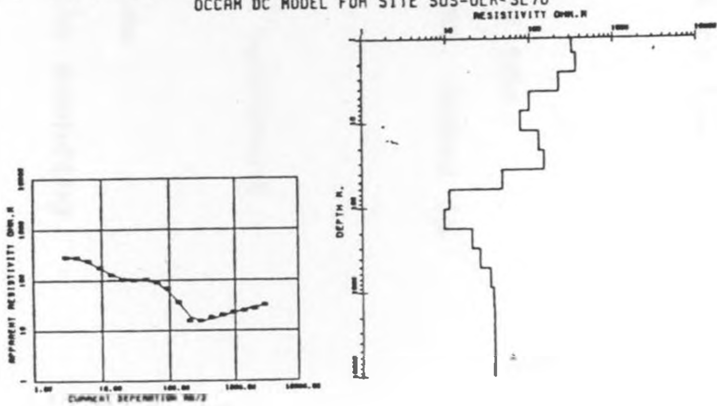

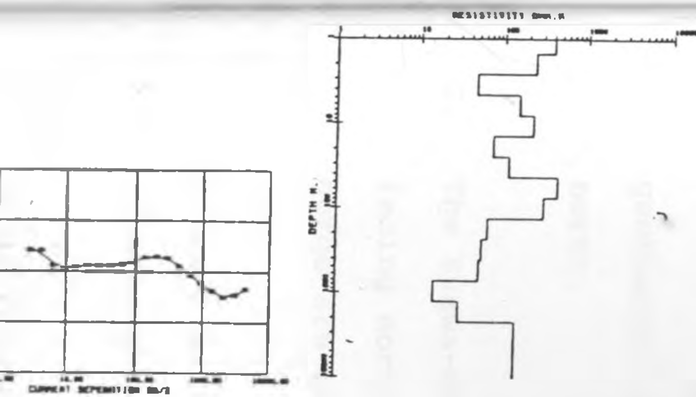

OCCAM DC MODEL FOR SITE SUS-OLK G25

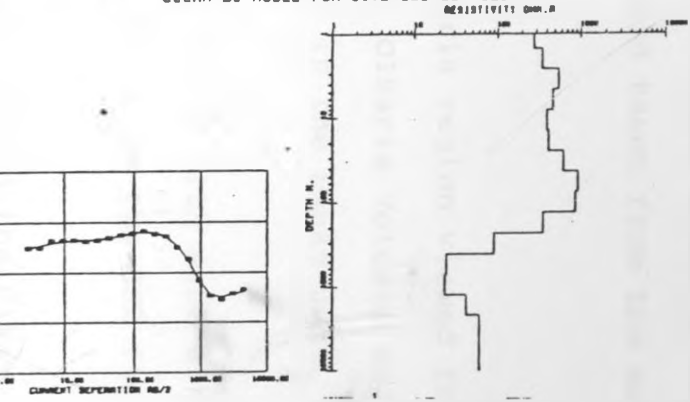

OCCAM DC MODEL FOR SITE SUS-OLK G29

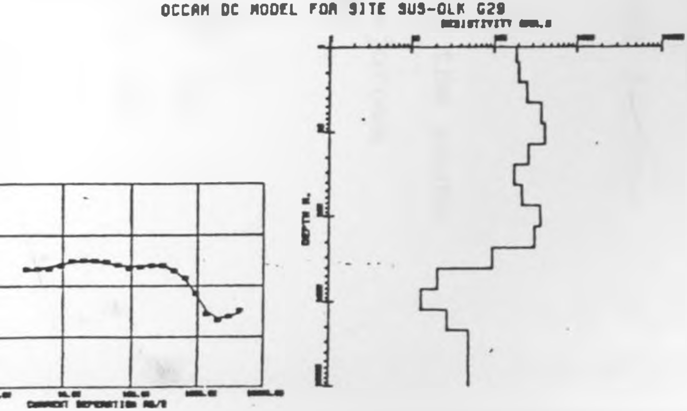

P L A T E S

1. Shows the hilly region south of the Olkaria geothermal field taken from the south facing north.

2. The Suswa-Olkaria region viewed from the south facing north. Olkaria Volcano and Njorowa gorge are seen in the background.

3. Suswa-Olkaria region with part of the Mau escarpment viewed from the SSE facing NNW.

4. Shows vegetation around the Olkaria volcanic complex viewed from the south facing north

5. Wildlife in the Hells gate area NE of the Olkaria geothermal field.

6. Part of the working crew offloading the equipment at a sounding station. Mt. Suswa is in the background.

7. Shows the field arrangement of the equipment.

8. Steel electrodes connected in series perpendicular to the azimuths of the sounding stations.

Plate 1

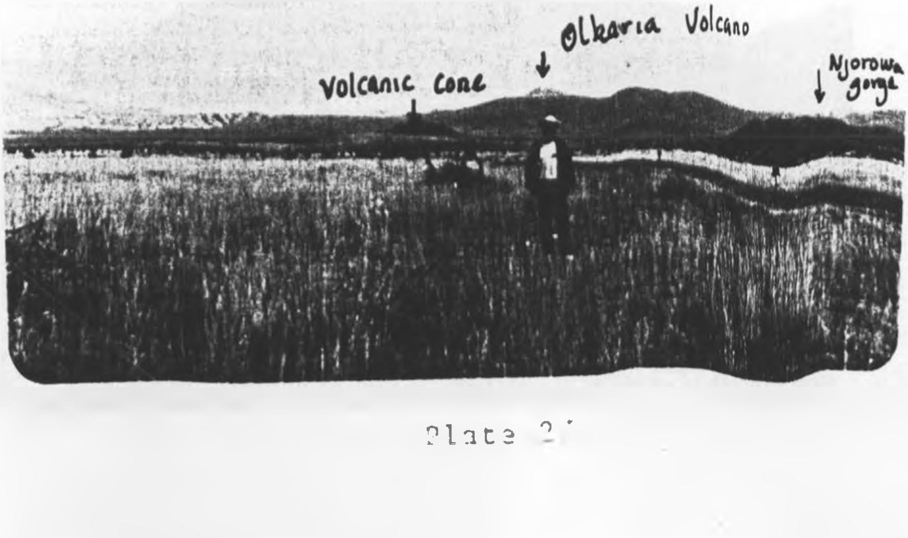

Plate 2

Plate 3

Plate 4

Plate 5

Plate 6

Plate 7

[illegible]